ELECTRON SPIN RESONANCE STUDY OF COPPER N,N-DIALKYLDISELENOCARBAMATES AND SOME RELATED COMPOUNDS

EXAMPLES OF NONCOINCIDING PRINCIPAL AXES

C.P. KEIJZERS

ELECTRON SPIN RESONANCE STUDY OF COPPER N,N-DIALKYLDISELENOCARBAMATES AND SOME RELATED COMPOUNDS

EXAMPLES OF NONCOINCIDING PRINCIPAL AXES

Promotor Prof Dr E de Boer

ELECTRON SPIN RESONANCE STUDY OF COPPER N,N-DIALKYLDISELENOCARBAMATES AND SOME RELATED COMPOUNDS

EXAMPLES OF NONCOINCIDING PRINCIPAL AXES

PROEFSCHRIFT

TER VERKRIJGING VAN DE GRAAD VAN DOCTOR IN DE WISKUNDE EN NATUURWETENSCHAPPEN AAN DE KATHOLIEKE UNIVERSITEIT TE NIJMEGEN, OP GEZAG VAN DE RECTOR MAGNIFICUS PROF Mr F J F.M DUYNSTEE VOLGENS BESLUIT VAN HET COLLEGE VAN DECANEN IN HET OPENBAAR TE VERDEDIGEN OP VRIJDAG 3 MEI 1974 DES NAMIDDAGS TE 2 UUR PRECIES.

DOOR

CORNELUS PETRUS KEIJZERS

GEBOREN TE OSS

1974

DRUK STICHTING STUDENTENPERS NIJMEGEN

Aan mijn ouders
Marian en Arya

Op deze plaats wil ik de medewerkers van de afdeling molecuulspectroscopie bedanken voor hun kollegialiteit en samenwerking gedurende de totstandkoming van dit proefschrift Met name Dr J G M van Rens ben ik erkentelijk voor de vele verhelderende diskussies die we gevoerd hebben over onze nauw verwante onderzoeken

Ik dank de heren Drs G F M Paulussen, P L A Chr M van der Meer, J T M Evers, Drs A W Gal, M H J M de Croon en Drs H L M van Gaal voor hun medewerking aan dit onderzoek tijdens hun hoofd- of bijvakstage

Drs J Willemse van de afdeling anorganische chemie en de heer H L Coenen ben ik dank verschuldigd voor de samenwerking bij de bereiding van de diselenocarbamaat verbindingen

Verder gaat mijn dank uit naar de medewerkers van de dienstverlenende afdelingen van de faculteit der Wiskunde en Natuurwetenschappen voor hun hulp bij het experimentele werk De afdeling illustratie, o l v de heer J Gerritsen, droeg zorg voor de figuren in dit proefschrift en voor de lay-out

Een gedeelte van het onderzoek is gefinancierd door de Stichting Scheikundig Onderzoek in Nederland (SON) met medewerking van de Nederlandse Organisatie voor Zuiver Wetenschappelijk Onderzoek (ZWO)

CONTENTS

CHAPTER I

INTRODUCTION

I A Introduction

This thesis deals with an electron spin resonance (ESR) study of bis(N,N-dialkyldiselenocarbamato)-copper(II) complexes {$Cu(R_2dsc)_2$, R=methyl(met), ethyl(et), n-butyl(but)}

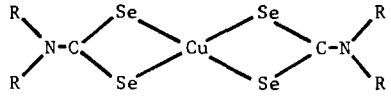

R = alkyl

and the related compounds bis(N,N diethyldithiocarbamato)-copper(II) {$Cu(et_2dtc)_2$} and bis(N,N-di n-butyldiselenocarbamato)-silver(II).

This study is a continuation of the investigations which are carried out at this University on the dithiocarbamato-, maleonitriledithiolato-(mnt), and other dithiolato-complexes of various metals [1-5]. A striking property of these ligands is their ability to stabilize metals with an unusually high oxidation number. Redox reactions of these complexes have been studied extensively in the Department of Inorganic Chemistry, resulting in the preparation of a large number of compounds with the metal ion in a high oxidation state [6-9].

Some of these compounds have been studied already with the aid of ESR spectroscopy. Of special interest for us are $Ag(et_2dtc)_2$, $Au(et_2dtc)_2$, and $Au(mnt)_2^{2-}$, which have been studied by van Rens in this department [5], and $Cu(et_2dtc)_2$ [10-13] and $Cu(mnt)_2^{2-}$ [14-16]. We have extended these studies to the diselenocarbamato-complexes. Since the natural abundance of selenium atoms with a nuclear spin is ten times larger than for sulphur, the hyperfine splitting (hfs) of the former atoms can be measured more easily than of the latter. These hyperfine splittings yield additional information about the electronic and molecular structure of the complexes. A disadvantage is the very large spin-orbit coupling of selenium, which results in a large influence of these ligand atoms on the g values. One of the consequences is an unexpected orientation of the $\bar{\bar{g}}$ tensor principal axes relative to the principal axes of the central metal hyperfine splitting tensor. A large part of this study is focussed on the explanation of this effect.

I B Survey of the present study

In section A of chapter II, expressions are derived for the resonance fields and the transition probabilities, using the formalism of the effective spin hamiltonian. These equations enable us to determine the spin hamiltonian parameters from the experimental spectra. In the sections II B, C, and D the parameters of the spin hamiltonian are expressed in the parameters occurring in the Molecular Orbital (MO) model. Special attention is paid to the influence of multicentre integrals and the problem of gauge invariance, because this is important if molecules are considered.

In chapter III the preparation of the various compounds and single crystals is given. Furthermore we discuss the derivation of the spin hamiltonian parameters from the experimental spectra.

The experimental results are presented in chapter IV. The main part is related to single crystal measurements in two different host lattices. Powder and glass spectra are also discussed.

The last chapter contains the results of extended Hückel calculations. The orientation of the principal axes in the diselenocarbamato complexes is explained.

CHAPTER II

THEORY

All systems considered in this thesis contain one unpaired electron and one or more nuclei with a magnetic moment. The hamiltonian of such a system can be divided into two parts: H_o and H_s. H_o is the Schrodinger hamiltonian, containing the kinetic energy and all Coulomb interactions of electrons and nuclei. H_s describes the electric multipole interactions and the magnetic interactions. The only electric multipole interaction of importance in our systems, is the quadrupole interaction. The magnetic interactions are the coupling between the electron spin and the nuclear spins, the coupling of these spins with the orbital angular momentum of the electron and (if present) with the external magnetic field.

In the Hartree Fock method, the eigenfunctions of H_o are approximated with determinant functions, consisting of one-electron spinorbitals $\psi\sigma$, where σ is the spinfunction. The spatial part ψ is a molecular orbital (MO), often approximated by a linear combination of atomic orbitals (LCAO). In chapter V we calculate these eigenfunctions in an approximate way. In the present chapter we assume an exact knowledge of these determinant functions and their energies. Moreover, in view of the low symmetry of the systems studied, we assume that the eigenvalues of H_o have no orbital degeneracy.

Expressions for the resonance fields and transition probabilities in the ESR spectrum are derived in section A, using the formalism of the effective spin hamiltonian. The physical background of some magnetic and electric interactions is discussed in sections B,C and D.

II A The spin hamiltonian and the esr spectrum

For the sake of simplicity, we restrict ourselves in this section to a paramagnetic molecule with only one nucleus with a magnetic moment. When such a system is placed in a homogeneous magnetic field, the spin hamiltonian of the system is given by

$$H_s = \mu_b \vec{B}.\bar{\bar{g}}.\vec{S} + \vec{S}.\bar{\bar{A}}.\vec{I} + \vec{I}.\bar{\bar{P}}.\vec{I} - g_n\mu_n\vec{B}.\vec{I}$$

$$= H_{EZ} + H_{HF} + H_Q + H_{NZ} \quad , \qquad (II.1)$$

where μ_b is the Bohr magneton, μ_n the nuclear magneton, g_n the gyromagnetic ratio of the nucleus and $\vec{B}$ the magnetic induction.

H_{EZ} is the electron Zeeman energy, representing the interaction of the electron spin $\vec{S}$ with the magnetic field. The generally anisotropic $\bar{\bar{g}}$ tensor will be discussed in section II B. When a magnetic induction of 0.32 Tesla is applied the magnitude of this interaction is of the order of 3000 $10^{-4}cm^{-1}$*.

H_{HF} is the magnetic hyperfine interaction between the nuclear spin $\vec{I}$ and the field produced by the electron spin $\vec{S}$. Generally the hyperfine coupling tensor $\bar{\bar{A}}$ is anisotropic, its principal axes do not necessarily coincide with those of $\bar{\bar{g}}$. The nature of this tensor will be discussed in section II C. The magnitude of this interaction is for copper: up to 150 $10^{-4}cm^{-1}$; for silver: 10 $10^{-4}cm^{-1}$; for selenium: up to 40 $10^{-4}cm^{-1}$.

H_Q is the nuclear quadrupole interaction, representing the interaction of the nuclear electric quadrupole moment with the electric field gradient. The tensor $\bar{\bar{P}}$ will be discussed in section II D. The magnitude of this interaction for copper in Cu(II)$(et_2dtc)_2$ diluted in Ni(II)$(et_2dtc)_2$ [17] or in tetraethylthiuramdisulphide [18] does not exceed 2 $10^{-4}cm^{-1}$. Silver and selenium do not posses a quadrupole moment.

H_{NZ} is the nuclear Zeeman energy, the interaction of the nuclear spin with the magnetic field. We neglect the chemical shielding in this interaction, because it is not likely to exceed 1,000 ppm, while the energy itself is small. Some magnitudes are: when using an induction of 1.2 Tesla: copper: 7 $10^{-4}cm^{-1}$; silver: 0.5 $10^{-4}cm^{-1}$; selenium: 2 $10^{-4}cm^{-1}$.

II A 1 Transformation of spincoordinates

Bleany [19] has derived expressions for the resonance magnetic field for the case of axially symmetric $\bar{\bar{g}}$ and $\bar{\bar{D}}$ (the zero field splitting tensor). Weger and Low [20] extended this calculation to the case of non-axially symmetric $\bar{\bar{D}}$. Golding and Tennant [18] handled the problem of axially symmetric $\bar{\bar{g}}$, $\bar{\bar{A}}$ and $\bar{\bar{P}}$. This calculation was extended by Golding [21] to the problem of non-axially symmetric $\bar{\bar{g}}$, $\bar{\bar{D}}$, $\bar{\bar{A}}$ and $\bar{\bar{P}}$, with the restriction, however, that the principal axes of all tensors coincide. The same restriction was made by McClung [22] who considered the case of non-axial $\bar{\bar{g}}$ and $\bar{\bar{A}}$. Recently Lin [23] discussed the problem of non-axial $\bar{\bar{g}}$, $\bar{\bar{D}}$, and $\bar{\bar{A}}$ without assuming that the tensors have the same set of principal axes.

*All formulas in this thesis will be in SI units. As is conventional in ESR spectroscopy, energies will be given in units of $10^{-4}cm^{-1}$. A unit of $10^{-4}cm^{-1}$ is equal to 1.9862 10^{-27} Joule.

Similarly Golding [24] did not make this assumption in deriving expressions for the resonance field in the case of rhombic $\bar{\bar{g}}$, $\bar{\bar{A}}$ and $\bar{\bar{D}}$. In all these derivations the nuclear Zeeman energy was neglected, although it can be important for the transition probabilities. In this section no restrictions are made for the orientation of the principal axes of the tensors. The ESR spectrum is calculated for the general case where the interactions can be represented by the spin hamiltonian (Eq.II.1). The applied magnetic induction is taken in an arbitrary direction:

$$\vec{B} = B\,\vec{k} \qquad \begin{aligned} k_x &= \sin\theta\cos\phi \\ k_y &= \sin\theta\sin\phi \\ k_z &= \cos\theta\ . \end{aligned} \qquad \text{(II.2)}$$

θ and ϕ are the spherical angles in the laboratory coordinate system.

Thus our goal is to calculate the eigenvalues and eigenvectors of the hamiltonian operator by means of a perturbation procedure. We start with a set of $(2S + 1)(2I + 1)$ states degenerate for H_o. Since the perturbations differ in order of magnitude ($H_{EZ} > H_{HF} > H_Q, H_{NZ}$), it is a good approximation first to diagonalize the largest term (H_{EZ}). This results into two sets of $(2I + 1)$ functions degenerate for $H_o + H_{EZ}$. Next the second largest term (H_{HF}) is diagonalized within each of these sets of $(2I + 1)$ degenerate functions. Thus we obtain the proper unperturbed functions which may be used in formulas for perturbation theory of non degenerate states [25].

The diagonalization of H_{EZ} amounts to the choice of a new basis set of electron spin functions. These are chosen to be eigenfunctions of the $\vec{S}$-component that is directed along the so-called "effective field"

$$\vec{B}_{ef} = \vec{B}.\bar{\bar{g}}\ . \qquad \text{(II.3)}$$

This $\vec{S}$-component may be called the z-component of a spin vector $\vec{S}'$ that can be obtained from $\vec{S}$ by the transformation

$$\vec{S} = \bar{\bar{U}}^{-1}.\vec{S}'\ , \qquad \text{(II.4)}$$

where $\bar{\bar{U}}$ is an orthogonal transformation matrix. Applying this transformation H_{EZ} can be rewritten:

$$H_{EZ} = \mu_b B\,\vec{k}.\bar{\bar{g}}.\bar{\bar{U}}^{-1}.\vec{S}'\ . \qquad \text{(II.5)}$$

A convenient expression for $\bar{\bar{U}}$ is:

$$\bar{\bar{U}}^{\star} = \begin{bmatrix} \frac{l_1 l_3}{\sqrt{l_1^2 + l_2^2}} & \frac{l_2 l_3}{\sqrt{l_1^2 + l_2^2}} & -\sqrt{l_1^2 + l_2^2} \\ \frac{-l_2}{\sqrt{l_1^2 + l_2^2}} & \frac{l_1}{\sqrt{l_1^2 + l_2^2}} & 0 \\ l_1 & l_2 & l_3 \end{bmatrix} \qquad \text{(II.6)}$$

where $\vec{l}$ is the unit vector along $\vec{B}_{ef}$:

$$\vec{l} = \frac{\vec{k}.\bar{\bar{g}}}{\sqrt{\vec{k}.\bar{\bar{g}}.\bar{\bar{g}}^t.\vec{k}^t}} \quad . \qquad \text{(II.7)}$$

Substitution of this expression for $\bar{\bar{U}}$ in Eq.II.5 yields:

$$H_{EZ} = \mu_b B \sqrt{\vec{k}.\bar{\bar{g}}.\bar{\bar{g}}^t.\vec{k}^t}\, S'_z \equiv \mu_b B\, g\, S'_z \; . \qquad \text{(II.8)}$$

We may interpret $g = \sqrt{\vec{k}.\bar{\bar{g}}.\bar{\bar{g}}^t.\vec{k}^t}$ as an "effective" g value in the direction of the applied field.

The next step is to diagonalize the second largest perturbation, H_{HF}, within a manifold of (2I + 1) degenerate functions for $H_o + H_{EZ}$:

$$\langle M_S, M_I^a \mid H_{HF} \mid M_S, M_I^b \rangle = 0 \qquad \text{if } M_I^a \neq M_I^b \quad . \qquad \text{(II.9)}$$

This means that off-diagonal matrix elements of H_{HF} exist only between levels of different M_S. These elements are small because the energy separation between the two manifolds of different M_S is much larger than the separations within such a manifold. In order to fulfil the condition (II.9) we introduce a transformation of the nuclear spin $\vec{I}$:

$$\vec{I} = \bar{\bar{V}}^{-1}.\vec{I}' \qquad \text{(II.10)}$$

where $\bar{\bar{V}}$ is an orthogonal transformation matrix and $\vec{I}'$ is the nuclear spin vector in a new coordinate system. Substituting the transformations (II.4) and (II.10) in H_{HF} results in:

*Obviously, a necessary condition for this expression is: $l_1^2 + l_2^2 \neq 0$. $l_1^2 + l_2^2 = 0$ implies that $l_3 = 1$, or $\vec{B}_{ef}$ is parallel to the laboratory z axis. In this case we have to take the unit matrix for $\bar{\bar{U}}$ and the electron spin functions are eigenfunctions of S_z.

$$H_{HF} = \vec{S}'.\bar{\bar{U}}.\bar{\bar{A}}.\bar{\bar{V}}^{-1}.\vec{I}' = \vec{S}'.\bar{\bar{T}}.\vec{I}' \qquad \text{(II.11)}$$

where we defined the effective hyperfine coupling tensor $\bar{\bar{T}}$. The row vector $\vec{S}'.\bar{\bar{U}}$ in (II.11) is obtained by transposing the column vector $\bar{\bar{U}}^{-1}.\vec{S}'$ in (II.4). Condition (II.9) is fulfilled if the matrix is taken for $\bar{\bar{V}}$ that is obtained from $\bar{\bar{U}}$ (Eq.II.6) by changing l_i to L_i, where $\vec{L}$ is the unit vector

$$\vec{L} = \frac{\vec{k}.\bar{\bar{g}}.\bar{\bar{A}}}{K} = \vec{I}.\bar{\bar{A}}\,\frac{\bar{\bar{g}}}{K} \qquad \text{(II.12)}$$

$$K = \sqrt{\vec{k}.\,\bar{\bar{g}}.\,\bar{\bar{A}}.\,\bar{\bar{A}}^{t}.\,\bar{\bar{g}}^{t}.\,\vec{k}^{t}} \quad . \qquad \text{(II.13)}$$

Since the remaining interactions (H_Q and H_{NZ}) are small, compared with H_{EZ} and H_{HF}, they will not yield off-diagonal elements comparable in magnitude with the diagonal ones. Therefore we simply apply the transformation (II.10) of the nuclear spin, and obtain

$$H_Q = \vec{I}.\bar{\bar{P}}.\vec{I} = \vec{I}'.\bar{\bar{V}}.\bar{\bar{P}}.\bar{\bar{V}}^{-1}.\vec{I}' = \vec{I}'.\bar{\bar{Q}}.\vec{I}' \qquad \text{(II.14)}$$

$$H_{NZ} = -g_n\mu_n\vec{B}.\vec{I} = -g_n\mu_n B\,\vec{k}.\bar{\bar{V}}^{-1}.\vec{I}' = -g_n\mu_n B\,\vec{Z}.\vec{I}' \quad . \qquad \text{(II.15)}$$

These equations define an effective quadrupole tensor $\bar{\bar{Q}}$ and a vector $\vec{Z}$.

The resulting spin hamiltonian for an arbitrary direction of the magnetic field is

$$H_s = g\,\mu_b B\,S_z' + \vec{S}'.\bar{\bar{T}}.\vec{I}' + \vec{I}'.\bar{\bar{Q}}.\vec{I}' - g_n\mu_n B\,\vec{Z}.\vec{I}' \quad . \qquad \text{(II.16)}$$

II A 2 Resonance fields

The energies, influenced by H_s are calculated with second order perturbation theory. The eigenfunctions of S_z' and I_z' are written as $|M_S, M_I\rangle$. The perturbed functions, originating from these, are denoted by $|M_S, M_I\rangle^{(1)}$ because they are not expected to deviate much from the functions $|M_S, M_I\rangle$. The resulting energy for $|M_S, M_I\rangle^{(1)}$ is

$$\begin{aligned} E(M_S,M_I) = {} & M_S g\,\mu_b B + M_S M_I T_{33} + \tfrac{1}{2}(3M_I^2 - I^2 - I)Q_{33} - g_n\mu_n M_I B\,Z_3 \\ & + \frac{F_1\{[\,\tfrac{1}{2}g_n\mu_n B\,Z_1 - F_7 Q_{13}\,]^2 + [\,\tfrac{1}{2}g_n\mu_n B\,Z_2 - F_7 Q_{23}\,]^2\}}{g_n\mu_n B\,Z_3 - M_S T_{33} - 3F_7 Q_{33}} \\ & + \frac{F_2\{[\,\tfrac{1}{2}g_n\mu_n B\,Z_2 - F_8 Q_{13}\,]^2 + [\,\tfrac{1}{2}g_n\mu_n B\,Z_2 - F_8 Q_{23}\,]^2\}}{-g_n\mu_n B\,Z_3 + M_S T_{33} + 3F_8 Q_{33}} \\ & + \frac{F_1 F_3\{(T_{11} - T_{22})^2 + (T_{12} + T_{21})^2\}}{-g\,\mu_b B + g_n\mu_n B\,Z_3 - (F_7 + F_9)T_{33} - 3F_7 Q_{33}} \end{aligned}$$

$$+\frac{F_2F_4\{(T_{11}+T_{22})^2+(T_{12}+T_{21})^2\}}{g\mu_bB-g_n\mu_nB\,Z_3+(F_8+F_{10})T_{33}+3F_8Q_{33}}$$

$$+\frac{F_2F_3\{(T_{11}+T_{22})^2+(T_{12}-T_{21})^2\}}{-g\mu_bB-g_n\mu_nB\,Z_3+(F_9-F_8)T_{33}+3F_8Q_{33}}$$

$$+\frac{F_1F_4\{(T_{11}+T_{22})^2+(T_{12}-T_{21})^2\}}{g\mu_bB+g_n\mu_nB\,Z_3+(F_7-F_{10})T_{33}-3F_7Q_{33}}$$

$$+\frac{F_1F_5\{(Q_{11}-Q_{22})^2+4Q_{12}^2\}}{g_n\mu_nB\,Z_3-M_ST_{33}-3F_7Q_{33}}$$

$$+\frac{F_2F_6\{(Q_{11}-Q_{22})^2+4Q_{12}^2\}}{-g_n\mu_nB\,Z_3+M_ST_{33}+3F_8Q_{33}}$$

$$+\frac{\frac{1}{2}M_SM_I^2\,(T_{13}^2+T_{23}^2)}{g\mu_bB+M_IT_{33}}\quad, \tag{II.17}$$

where
$$F_1=(I+M_I+1)(I-M_I)$$
$$F_2=(I-M_I+1)(I+M_I)$$
$$F_3=1/16(3/2+M_S)(1/2-M_S)$$
$$F_4=1/16(3/2-M_S)(1/2+M_S)$$
$$F_5=1/32(I+M_I+2)(I-M_I-1)$$
$$F_6=1/32(I-M_I+2)(I+M_I-1)$$
$$F_7=M_I+1/2$$
$$F_8=M_I-1/2$$
$$F_9=M_S+1/2$$
$$F_{10}=M_S-1/2\ .$$

From these energies one obtains the required field strength for the $\Delta M_S=\pm1$, $\Delta M_I=m(m=0,\pm1,+2,+3)$ transition by demanding

$$h\nu=E(\tfrac{1}{2},M_I)-E(-\tfrac{1}{2},M_I+m). \tag{II.18}$$

In the case of copper ($I=3/2$) this leads to 4 $\Delta M_I=0$ transitions, 6 $\Delta M_I=+1$, 4 $\Delta M_I=\pm2$ and 2 $\Delta M_I=\pm3$ transitions. If the second order energy corrections are small compared with the first order contributions, the energy level scheme may be the one of Fig.1A and the ESR spectrum may show the pattern of Fig.1B.

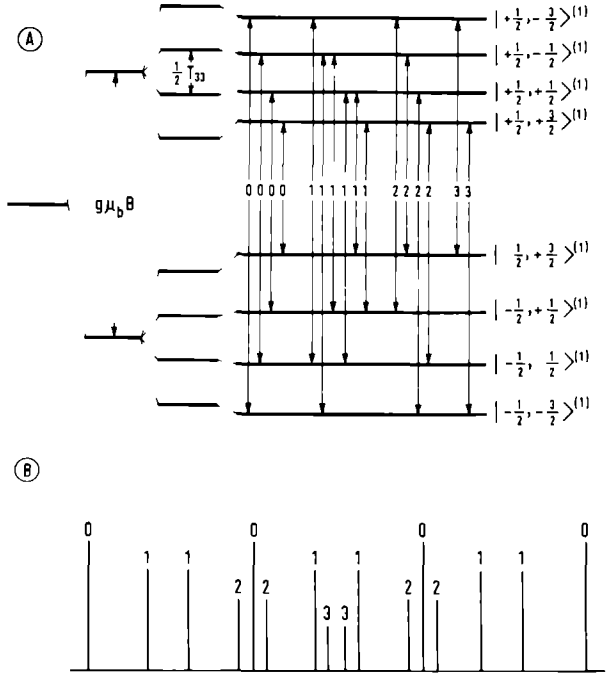

Fig.1A Energy level scheme and ESR transitions of a copper complex for an arbitrary orientation of the magnetic field. Distances are not to scale.

B Stick spectrum in case the second order energy corrections are small compared with the first order energies. The height of a peak does not represent its intensity.

II A 3 Transition probabilities

To derive expressions for the transition probabilities, the perturbed eigenfunctions have to be calculated. Up to first order they are

$$\frac{1}{N}\,|M_S,M_I\rangle^{(1)} = |M_S,M_I\rangle$$

$$+\frac{F_1^{\frac{1}{2}}[\,-\frac{1}{2}g_n\mu_n B(Z_1 - iZ_2) + F_7(Q_{13} - iQ_{23})\,]}{g_n\mu_n B\,Z_3 - M_S T_{33} - 3F_7 Q_{33}}\,|M_S,M_I + 1\rangle$$

$$+\frac{F_2^{\frac{1}{2}}[\,-\frac{1}{2}g_n\mu_n B(Z_1 + iZ_2) + F_8(Q_{13} + iQ_{23})\,]}{-g_n\mu_n B\,Z_3 + M_S T_{33} + 3F_8 Q_{33}}\,|M_S,M_I - 1\rangle$$

$$+\frac{[\,\frac{1}{2}F_2F_6\,]^{\frac{1}{2}}\,[\,Q_{11} - Q_{22} + 2iQ_{12}\,]}{-g_n\mu_n B\,Z_3 + M_S T_{33} + 3(F_8 - \frac{1}{2})Q_{33}}\,|M_S,M_I - 2\rangle$$

$$+\frac{[\tfrac{1}{2}F_1F_5]^{\frac{1}{2}}[Q_{11}-Q_{22}-2iQ_{12}]}{g_n\mu_nB\,Z_3-M_ST_{33}-3(F_7+\tfrac{1}{2})Q_{33}}|M_S,M_I+2\rangle$$

$$+\frac{[F_1F_3]^{\frac{1}{2}}[T_{11}-T_{22}-iT_{12}-iT_{21}]}{-g\,\mu_bB+g_n\mu_nB\,Z_3-(F_7+F_9)T_{33}-3F_7Q_{33}}|M_S+1,M_I+1\rangle$$

$$+\frac{[F_2F_3]^{\frac{1}{2}}[T_{11}+T_{22}+iT_{12}-iT_{21}]}{-g\,\mu_bB-g_n\mu_nB\,Z_3+(F_9-F_8)T_{33}+3F_8Q_{33}}|M_S+1,M_I-1\rangle$$

$$+\frac{[F_1F_4]^{\frac{1}{2}}[T_{11}+T_{22}-iT_{12}+iT_{21}]}{g\,\mu_bB+g_n\mu_nB\,Z_3+(F_7-F_{10})T_{33}-3F_7Q_{33}}|M_S-1,M_I+1\rangle$$

$$+\frac{[F_2F_4]^{\frac{1}{2}}[T_{11}-T_{22}+iT_{12}+iT_{21}]}{g\,\mu_bB-g_n\mu_nB\,Z_3+(F_8+F_{10})T_{33}+3F_8Q_{33}}|M_S-1,M_I-1\rangle$$

$$+\frac{2F_3^{\frac{1}{2}}M_I[T_{13}-iT_{23}]}{-g\,\mu_bB-M_IT_{33}}|M_S+1,M_I\rangle$$

$$+\frac{2F_4^{\frac{1}{2}}M_I[T_{13}+iT_{23}]}{g\,\mu_bB+M_IT_{33}}|M_S-1,M_I\rangle\quad, \tag{II.19}$$

where N is a normalization constant and the F_i have been defined in the preceding paragraph.

Transitions between the states described in Eq.II.19, are induced by a linearly polarized oscillatory field $\vec{B}_1\cos\omega t$, normal to the static magnetic field. The direction of $\vec{B}_1$ is given by a unit vector $\vec{k}_1$ in the laboratory coordinate system. The probability of the transition between the states $|\tfrac{1}{2},M_I^a\rangle^{(1)}$ and $|-\tfrac{1}{2},M_I^b\rangle^{(1)}$ is proportional to [26]

$$P(\tfrac{1}{2},M_I^a;-\tfrac{1}{2},M_I^b)\ (:)\ |{}^{(1)}\langle\tfrac{1}{2},M_I^a|\mu_b\vec{B}_1.\bar{\bar{g}}.\vec{S}-g_n\mu_n\vec{B}_1.\vec{I}|-\tfrac{1}{2},M_I^b\rangle^{(1)}|^2\ .$$

Neglecting the nuclear Zeeman term and omitting constant factors, this expression becomes

$$(:)\ |{}^{(1)}\langle\tfrac{1}{2},M_I^a|\vec{O}.\vec{S}'|-\tfrac{1}{2},M_I^b\rangle^{(1)}|^2\ , \tag{II.20}$$

where we substituted the transformation (II.4) and defined the vector

$$\vec{O}=\vec{k}_1.\bar{\bar{g}}.\bar{\bar{U}}^{-1}\ . \tag{II.21}$$

The results of this section, as far as the resonance fields are

concerned, are used to determine the ESR parameters from single crystal spectra. To verify these results the transition probabilities are calculated and compared with the measured spectra. The method is outlined in section III E.

II B The g tensor

The theory of the $\overline{\overline{g}}$ tensor, and especially the problem of gauge invariance, has been discussed extensively by Stone [27,28] and Slichter [29]. In this section we follow the derivation given by Stone. Consider a molecule, containing N nuclei and 2n-1 electrons, one of which is unpaired in the ground state. The hamiltonian is :

$$H = H_o + H_{pert} \qquad (II.22)$$

where H_o is the hamiltonian of the unperturbed system, as defined in section A of this chapter. H_{pert} is the perturbation describing the interaction between the electron spin and electric and magnetic field. The eigenfunctions $|n,m_\sigma\rangle$ of H_o are approximated with one or more Slater determinants. In this notation "n" denotes the spatial function and "m_σ" is the z-component of the electron spin $\vec{S}$. The ground state $|o,m_\sigma\rangle$ is assumed to be orbitally non-degenerate, with a twofold spin degeneracy. The Slater determinants are composed of one-electron spin orbitals $\psi\sigma$. The spatial part ψ of a spin orbital is a molecular orbital, consisting of a linear combination of atomic orbitals, (AO's), ϕ. Omitting a normalization factor $N = \{(2n-1)!\}^{-\frac{1}{2}}$, the unperturbed functions of the ground and excited states are·

a. Ground state,

$$|o,m_\sigma\rangle = |\psi_1\alpha(1)\psi_1\beta(2).....\psi_{n-1}\alpha(2n-3)\psi_{n-1}\beta(2n-2)\psi_n\sigma(2n-1)|. \qquad (II.23a)$$

b. Excited states with one electron excited into the MO of the unpaired electron,

$$|k,m_\sigma\rangle = |\psi_1\alpha(1)\psi_1\beta(2)...\psi_k\sigma(2k-1)...\psi_n\alpha(2n-2)\psi_n\beta(2n-1)|, \quad k<n. \qquad (II.23b)$$

c. Excited states with the unpaired electron excited into an initially empty MO,

$$|h,m_\sigma\rangle = |\psi_1\alpha(1)\psi_1\beta(2)...\psi_{n-1}\alpha(2n-3)\psi_{n-1}\beta(2n-2)\psi_h\sigma(2n-1)|, \quad h>n \qquad (II.23c)$$

d. Excited states with one electron excited from a doubly occupied MO into an empty one. These excitations give rise to two doublets and one

quartet state. The doublet functions are:

$$|d_1,m_\sigma> = \frac{1}{\sqrt{2}}\{|\psi_1\alpha(1)\psi_1\beta(2)\ldots\psi_k\sigma(2k-1)\ldots\psi_n\sigma(2n-2)\psi_h\sigma'(2n-1)| - |\psi_1\alpha(1)\psi_1\beta(2)\ldots\psi_k\sigma'(2k-1)\ldots\psi_n\sigma(2n-2)\psi_h\sigma(2n-1)|\}, \quad k<n,\ h>n,\ \sigma\neq\sigma', \qquad (II.23d)$$

$$|d_2,m_\sigma> = \frac{1}{\sqrt{6}}\{2|\psi_1\alpha(1)\psi_1\beta(2)\ldots\psi_k\sigma(2k-1)\ldots\psi_n\sigma'(2n-2)\psi_h\sigma(2n-1)| - |\psi_1\alpha(1)\psi_1\beta(2)\ldots\psi_k\sigma(2k-1)\ldots\psi_n\sigma(2n-2)\psi_h\sigma'(2n-1)| - |\psi_1\alpha(1)\psi_1\beta(2)\ldots\psi_k\sigma'(2k-1)\ldots\psi_n\sigma(2n-2)\psi_h\sigma(2n-1)|\}, \quad k<n,\ h>n,\ \sigma\neq\sigma'. \qquad (II.23e)$$

The spin components of the quartet states are:

$$|q,m_\sigma> = \frac{1}{\sqrt{3}}\{|\psi_1\alpha(1)\psi_1\beta(2)\ldots\psi_k\sigma(2k-1)\ldots\psi_n\sigma'(2n-2)\psi_h\sigma(2n-1)| + |\psi_1\alpha(1)\psi_1\beta(2)\ldots\psi_k\sigma(2k-1)\ldots\psi_n\sigma(2n-2)\psi_h\sigma'(2n-1)| + |\psi_1\alpha(1)\psi_1\beta(2)\ldots\psi_k\sigma'(2k-1)\ldots\psi_n\sigma(2n-2)\psi_h\sigma(2n-1)|\}, \quad k<n,\ h>n,\ \sigma\neq\sigma', \qquad (II.23f)$$

$$|q,3m_\sigma> = |\psi_1\alpha(1)\psi_1\beta(2)\ldots\psi_k\sigma(2k-1)\ldots\psi_n\sigma(2n-2)\psi_h\sigma(2n-1)|, \quad k<n,\ h>n. \qquad (II.23g)$$

e. As will be shown, states with more than one electron excited do not contribute.

Assuming a complete knowledge of the unperturbed states and their energies, the goal is to calculate the perturbed energy levels, using second order perturbation theory. Since the ground state of the unperturbed system is twofold degenerate it is necessary to solve a two dimensional secular equation. It was shown that up to second order the energy levels are the eigenvalues of the following hamiltonian [30]

$$\tilde{H} = E_o + P_o H_{pert} P_o + \frac{P_o H_{pert} P_n H_{pert} P_o}{E_o - E_n} \qquad (II.24)$$

E_o and E_n are the unperturbed energies of the ground state $|o>$ and the excited states $|n>$; P_o and P_n are projection operators for the states $|o>$ and $|n>$

$$P_o = \sum_{m_\sigma} |o,m_\sigma><m_\sigma,o| \qquad P_n = \sum_{m_\sigma} |n,m_\sigma><m_\sigma,n| \ . \qquad (II.25)$$

II B 1 The hamiltonian of the system

For a one electron system, an expression for H_{pert} can be derived from Dirac's relativistic wave equation [27,28,31,32]

$$H_{pert} = H_{SZ} + H_{SO} + H_{OZ} + H_{DIA} \tag{II.26}$$

where H_{SZ} is the spin Zeeman energy

$$H_{SZ} = g_e \mu_b k \vec{S}.\vec{B} \ , \tag{II.27}$$

H_{SO} is the spin-orbit coupling energy

$$H_{SO} = \frac{g_e k^2}{2mc} \mu_b \vec{S}.[\vec{E} \times (\vec{p} + e\vec{A})] \ , \tag{II.28}$$

H_{OZ} is the orbital Zeeman energy

$$H_{OZ} = \frac{ek}{m} \vec{A}.\vec{p} \ , \tag{II.29}$$

and H_{DIA} is the diamagnetic energy

$$H_{DIA} = \frac{e^2}{2m} k\vec{A}.\vec{A} \ . \tag{II.30}$$

(As H_{DIA} does not play a role in this derivation, it will be omitted in the rest of this section.)

In these interactions $\vec{p}$ is the electron momentum and -e is the electron charge. $\vec{E}$ is the electric field and $\vec{A}$ is the magnetic vector potential [33] describing the magnetic field. g_e is the free electron g value, being 2.00229. The function k is

$$k = 2mc^2(W + eA_o + 2mc^2)^{-1} \ , \tag{II.31}$$

where A_o is the scalar potential [33]. The energy $W + mc^2$ of the system usually lies close to the rest energy mc^2, hence W is a small number. In lowest order approximation k = 1.

In a free atom the electric field $\vec{E}$ is exactly parallel to the radius vector $\vec{r}$ of the electron relative to the nucleus

$$\vec{E} = \frac{2m^2c^2}{e\hbar^2} \xi(r) \vec{r} \ , \tag{II.32}$$

where the spin-orbit coupling operator $\xi(r)$ is a function of the distance from the nucleus. Substituting II.32 and the electron spin $\vec{S}$, the perturbations become

$$H_{SZ} = \mu_b g_e \vec{S}.\vec{B} \ , \tag{II.33a}$$

$$H_{SO} = \frac{g_e}{2\hbar}\,\xi(r)\,\vec{S}.[\,\vec{r}\times(\vec{p}+e\vec{A})\,]\ , \qquad \text{(II.33b)}$$

$$H_{OZ} = \frac{e}{m}\,\vec{A}.\vec{p}\ . \qquad \text{(II.33c)}$$

Since our system contains N atoms and 2n-1 electrons, we have to generalize equations II.33. This can be done by

a. assuming the electric field to be a sum of central fields

$$\vec{E} = \frac{2m^2c^2}{e\hbar^2}\sum_{k=1}^{N}\xi_k(r^k)\,\vec{r}^k\ , \qquad \text{(II.34)}$$

b. summing the perturbations of II.33 for each electron. The resulting perturbations are

$$H_{SZ} = \mu_b g_e \sum_i \vec{S}^i.\vec{B}\ , \qquad \text{(II.35a)}$$

$$H_{SO} = \frac{g_e}{2\hbar}\sum_{k,i}\xi_k(r^{ki})\,\vec{S}^i.[\,\vec{r}^{ki}\times(\vec{p}^i+e\vec{A}^i)\,]\ , \qquad \text{(II.35b)}$$

$$H_{OZ} = \frac{e}{m}\sum_i \vec{A}^i.\vec{p}^i\ . \qquad \text{(II.35c)}$$

In these equations i runs over all electrons and k over all nuclei. $\vec{A}^i$ is the vector potential at the position of the electron i and $\vec{r}^{ki}$ is the position vector of electron i relative to the nucleus k.
The vector potential $\vec{A}^i$ has the value

$$\vec{A}^i = \tfrac{1}{2}\vec{B}\times(\vec{r}^i-\vec{R})\ , \qquad \text{(II.36)}$$

where $\vec{R}$ is an arbitrary constant vector and $\vec{r}^i$ the position vector of electron i relative to an arbitrarily chosen origin. In the Coulomb gauge [34] the requirements for $\vec{A}$ are:

$$\text{curl}\ \vec{A} = \vec{\nabla}\times\vec{A} = \vec{B} \qquad \text{(II.37a)}$$

$$\text{div}\ \vec{A} = \vec{\nabla}\,.\,\vec{A} = 0 \qquad \text{(II.37b)}$$

and it is clear that $\vec{A}^i$ of Eq.II.36 fulfils the conditions II.37, independent of the choice of $\vec{R}$.
Substituting $\vec{A}$ and defining $\hbar\vec{L}^{ki} = \vec{r}^{ki}\times\vec{p}^i$ to be the angular momentum of electron i about the nucleus k, the perturbations become

$$H_{SZ} = \mu_b g_e \sum_i \vec{S}^i.\vec{B}\ , \qquad \text{(II.38a)}$$

$$H_{SO} = \frac{g_e}{2\hbar}\sum_{k,i}\xi_k(r^{ki})\,\vec{S}^i.[\,\hbar\vec{L}^{ki}+\frac{e}{2}\vec{r}^{ki}\times\{\vec{B}\times(\vec{r}^i-\vec{R})\}\,]\ , \qquad \text{(II.38b)}$$

$$H_{OZ} = \mu_b \sum_i \vec{B}\,.\,\vec{L}^{,i}\ . \qquad \text{(II.38c)}$$

In Eq.II.38c $\hbar\vec{L}'^{,i}$ is the angular momentum of the electron i about the origin of the vector potential.

II B. 2 Calculation of the $\bar{\bar{g}}$ tensor

To calculate the $\bar{\bar{g}}$ tensor we collect those terms of Eq.II.24 which are linear in the magnetic field and the electron spin and define them as $\tilde{H}_g$. Defining H_{SOB} as the term of H_{SO} involving the magnetic field and H_{SON} as the term that does not, $\tilde{H}_g$ becomes

$$\tilde{H}_g = P_o H_{SZ} P_o + P_o H_{SOB} P_o + \sum_{n\neq o} \frac{P_o H_{SON} P_n H_{OZ} P_o + P_o H_{OZ} P_n H_{SON} P_o}{E_o - E_n} \quad . \qquad \text{(II.39)}$$

Since P_o is the projection operator for the ground state, we may take matrix elements of $\tilde{H}_g$ diagonal in the orbital ground state

$$\langle o,\sigma|\tilde{H}_g|o,\sigma'\rangle = \langle o,\sigma|H_{SZ}|o,\sigma'\rangle + \langle o,\sigma|H_{SOB}|o,\sigma'\rangle + \sum_{n\neq o}\sum_{\sigma''} \frac{\langle o,\sigma|H_{SON}|n,\sigma''\rangle\langle n,\sigma''|H_{OZ}|o,\sigma'\rangle + \langle o,\sigma|H_{OZ}|n,\sigma''\rangle\langle n,\sigma''|H_{SON}|o,\sigma'\rangle}{E_o - E_n} \qquad \text{(II.40)}$$

Substituting the functions II.23a-II.23g, the various contributions become:

a. First order contributions,

$$\langle o,\sigma|H_{SZ}|o,\sigma'\rangle = \mu_b g_e \vec{B} \cdot \langle\sigma|\vec{S}|\sigma'\rangle \ , \qquad \text{(II.41a)}$$

$$\langle o,\sigma|H_{SOB}|o,\sigma'\rangle = g_e \frac{e}{4\hbar} \sum_k \langle\sigma|\vec{S}|\sigma'\rangle \cdot \langle\psi_n|\xi_k(r^k)\vec{r}^k \times \{\vec{B}\times(\vec{r}-\vec{R})\}|\psi_n\rangle =$$
$$= g_e \frac{e}{4\hbar} \sum_k \langle\sigma|\vec{S}|\sigma'\rangle \cdot \langle\psi_n|\xi_k(r^k)\{\vec{r}^k\cdot(\vec{r}-\vec{R})\vec{B} - \vec{B}\cdot(\vec{r}-\vec{R})\vec{r}^k\}|\psi_n\rangle . \qquad \text{(II.41b)}$$

b. Second order contributions.

Approximating the energies as a sum of one-electron MO energies, the total contribution of the states $|k,\sigma\rangle$ and $|h,\sigma\rangle$ becomes

$$\frac{g_e}{2}\mu_b \sum_{m\neq n}\sum_k \langle\sigma|\vec{S}|\sigma'\rangle \cdot \left\{ \frac{\langle\psi_n|\xi_k(r^k)\vec{L}^k|\psi_m\rangle\langle\psi_m|\vec{L}'|\psi_n\rangle\cdot\vec{B} + \langle\psi_m|\xi_k(r^k)\vec{L}^k|\psi_n\rangle\langle\psi_n|\vec{L}'|\psi_m\rangle\cdot\vec{B}}{\varepsilon_n - \varepsilon_m} \right\} , \qquad \text{(II.42)}$$

where ε_n is the one-electron energy of the n^{th} MO. As the functions ψ are taken real and because the angular momentum operators are Hermitian and purely imaginary, this results in

$$g_e \mu_b \sum_{m \neq n} \sum_k \langle \sigma | \vec{S} | \sigma' \rangle \cdot \frac{\langle \psi_n | \xi_k(r^k) \vec{L}^k | \psi_m \rangle \langle \psi_m | \vec{L}' | \psi_n \rangle \cdot \vec{B}}{\epsilon_n - \epsilon_m} \quad . \qquad \text{(II.43)}$$

It can be proven that the states $|d_1, m_\sigma\rangle$ and $|d_2, m_\sigma\rangle$ give no contribution. The quartet states $|q, m_\sigma\rangle$ and $|q, 3m_\sigma\rangle$ do not contribute at all because H_{OZ} does not depend on spin. Excited states with two or more excited electrons do not contribute because only one-electron operators are involved.

c. Third order contributions.

Tippins [35] published a formula for the third order corrections, using the same perturbation procedure. These terms are significant only when spin-orbit coupling is important and the energy separations $\epsilon_n - \epsilon_m$ are small. Therefore, it seems justified to neglect these contributions for the first row transition metal complexes. This formula is not gauge invariant (see section II B.3), as was shown by Atkins and Jamieson [36]. These authors derived a third order gauge invariant formula. Compared with the formula of Tippens, this involved some additional terms which are much smaller than those obtained by Tippens.

The following formula for the $\bar{\bar{g}}$ tensor can be derived from the expressions II.41 and II.43:

$$g_{\alpha\beta} = g_e \delta_{\alpha\beta} + \sum_k \left[\frac{g_e m}{2\hbar^2} \{ \langle \psi_n | \xi_k(r^k) \vec{r}^k \cdot (\vec{r} - \vec{R}) | \psi_n \rangle \delta_{\alpha\beta} - \langle \psi_n | \xi_k(r^k) r_\alpha^k (\vec{r} - \vec{R})_\beta | \psi_n \rangle \} \right.$$

$$\left. + g_e \sum_{m \neq n} \frac{\langle \psi_n | \xi_k(r^k) L_\alpha^k | \psi_m \rangle \langle \psi_m | L'_\beta | \psi_n \rangle}{\epsilon_n - \epsilon_m} \right] . \qquad \text{(II.44)}$$

II B 3 Gauge invariance

The bracketed first order terms in Eq.II.44 depend on the choice of $\vec{R}$ so that their values are not uniquely defined. Since the total expression for the g shift in II.44 has to be gauge invariant, the second order terms must compensate the gauge dependence in the first order terms. In fact, it was shown by Stone [27,28] that each term in the sum over k, (k refers to one particular nucleus), is gauge invariant. Hence it is allowed to take $\vec{R} = \vec{R}^k$, so that $\vec{r} - \vec{R}^k = \vec{r}^k$ and $\vec{L}' = \vec{L}^k$. This choice of origin for $\vec{R}$ has been named the "natural" gauge. Expression II.44 becomes:

$$g_{\alpha\beta} = g_e\delta_{\alpha\beta} + \sum_k \left[\frac{g_e m}{2\hbar^2}\{\langle\psi_n|\xi_k(r^k)\,\vec{r}^k.\vec{r}^k|\psi_n\rangle\delta_{\alpha\beta} - \langle\psi_n|\xi_k(r^k)\,r^k_\alpha r^k_\beta|\psi_n\rangle\}\right.$$

$$\left. + g_e \sum_{m\neq n} \frac{\langle\psi_n|\xi_k(r^k)\,L^k_\alpha|\psi_m\rangle\langle\psi_m|L^k_\beta|\psi_n\rangle}{\varepsilon_n - \varepsilon_m}\right] . \qquad \text{(II.45)}$$

II B 4 Approximations

a. The advantage of using the natural gauge is that the first order terms become negligible. In a Coulomb potential we have [37]

$$\frac{mr^2}{\hbar^2}\,\xi(r) = \frac{e^2}{2mc^2}\,Z\,\frac{1}{r} \quad , \qquad \text{(II.46)}$$

where Z is the effective nuclear charge. The integral $\langle\psi_n|\frac{1}{r}|\psi_n\rangle$ is of the order $\frac{1}{a_o}$ (a_o is the Bohr radius $\frac{\hbar^2}{me^2}$), thus the first order contribution is of the order $\frac{e^4}{\hbar^2c^2} \simeq 10^{-5}$ and is negligible for transition metal complexes where g shifts are of the order 10^{-1}.

b. Expanding ψ in a linear combination of atomic orbitals, $\psi_n = \sum_k \chi^k_n$, the matrix elements $\langle\psi_m|L^k_\beta|\psi_n\rangle$ can be written:

$$\langle\psi_m|L^k_\beta|\psi_n\rangle = \sum_{k'}\langle\psi_m|L^k_\beta|\chi^{k'}_n\rangle \quad , \qquad \text{(II.47)}$$

where $\chi^{k'}_n$ is that part of the n-th MO that is centred on the atom k'. If $\vec{R}^{kk'}$ is the vector from the atom k to the atom k', the linear transformation between L^k_β and $L^{k'}_\beta$ is given by

$$L^k_\beta = L^{k'}_\beta + \frac{1}{\hbar}\,(\vec{R}^{kk'} \times \vec{p}^k)_\beta \quad . \qquad \text{(II.48)}$$

Substituting this into II.45, the second order contribution becomes

$$g_e \sum_{m\neq n}\sum_{k,k'} \frac{\langle\psi_n|\xi_k(r^k)L^k_\alpha|\psi_m\rangle\langle\psi_m|L^{k'}_\beta|\chi^{k'}_n\rangle}{\varepsilon_n - \varepsilon_m}$$

$$+ \frac{g_e}{\hbar}\sum_{m\neq n}\sum_k\sum_{k'\neq k}\sum_{\gamma,\delta} \frac{\langle\psi_n|\xi_k(r^k)L^k_\alpha|\psi_m\rangle\langle\psi_m|p^k_\delta|\chi^{k'}_n\rangle}{\varepsilon_n - \varepsilon_m}\,\epsilon^{\beta\gamma\delta}\,R^{kk'}_\gamma \,, \qquad \text{(II.49)}$$

in which $\epsilon^{\beta\gamma\delta}$ is the alternating tensor, which is defined as

$$\epsilon^{\beta\gamma\delta} \begin{cases} 0 \text{ if any two of } \beta,\gamma,\delta \text{ are equal.} \\ +1 \text{ if } \beta\gamma\delta \text{ is an even permutation of xyz.} \\ -1 \text{ if } \beta\gamma\delta \text{ is an odd permutation of xyz.} \end{cases}$$

If h is the one-electron hamiltonian of which the MO's ψ are eigenfunctions, $\vec{p}$ is given by

$$\vec{p} = \frac{m}{i\hbar} (\vec{r}h - h\vec{r}) \quad . \tag{II.50}$$

The matrix element $\langle\psi_m|p_\delta^k|\psi_n^{k'}\rangle$ can therefore be rewritten as

$$\frac{m}{i\hbar} \{\langle\psi_m|r_\delta^k h|\chi_n^{k'}\rangle - \varepsilon_m\langle\psi_m|r_\delta^k|\chi_n^{k'}\rangle\} \quad . \tag{II.51}$$

If the zero differential overlap approximation (ZDO) [38] is applied, II.51 becomes

$$\frac{m}{i\hbar} (\varepsilon_n - \varepsilon_m) \langle\psi_m|r_\delta^k|\chi_n^{k'}\rangle \quad . \tag{II.52}$$

Substitution of II.52 in the second term of II.49 gives

$$-\frac{mg_e}{i\hbar^2} \sum_k \sum_{k'\neq k} \sum_{\gamma,\delta} \langle\psi_n|\xi_k(r^k)L_\alpha^k r_\delta^k|\chi_n^{k'}\rangle \epsilon^{\beta\gamma\delta} R_\gamma^{kk'} \quad . \tag{II.53}$$

Use was made of the fact that L_α^k is Hermitian and purely imaginary, and the closure relation, $\sum_m |\psi_m\rangle\langle\psi_m| = 1$, was applied. After some tedious calculations, Eq.II.53 can be transformed into:

$$-\frac{mg_e}{2\hbar^2} \sum_k \sum_{k'\neq k} \sum_{\gamma,\delta} \langle\psi_n|\xi_k(r^k)\{\vec{r}^k.\vec{R}^{kk'}\delta_{\alpha\beta} - R_\alpha^{kk'} r_\beta^k\}|\chi_n^{k'}\rangle \quad . \tag{II.54}$$

Since this term is of the same order of magnitude as the first order contribution, it is negligibly small. Therefore only the first term of Eq.II.49 will be retained.

Now the question arises whether the ZDO approximation is justified for these matrix elements. Smith calculated the g values of some tetragonal copper(II) compounds with inclusion of both charge transfer (CT) and d-d transitions [39]. His results show that the contributions to the matrix elements $\langle\psi_m|p_\delta^k|\chi_n^{k'}\rangle$ of the CT states are larger than those of the d-d transitions. This is in accordance with II.52, because for these compounds the transition energies of the CT states are larger than the d-d transition energies. Furthermore, it appears that a partial cancellation of terms occurs, rendering II.54 rather small. Hence, the g shift is mainly determined by the first term in II.49.

It should be noted that the contributions of the excited states to the second term of II.49 are independent of the transition energies (see II.49 and II.52). Therefore, all excited states must be included in the calculation of the second term of II.49. If the low lying excited states

are taken into account only, large errors may result [40,41].

c. Since $\xi(r)$ behaves as r^{-3} for large r, all multicentre terms in the spin-orbit matrix elements may be neglected, so that

$$\langle\psi_n|\xi_k(r^k)L_\alpha^k|\psi_m\rangle = \langle\chi_n^k|\xi_k(r^k)L_\alpha^k|\chi_m^k\rangle \quad . \tag{II.55}$$

The radial parts of these integrals have not been calculated, but are approximated by the empirical spin-orbit coupling constants. (Table V.1) Moores and McWeeny showed that this approximation, and the use of one-centre integrals only, gives considerably better results then an ab initio calculation [42].

We are thus left with the formula.

$$g_{\alpha\beta} = g_e\delta_{\alpha\beta} + g_e \sum_{m\neq n} \sum_{k,k'} \frac{\langle\chi_n^k|\xi_k(r^k)L_\alpha^k|\chi_m^k\rangle\langle\psi_m|L_\beta^{k'}|\chi_n^{k'}\rangle}{\varepsilon_n - \varepsilon_m} \quad . \tag{II.56}$$

For one of the systems studied (i.e. $Cu/Ni(et_2dtc_2)$ we have taken into account the two-centre contributions in $\langle\psi_m|L_\beta^{k'}|\chi_n^{k'}\rangle$. The values obtained were less than 10% higher than the Δg values calculated with one-centre integrals only. Therefore, these integrals have been neglected and in all calculations the following approximate, gauge invariant formula has been used:

$$g_{\alpha\beta} = g_e\delta_{\alpha\beta} + g_e \sum_{m\neq n} \sum_{k,k'} \frac{\langle\chi_n^k|\xi_k(r^k)L_\alpha^k|\chi_m^k\rangle\langle\chi_m^{k'}|L_\beta^{k'}|\chi_n^{k'}\rangle}{\varepsilon_n - \varepsilon_m} \quad . \tag{II.57}$$

II C The hyperfine coupling tensor

Again we consider the system of the preceding section but include interactions with the nuclear spin $\vec{I}$ of one nucleus K. Because of the unpaired electron the total spin degeneracy is 2(2I + 1)-fold in the unperturbed system. The eigenfunctions are represented by $|n,m_\sigma\rangle|I,\pi\rangle$, where $|I,\pi\rangle$ is the nuclear function, π is the expectation value of I_z.

The perturbed energy levels are the eigenvalues of the hamiltonian II 24. The projection operators P_o and P_n of the states $|o\rangle$ and $|n\rangle$ are

$$P_o = \sum_{m_\sigma} \sum_{\pi} |o,m_\sigma\rangle |I,\pi\rangle \langle I,\pi| \langle o,m_\sigma|$$

$$P_n = \sum_{m_\sigma} \sum_{\pi} |n,m_\sigma\rangle |I,\pi\rangle \langle I,\pi| \langle n,m_\sigma| \quad . \tag{II.58}$$

II C 1 The hamiltonian of the system

The influence of the nuclear spin $\vec{I}$ can be taken into account in the same way as was done for the external magnetic field in section II B. The hamiltonian for this interaction contains the terms corresponding with those of Eq.II.35a-35c, where $\vec{B}$ and $\vec{A}$ are now caused by the nuclear spin. In the absence of an external field, the vector potential is [43]

$$\vec{A}^1 = \frac{\mu_o}{4\pi} \frac{g_K \mu_n \vec{I} \times \vec{r}^{K1}}{r^{K1^3}} \qquad \text{(II 59)}$$

and, consequently,

$$\vec{B}^1 = \frac{\mu_o}{4\pi} g_K \mu_n \left[- \frac{\vec{I}}{r^{K1^3}} + \frac{3\vec{I}.\vec{r}^{K1}}{r^{K1^5}} \vec{r}_{K1} \right] , \qquad \text{(II.60)}$$

where μ_o is the magnetic permeability of free space and g_K the g value of the nucleus K.

In this magnetic field the various terms of the hamiltonian become

$$\begin{aligned} H^1_{SZ} &= \frac{\mu_o}{4\pi} \mu_b \mu_n g_e g_K \sum_1 \{ - \frac{\vec{S}^1.\vec{I}}{r^{K1^3}} + \frac{3(\vec{r}^{K1}.\vec{S}^1)(\vec{r}^{K1}.\vec{I})}{r^{K1^5}} \} \\ &= \frac{P}{r^{K1^3}} \left(\frac{4\pi}{5} \right)^{\frac{1}{2}} \{ I_x S^1_x (\sqrt{3} Z_{x^2-y^2} - Z_{z^2})^1 + I_y S^1_y (-\sqrt{3} Z_{x^2-y^2} - Z_{z^2})^1 \\ &\quad + I_z S^1_z (2 Z_{z^2})^1 + (I_y S^1_x + I_x S^1_y)(\sqrt{3} Z_{xy})^1 \\ &\quad + (I_z S^1_x + I_x S^1_z)(\sqrt{3} Z_{xz})^1 + (I_z S^1_y + I_y S^1_z)(\sqrt{3} Z_{yz})^1 \} \\ &\equiv \frac{P}{r^{K1^3}} \sum_{\alpha,\beta=x,y,z} I_\alpha S^1_\beta F^{K1}_{\alpha\beta} , \end{aligned} \qquad \text{(II.61a)}$$

where each Z function is a normalized real combination of spherical harmonics $Y_{2,m}$ centred on the nucleus K. P has been defined as $\frac{\mu_o}{4\pi} \mu_b \mu_n g_e g_K$; $F^{K1}_{\alpha\beta}$ are the components of a symmetrical, traceless tensor operator.

$$H^1_{SON} = \frac{g_e}{2} \sum_{k,1} \xi_k(r^{K1}) \vec{S}^1.\vec{L}^{K1} \qquad \text{(II.61b)}$$

$$H^1_{SOB} = \frac{mP}{\hbar^2} \sum_{k,1} \xi_k(r^{K1}) \{ \frac{\vec{S}^1.\vec{I})(\vec{r}^{K1}.\vec{r}^{K1}) - (\vec{S}^1.\vec{r}^{K1})(\vec{I}.\vec{r}^{K1})}{r^{K1^3}} \} \qquad \text{(II.61c)}$$

$$H^1_{OZ} = \frac{2P}{g_e} \sum_1 \frac{\vec{I}.\vec{L}^{K1}}{r^{Ki^3}} \qquad \text{(II.61d)}$$

The terms of the hamiltonian II.61a-d are substituted in Eq.II.24. Only those terms which are linear in the electron spin and the nuclear spin are retained and form the hamiltonian $\tilde{H}_A$. Matrix elements of $\tilde{H}_A$ are calculated which are diagonal in the ground state orbital:

$$\langle I,\pi|\langle o,\sigma|\tilde{H}_A|o,\sigma'\rangle|I,\pi'\rangle = \langle I,\pi|\langle o,\sigma|H_{SOB}+H_{SZ}|o,\sigma'\rangle|I,\pi'\rangle$$

$$+ \sum_{n\neq o} \frac{\langle I,\pi|\langle o,\sigma|H_{OZ}P_nH_{SON}|o,\sigma'\rangle|I,\pi'\rangle + \text{p.o.i.}}{E_o - E_n}$$

$$+ \sum_{n\neq o} \frac{\langle I,\pi|\langle o,\sigma|H_{SZ}P_nH_{SON}|o,\sigma'\rangle|I,\pi'\rangle + \text{p.o.i.}}{E_o - E_n} \quad , \qquad \text{(II.62)}$$

where p.o.i. means the similar product with the operators interchanged. The various contributions can be calculated through substitution of the functions II.23a -II.23g.

a. First order contributions.

The interactions H_{SZ} and H_{SOB} give a first order contribution to the hyperfine coupling tensor $\bar{\bar{A}}^K$ of the spin hamiltonian. A traceless, symmetrical tensor is obtained from H_{SZ}, with elements

$$A^K_{\alpha\beta} = P\,\langle\psi_n|\,\frac{F^K_{\alpha\beta}}{r^{K3}}\,|\,\psi_n\rangle \qquad \text{(II.63)}$$

As discussed by several authors [44], the term H_{SOB} is of the order of $\frac{1}{r^4}$ and behaves on an atomic scale almost like a delta function. Therefore, its contribution to the hyperfine coupling of non s electrons is small compared to the contribution of H_{SZ} and can be neglected.

b. Second order contributions.

In Eq.II.62 all terms have been neglected which explicitly contain $\langle r^{-3}\rangle$ twice. The energies of the states are calculated by summing one-electron MO energies.

It can be deduced that second order contributions from terms in II.62 containing the operator $H_{OZ}P\,H_{SON}$ yield a non traceless tensor

$$A^K_{\alpha\beta} = 2P \sum_{m\neq n} \sum_{k} \frac{\langle\psi_n|\xi_k(r^k)\,L^k_\alpha|\psi_m\rangle\,\langle\psi_m|\frac{L^K_\beta}{r^{K3}}|\psi_n\rangle}{\epsilon_n - \epsilon_m} \quad . \qquad \text{(II.64)}$$

This contribution is due to excited states $|k,m_\sigma\rangle$ and $|h,m_\sigma\rangle$; other excited states do not contribute.

Similarly, the terms in II.62 containing the operator H_{SZ} P H_{SON} give a contribution which is due only to the excited states $|k,\sigma>$ and $|h,\sigma>$:

$$A^K_{\alpha\beta} = P \sum_{m\neq n} \sum_{k} \sum_{\gamma,\delta} \frac{i\epsilon^{\gamma\delta\alpha} <\psi_n|\xi_k(r^k)\ L^k_\gamma|\psi_m><\psi_m|\frac{F^K_{\delta\beta}}{r^3}|\psi_n>}{\epsilon_n - \epsilon_m} \quad . \qquad (II.65)$$

The summations γ and δ run over the Cartesian coordinates x, y, and z. The excited states $|d_1,m_\sigma>$ do not give a contribution, while the contributions from the states $|d_2,m_\sigma>$, $|q,m_\sigma>$, and $|q,3m_\sigma>$ cancel each other. Summing up, the expression for a general tensor element is:

$$A^K_{\alpha\beta} = P\Big[<\psi_n|\frac{F^K_{\alpha\beta}}{r^3}|\psi_n> + \sum_{m\neq n} \sum_{k} \Big\{\frac{2<\psi_n|\xi_k(r^k)\ L^k_\alpha|\psi_m><\psi_m|\frac{L^K_\beta}{r^3}|\psi_n>}{\epsilon_n - \epsilon_m}$$

$$+ \sum_{\gamma,\delta} \frac{i\,\epsilon^{\gamma\delta\alpha} <\psi_n|\xi_k(r^k)\ L^k_\gamma|\psi_m><\psi_m|\frac{F^K_{\delta\beta}}{r^3}|\psi_n>}{\epsilon_n - \epsilon_m}\Big\}\Big] \quad . \qquad (II.66)$$

Since all operators depend on $\frac{1}{r^3}$, it is expected that more-centre integrals can be neglected.

II C 3 The hyperfine coupling of s electrons

Whereas for non s electrons the contribution of H_{SZ} dominates the one of H_{SOB}, the situation is reversed for s electrons: H_{SZ} vanishes because of the spherical symmetry and only H_{SOB} is left [43]. The resulting contribution to the $\bar{\bar{A}}^K$ tensor is isotropic, and in a good approximation is equal to

$$A^K_{\alpha\alpha} = \frac{8\pi}{3} P\ |\psi_n(o)|^2 \quad . \qquad (II.67)$$

This term in the hyperfine coupling is often called the contact term, since it arises from the density of the electron at the nucleus: $|\psi_n(o)|^2$.

II D The nuclear quadrupole coupling tensor

The nuclear quadrupole interaction is an electrical interaction between the quadrupole moment of the nucleus and the electric field gradient. The hamiltonian for this interaction can be written as [45]

$$H_Q = \frac{1}{6} \sum_{\alpha,\beta} V^K_{\alpha\beta} Q^K_{\alpha\beta} \quad , \tag{II.68}$$

where $\bar{\bar{V}}^K$ and $\bar{\bar{Q}}^K$ are symmetric traceless tensors of second rank

$$V^K_{\alpha\beta} = \frac{\delta^2 V}{\delta x_\alpha \delta x_\beta}(\vec{o}) \tag{II.69a}$$

$$Q^K_{\alpha\beta} = \int^{V_K} (3x_\alpha x_\beta - \delta_{\alpha\beta} r^2)\, \rho(\vec{r})\, d\tau \quad , \tag{II.69b}$$

$\rho(\vec{r})$ is the nuclear charge density in a scalar potential $V(\vec{r})$ and x_α is the α-component of $\vec{r}$. V_K is the nuclear volume. As in section II C, the ground state wave function can be represented by $|o,m_\sigma>|I,\pi>$, where $|I,\pi>$ is a nuclear function and $|o,m_\sigma>$ describes the electronic charges outside the nucleus. To derive an expression for the elements of the $\bar{\bar{P}}^K$ tensor (section II A) we calculate the energy of H_Q in first order

$$<o,m_\sigma|<I,\pi|H_Q|I,\pi'>|o,m_\sigma> = \frac{1}{6} \sum_{\alpha,\beta} <o,m_\sigma|V^K_{\alpha\beta}|o,m_\sigma><I,\pi|Q^K_{\alpha\beta}|I,\pi'> \, . \tag{II.70}$$

Using the Wigner-Eckardt theorem, the matrix elements of $\bar{\bar{Q}}^K$ can be rewritten

$$<I,\pi|Q^K_{\alpha\beta}|I,\pi'> = \frac{eQ}{I(2I-1)} <I,\pi|3\frac{I_\alpha I_\beta + I_\beta I_\alpha}{2} - \delta_{\alpha\beta} I^2|I,\pi'>, \tag{II.71}$$

where Q is the nuclear quadrupole moment defined as $<I,I|Q^K_{zz}|I,I>$. Comparison of II.70 and II.71 with the spin hamiltonian (II.1) yields for the elements of the $\bar{\bar{P}}^K$ tensor

$$P^K_{\alpha\beta} = \frac{eQ}{2I(2I-1)} V^K_{\alpha\beta} \, . \tag{II.72}$$

Here and in the following $V^K_{\alpha\beta}$ is the expectation value of the element $\alpha\beta$ of the electric field gradient (EFG) tensor at nucleus K and has the form [46]:

$$V^K_{\alpha\beta} = \frac{e}{4\pi\epsilon_o} \{ \sum_{A \neq K} [\frac{Z_A (3(X_\alpha X_\beta)_{AK} - \delta_{\alpha\beta} R^2_{AK})}{R^5_{AK}}]$$

$$- <o,m_\sigma| \sum_{k=1}^{2n-1} [\frac{(3(x_\alpha x_\beta)_{Kk} - \delta_{\alpha\beta} r^2_{Kk})}{r^5_{Kk}}] |o,m_\sigma> \} \, , \tag{II.73}$$

where $\vec{R}_{AK}$ is the radius vector connecting the nuclei A and K, $(X_\alpha)_{AK}$ is its component along the molecular α axis, $\vec{r}_{Kk}$ is the radius vector

connecting the nucleus K and the electron k, and $(x_\alpha)_{Kk}$ is its α component. The nuclear charge of the atom A is given by eZ_A. Substitution of $|o,m_o>$ (Eq.II.23a) and writing the MO's as linear combinations of AO's ϕ, the electronic part of II.73 can be split up in terms, involving a different number of centres

$$V^K_{\alpha\beta}(el) = -\frac{e}{4\pi\epsilon_o}\sum_u N_u \Big[\sum_{k,k'}^{K} C_{ku}C_{k'u}\langle\phi_k|\frac{F^K_{\alpha\beta}}{r_K^3}|\phi_{k'}\rangle + 2\sum_k^K \sum_{A\neq K}\sum_a^A C_{au}C_{ku}\langle\phi_a|\frac{F^K_{\alpha\beta}}{r_K^3}|\phi_k\rangle$$

$$+ \sum_{A\neq K}\sum_{a,a'}^{A} C_{au}C_{a'u}\langle\phi_a|\frac{F^K_{\alpha\beta}}{r_K^3}|\phi_{a'}\rangle + \sum_{\substack{A\neq K\\ A\neq B}}\sum_{B\neq K}\sum_a^A\sum_b^B C_{au}C_{bu}\langle\phi_a|\frac{F^K_{\alpha\beta}}{r_K^3}|\phi_b\rangle \Big] . \tag{II.74}$$

The operator $F^K_{\alpha\beta}$ is defined in section C of this chapter.

$$F^K_{\alpha\beta} = \frac{3x_\alpha x_\beta - r^2\delta_{\alpha\beta}}{r^2} . \tag{II.75}$$

N_u is the occupation number of the u-th MO. C_{au} is the LCAO coefficient of the AO ϕ_a in the u-th MO.

White and Drago [47] have pointed out, for nuclei of the third row and higher, that the sum of the two-centre nuclear and electronic contributions (being opposite in sign) to $V^K_{\alpha\beta}$ is small compared to the one-centre contribution. For the EFG on the nitrogen atom in HCN and NH_3 O'Konski and Ha [48] have shown that the last term, which is a three-centre contribution, is negligibly small. Thus for practical purposes we can use the relationship:

$$V^K_{\alpha\beta} = -\Sigma N_u \sum_k^K C^2_{ku} V^{kk}_{\alpha\beta} - 2\Sigma_u N_u \sum_{k<k'}^K C_{ku}C_{k'u}V^{kk'}_{\alpha\beta} , \tag{II.76}$$

where

$$V^{kk'}_{\alpha\beta} = \frac{e}{4\pi\epsilon_o}\langle\phi_k|\frac{F^K_{\alpha\beta}}{r_K^3}|\phi_{k'}\rangle . \tag{II.77}$$

The effect of neglecting the sum of the multicentre contributions has been discussed by de Vries et.al [3,46]. It was found that for $Fe(dtc)_2Cl$ these terms increased V^{Fe}_{zz} by 10%.

Utilizing the atomic orbital net populations according to Mulliken [49]

$$n(a) = \sum_u N_u C^2_{au} \tag{II.78}$$

and defining

$$n(a,a') = \sum_u N_u C_{au} C_{a'u} \qquad \text{(II.79)}$$

Eq.II.72 can be rewritten:

$$P^K_{\alpha\beta} = - \frac{eQ}{2I(2I-1)} \left\{ \sum_k^K n(k) V^{kk}_{\alpha\beta} + 2 \sum_{k<k'}^K n(k,k') V^{kk'}_{\alpha\beta} \right\} . \qquad \text{(II.80)}$$

Formula II.80 is used for the calculation of the quadrupole coupling tensor in chapter V.

CHAPTER III

EXPERIMENTAL

III A. Preparation of the compounds

III A 1 Diselenocarbamate complexes

The complexes have been synthesized according to the method of Barnard and Woodbridge [50].In this method a solution of CSe_2 in dioxane is added to a vigorously stirred alkaline solution of a secondary amine in water:

$$CSe_2 + NaOH + R_2NH \rightarrow Na(R_2NCSe_2) + H_2O.$$

The proces takes place in a nitrogen atmosphere at a temperature of about $-10^{o}C$. A solution of a metal salt in water is added to the solution of the sodium compound:

$$2\ Na(R_2NCSe_2) + M(II)X_2 \rightarrow M(II)(R_2NCSe_2)_2 + 2NaX, \qquad (X = Cl,Br)$$

after which the normal purifications are carried out.

The CSe_2 has been prepared according to the method of Gattow and Drager [51]. By means of a constant nitrogen flow, CH_2Cl_2 is led over molten selenium, at a temperature of 580-600^{o}C:

$$CH_2Cl_2 + 2\ Se \rightarrow CSe_2 + 2\ HCl.$$

Because of the very poisonous products, formed during this reaction, some special precautions have to be taken. An apparatus has been used, equipped with a temperature control unit and a pressure slot and suited for continuous processing. After filtration, the CSe_2 has been used without further purification.

In this way the Zn(II) complexes with methyl, ethyl and n-butyl groups have been prepared. The Cu(II), Ag(I) and Ni(II) complexes have been prepared by replacement of Zn by Cu, Ag or Ni respectively. Although special precautions have been taken, contamination with copper of the latter two complexes could not be prevented.

III A 2 Dithiocarbamate complexes

The $Zn(et_2dtc)_2$ complex has been prepared according to the literature [1], using $ZnCl_2$ and $Na(et_2dtc)$.

III B. Preparation of the single crystals and powders

The systems will be denoted $Mp/Md(R_2lig)_2$, where $Md(R_2lig)_2$ is the

diamagnetic host compound and Mp the guest paramagnetic metal ion. R_2lig is the ligand, either R_2dtc or R_2dsc, R is the alkyl group.

III B 1 Crystals and powders doped with Cu(II)

Single crystals and powders of the Ni(II) or Zn(II) complexes, doped with Cu(II), have been prepared by mixing a chloroform solution of the diamagnetic host with a DMF solution of $CuBr_2$, followed by slow evaporation of the solvent. The concentration ratios Zn or Ni : Cu are about 100 : 1.

III B 2 Crystals doped with Ag(II)

For the preparation of Ag/Ni$(but_2dsc)_2$ a 1 : 1 mixture of selenurammonoselenide (SMS) and selenuramtriselenide (STS) is used as an oxidizing reagent:

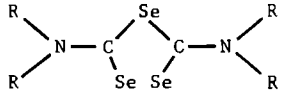

SMS

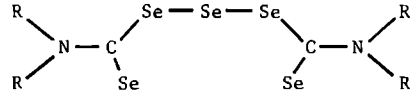

STS

This mixture has been prepared according to the literature [50]: A suspension of Zn$(but_2dsc)_2$ in H_2O is oxidized by adding very slowly equal amounts of H_2O_2 (30%) and sulfuric acid (23%).

The crystals have been prepared by adding 0.0025 mmol SMS/STS(1:1) to a chloroform solution of 0.1 mmol Ni(II)$(but_2dsc)_2$ and 0.005 mmol Ag(I)(but_2dsc):

$$4\ Ag(I)(but_2dsc) + 1\ SMS + 1\ STS \rightarrow 4\ Ag(II)(but_2dsc)_2.$$

By slow evaporation at room temperature, the unstable Ag(II) complex is built in in the Ni(II) lattice.

III C Apparatus

The ESR liquid solution spectra have been taken at the X-band frequency (9 GHz), using a Varian 4502 or an AEG spectrometer.

Single crystal, powder and frozen glass spectra have been recorded at the Q-band frequency (35 GHz) with a Varian 4503 spectrometer, equipped with a variable temperature control.

The magnetic field has been measured with an AEG gaussmeter and the X-band microwave frequency was monitored with a HP 5245L frequency counter. Because of the lack of a suitable counter, the Q-band microwave frequency has been calculated from the ESR signal of a polycrystalline DPPH sample (g = 2.0036).

Except for the frozen glass samples, all measurements have been carried out at room temperature.

The computer calculations have been carried out on the IBM computers 360/50 and 370/155, at the University Computing Centre.

III D Single crystal measurements

For single crystal measurements, the crystals were embedded in paraffine wax and mounted on a glass rod. Measurements in one plane have been carried out by rotating the magnet around the cylindrical Q-band cavity. The axis of rotation could be changed with the aid of a specially designed apparatus. Although the computer programs "SPINHAM" and "GAPLSD" (section III E.) make it unnecessary to have angles of 90° between the axes of rotation, it has been tried to reach this value as close as possible.

III E. Calculation of the spin hamiltonian parameters from the spectra

III E 1 Determination of the full spin hamiltonian

A FORTRAN IV computerprogram called "SPINHAM" has been written to calculate spectra according to the theory presented in section II A.

The required inputdata are:

a. For the calculation of the resonance fields:
   1. $\bar{\bar{g}}$-, $\bar{\bar{A}}$-, and $\bar{\bar{P}}$-tensor, (see II.1)
   2. klystron frequency for every spectrum,
   3. vector $\vec{k}$ (Eq. II.2) for every spectrum,
   4. resonance field of every line.

b. For the transition probabilities:
   1. vector $\vec{k}_1$ for every spectrum.

The output for each spectrum is:

1. g(Eq. II.8), $\bar{\bar{T}}$ (Eq. II.11), $\bar{\bar{Q}}$ (Eq. II.14) and $\vec{Z}$ (Eq. II.15),
2. $\vec{O}$ (Eq. II.21),
3. resonance fields, calculated by rewriting Eq. II.18:

$$B = -\frac{1}{g\mu_b}\,(-h\nu + M_I T_{33} + \text{first and second order terms}),$$

4. transition probabilities, calculated according to Eq. II.20.

Since the second order terms depend on B, the program is, properly speaking, a fitting program. It has been linked to the minimization program "MINUITS", [52] that minimizes the function

$$\{\frac{1}{N}\sum_{i=1}^{N}(B^{i}_{observed} - B^{i}_{calculated})^{2}\}^{\frac{1}{2}},$$

where N is the number of resonance lines including $\Delta M_I > o$ transitions. The minimization takes place by varying the elements of $\bar{\bar{g}}$, $\bar{\bar{A}}$ and $\bar{\bar{P}}$. In this way this procedure enables us to find accurate values for these tensors, even if no good guess of the tensorelements is available. Since the experimental error in the measured intensities is rather large, the transition probabilities have been used only to check the calculated spin hamiltonian parameters.

III E 2 Calculation of the spin hamiltonian in the strong field approximation

To save computertime, it is recommendable to start the program "SPINHAM" with initial values for $\bar{\bar{g}}$, $\bar{\bar{A}}$ and $\bar{\bar{P}}$ being as close as possible to the final ones. In addition, this program has been written for just one nuclear spin, thus ligand hyperfine splittings can not be handled. Therefore, another, if less accurate, method has been developed to calculate tentative values for the elements of the $\bar{\bar{g}}$ and $\bar{\bar{A}}$ tensors, which can be used as starting values for the program "SPINHAM". In this method, the nuclear Zeeman and quadrupole interactions are neglected, because both are (in our systems) small compared with the hyperfine interactions. Furthermore, all non-diagonal elements in the hamilton matrix, caused by the hyperfine interaction term, are neglected, which means that the so called "strong field approximation" is made. The resulting hamiltonian is:

$$H_s = g_{ef}\mu_b B S'_z + a_{ef} S'_z I'_z, \qquad \text{(III.1)}$$

where

$$g_{ef}(\theta,\phi) = \sqrt{\vec{k}.\,\bar{\bar{g}}.\,\bar{\bar{g}}^{t}.\,\vec{k}^{t}} \qquad \text{(III.2)}$$

$$a_{ef}(\theta,\phi) = T_{33} = \frac{\sqrt{\vec{k}.\,\bar{\bar{g}}.\,\bar{\bar{A}}.\,\bar{\bar{A}}^{t}.\,\bar{\bar{g}}^{t}.\,\vec{k}^{t}}}{g_{ef}(\theta,\phi)} \qquad \text{(III.3)}$$

The procedure is as follows:

a. Spectra are measured in three planes, not necessarily perpendicular to each other. Depending on the complexity, the spectra are measured every 5^{o} or 15^{o}. The position of the magnetic field is given by an angle α relative to an arbitrary chosen axis in the plane. For every orientation g_{ef} and a_{ef} is measured according to Eq. III.1 and where possible corrected for second order shifts. To recognize errors in the measurements, the data measured in one plane are fitted to the theoretical expressions III.2 and III.3. To

this end a program "PLANE" has been written, making use of a least squares procedure.

b. After enough reliable measuring points have been obtained in this way, the next step is to determine the positions of the intersecting lines of one plane with the two other planes. These positions are determined with the aid of a program "SNIJLIJN", which seeks identical values of g_{ef} and a_{ef} in different planes.

c. The measured values of g_{ef} and a_{ef}, the angle α of every spectrum, and the positions of the three intersecting lines, are the input for the program "GAPLSD". In this program, a coordinate system is chosen, as is shown in Figure 2. The measured plane I is chosen to be the xy plane, the intersecting line with plane II is taken as the x-axis. Next the spherical angles θ and ϕ of the magnetic field of every measured spectrum are calculated. These angles can be determined from the angle α and the dihedral angles η and ω (see Figure 2). The dihedral angles are calculated from the equations

$$\cos\omega = \frac{\cos\gamma_2 - \cos\gamma_1 \cos\gamma_3}{\sin\gamma_1 \sin\gamma_3} \qquad \text{(III.4)}$$

$$\cos\eta = \frac{\cos\gamma_3 - \cos\gamma_1 \cos\gamma_2}{\sin\gamma_1 \sin\gamma_2} \quad , \qquad \text{(III.5)}$$

where the angles γ are denoted in the figure and are known from the positions of the intersecting lines.

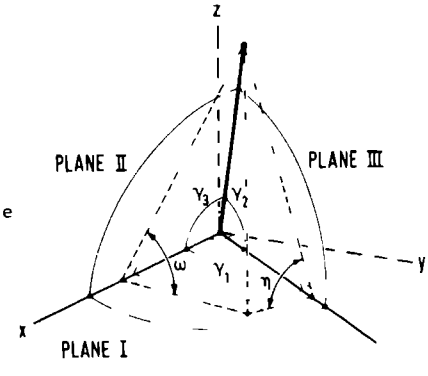

Fig. 2 Chosen coordinate system in case the angles γ between the intersecting lines of the measuring planes are not equal to 90°.

Thereafter, the tensor $\bar{\bar{g}}^2 = \bar{\bar{g}}.\bar{\bar{g}}^t$ is calculated and diagonalized using formula III.2 and a least squares method. This yields the directions of the principal axes in the chosen coordinate system and the eigenvalues of the $\bar{\bar{g}}^2$ tensor, which are the squares of the principal values of the $\bar{\bar{g}}$ tensor. The signs of the principal values of the $\bar{\bar{g}}$ tensor can not be determined, they have been assumed to be positive. Moreover, $\bar{\bar{g}}$ is assumed to be symmetrical. With the aid of the principal values of $\bar{\bar{g}}$ and its eigenvectors, which are the same as those for $\bar{\bar{g}}^2$, the $\bar{\bar{g}}$ tensor in the coordinate system of Fig. 2 can be constructed.

In an analogous way, the tensor $\bar{\bar{g}}.\bar{\bar{A}}.\bar{\bar{A}}^t.\bar{\bar{g}}^t$ is calculated. Multiplying from left and right with $\bar{\bar{g}}^{-1}$ yields $\bar{\bar{A}}^2 = \bar{\bar{A}}.\bar{\bar{A}}^t$. The principal axes and the squares of the principal values of $\bar{\bar{A}}$ are obtained by diagonalization of $\bar{\bar{A}}^2$. As for the $\bar{\bar{g}}$ tensor, the sign of the hyperfine splittings can not be determined. In all cases comparison of the average hyperfine splitting with the isotropic splitting (measured in liquid solution) led to the conclusion that all three principal values had the same sign. All principal values of copper have been taken negative and those of selenium positive, in agreement with a) the negative sign of the isotropic hyperfine splitting of copper, as given in the literature [53] and b) with the signs of the anisotropic splittings of copper and selenium as calculated by the extended Huckel Molecular Orbital method (Chapter V). The negative hyperfine interaction of copper is caused by a negative spin density and a positive magnetic moment, therefore the hyperfine interaction of silver has been taken positive, because of the negative sign of its magnetic moment. The $\bar{\bar{A}}$ tensors of copper and silver and the $\bar{\bar{g}}$ tensors, as calculated by "GAPLSD", were used as the initial values for the program "SPINHAM". The $\bar{\bar{A}}$ tensors of selenium have not been refined further.

III E 3 Ambiguity in the determination

As is well known [54], an ambiguity arises in the calculation of the tensors, because in general the relative directions of the rotations in the planes is not known, when more than one crystal is used to obtain a complete set of measurements. This leads to two distinct possibilities, because the direction of rotation of two planes can be chosen arbitrarily, leaving two different choices for the third plane. In practice this gave no problems, because in all systems studied one of these possibilities yielded imaginary hyperfine splittings.

III E 4 Angles between the principal axes and the b-axis

To situate the principal axes in the molecular frames, we have used the fact that all host crystals are monoclinic (space group $P_{2_1/c}$), with two magnetically non-equivalent sites in a unit cell. Since the crystallographic b-axis is a twofold (screw-) axis, it bisects the angle between two corresponding principal axes of the two sites. As the latter angle can be determined, comparison of this angle with crystallographic data may help to locate the direction in the molecule, along which the principal axis is situated.

III E 5 Experimental errors

It turned out that the $\bar{\bar{g}}$ tensors could be determined very accurately with the program "GAPLSD"; the minimization in "SPINHAM" resulted in a negligible change of these tensors. By comparing the values obtained for the two different sites, the accuracy is estimated to be of the order of 0.0002. The accuracy of the $\bar{\bar{A}}$ tensors of copper and silver was improved by the use of "SPINHAM". The error in the largest splittings is of the order of $0.2\ 10^{-4}cm^{-1}$, the errors in the smaller ones are somewhat larger, even in absolute sense. Through comparison of the values obtained for the two sites, the errors in the "axial" selenium splittings are estimated to be $\sim 0.5\ 10^{-4}cm^{-1}$, the errors in the "equatorial" splittings are much larger and can be $2\ 10^{-4}cm^{-1}$.

The principal values of the quadrupole tensors as determined with "SPINHAM" turned out to be very small, they do not exceed $3\ 10^{-4}cm^{-1}$. Since the absolute error is of the order of $0.2\ 10^{-4}cm^{-1}$, the relative error is large.

The errors in the directions of the principal axes are strongly correlated with the errors in the principal values belonging to them. For the $\bar{\bar{g}}$ tensors and the $\bar{\bar{A}}$ tensors of copper and silver, and the "axial" hyperfine values of selenium, the errors are estimated to be less than 2°. For the "equatorial" selenium hyperfine axes and the axes of the $\bar{\bar{P}}$ tensors, the errors are much larger and may be 10° or more.

CHAPTER IV

RESULTS OF ESR MEASUREMENTS

In this chapter the experimentally obtained results are presented, divided into single crystal, powder and liquid solution measurements. We list in Table IV.1 the characteristics of those nuclei of which the hfs has been measured. The hyperfine couplings of ^{65}Cu will not be given. The splitting due to the silver isotopes ^{107}Ag and ^{109}Ag has not been detected.

Table IV.1 Characteristics of nuclei

isotope	natural abundance (in %) [55]	I	magnetic moment [55] (in units of μ_n)	quadrupole moment (in $10^{-24}cm^2$) [55,56]
^{33}S	0.76	3/2	+0.6433	-0.055
^{63}Cu	69.09	3/2	+2.226	-0.211
^{65}Cu	30.91	3/2	+2.385	-0.195
^{77}Se	7.58	1/2	+0.534	-
^{107}Ag	51.82	1/2	-0.1135	-
^{109}Ag	48.18	1/2	-0.1305	-

IV A Measurements on $Cu(dsc)_2$ and $Ag(dsc)_2$ diluted in single crystals of $Ni(dsc)_2$

The diselenocarbamate complexes of copper have been studied in single crystals of the diamagnetic nickel complexes: After examining the system $Cu/Ni(but_2dsc)_2$ [57], we continued our study by investigating the systems $Cu/Ni(met_2dsc)_2$ and $Cu/Ni(et_2dsc)_2$. Silver diselenocarbamate was studied, diluted in $Ni(but_2dsc)_2$. Attempts to grow single crystals of $Ni(met_2dsc)_2$ failed, because of insolubility of this complex.

IV A 1 Crystal structures

The crystallographic structure of $Ni(et_2dsc)_2$ has been determined by Bonamico et al. [58]. The structure of the $Ni(but_2dsc)_2$ complex was determined by Noordik at the Crystallography Laboratory of our university [59]. This latter determination was done because striking differences were found in the results of the ESR measurements on the systems $Cu/Ni(et_2dsc)_2$ and $Cu/Ni(but_2dsc)_2$. Both crystals belong to the space group $P2_1/c$, and contain two molecules in a unit cell. In each molecule the Ni atom occupies an inversion centre, which means that the central part of the molecules

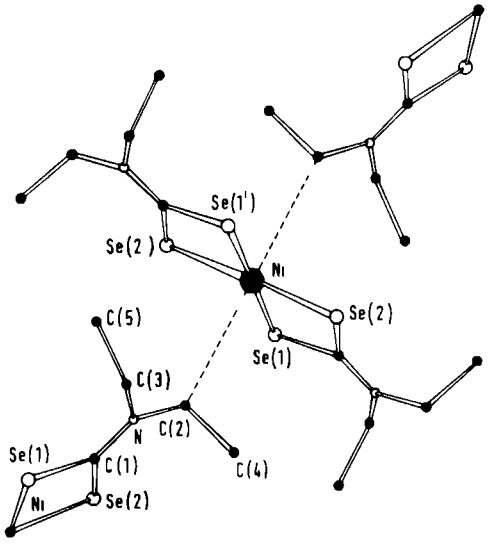

Fig.3 Projection of the structure of $Ni(et_2dsc)_2$ along the a axis [58].

(consisting of Ni and four Se atoms) forms a plane. The structure of the ethyl compound is illustrated in Fig. 3. Table IV.2 gives a number of distances and angles of importance for the interpretation of the ESR spectra. In $Ni(et_2dsc)_2$ the central part of the molecule has nearly D_{2h} symmetry. The deviation from this symmetry is larger in the n-butyl complex and also in the thio compound. This accounts for the above mentioned differences in the ESR results, as will be discussed later. The Se atoms of

Table IV.2 Bonding distances (in Å) and angles of $Ni(et_2dsc)_2$ [58], $Ni(but_2dsc)_2$ [59] and $Ni(et_2dtc)_2$ [60]. α is the angle between the crystallographic b axis and the bonding directions Ni - S(e)*.

	$Ni(et_2dsc)_2$		$Ni(but_2dsc)_2$		$Ni(et_2dtc)_2$	
	distance	α	distance	α	distance	α
$Ni-S(e)_1$	2.316	28.5°	2.317	61.5°	2.195	28.7°
$Ni-S(e)_2$	2.318	76.3°	2.307	49.4°	2.207	76.1°
angles						
$S(e)_1-Ni-S(e)_2$	81.8°		81.3°		79.2°	

*S(e) means S or Se

the neighbouring molecules are at such large distances that intermolecular effects on the ESR parameters can be neglected, provided the guest molecules accept the structure of the host crystal. The latter cannot be taken for granted, because the pure copper complex has a totally different structure [58]. In Fig. 4 and Table IV.6 the structure, bonding distances and bonding angles are given of the $Cu(et_2dsc)_2$ compound.

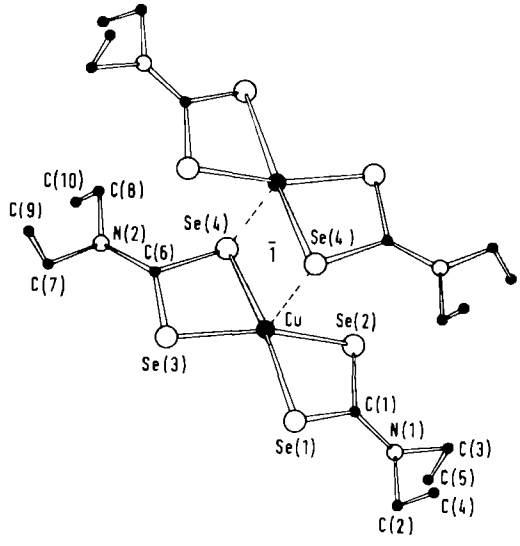

Fig. 4 Bimolecular unit of $Cu(et_2dsc)_2$ [58].

This crystal too belongs to the space group $P2_{1/c}$, but consists of dimeric units with Cu atoms surrounded by five Se atoms in an approximately tetragonal pyramidal structure. Because the Cu complex is monomeric in liquid solution it is not unlikely that it occurs as a monomer in the Ni crystal. The fact that the highest possible concentration that yields single crystals is about 2%, indicates that the doping of the crystal is accompanied with considerable lattice tension.

Since the pure Ag(II) compound cannot be isolated, its structure is unknown. Van Rens [5] concluded for the structures of the Ag and Cu dithiocarbamate compounds that they have similar structures. The structures of the diselenocarbamato complexes of Cu, Ni and Zn resemble very much the structures of the dithio complexes [60-62], hence one may expect that the $Ag(dsc)_2$ and $Cu(dsc)_2$ compounds have also similar structures.

IV A 2 Single crystal spectra

Generally the ESR spectra show the signals of two magnetically nonequivalent molecules. The two signals coincide when the magnetic field is parallel to the crystallographic monoclinic b-axis or when the field lies in the ac plane. The presence of the ^{77}Se isotope in general gave rise to two pairs of satellites having an intensity of 8% of the major peaks. These satellites are due to molecules with only one ^{77}Se atom. Using higher amplification, satellites due to molecules with two ^{77}Se atoms could be easely observed. As these do not yield additional information, they have been ignored. Because only two different satellites could be detected, we conclude that the inversion centre has been retained in the guest molecules.

Three representative spectra are reproduced in Fig. 5, 6 and 7. In Fig. 5 the magnetic field is located in the ac plane, so that the two molecules in the unit cell are magnetically equivalent. The hyperfine lines in this spectrum show a linewidth dependence on the Cu nuclear quantum number. Such a large linewidth variation is found only for some orientations in $Cu/Ni(but_2dsc)_2$ but is absent in ESR spectra recorded at $4.2^{o}K$. An explanation could be the occurrence of lattice distortions giving rise to a distribution of $Cu(but_2dsc)_2$ molecules over a small range of orientations. This explanation is supported by the X-ray results of Noordik who found a wide mosaic spread in $Ni(but_2dsc)_2$ [63].

Fig. 6 shows clearly the anisotropy in the copper hyperfine interactions. In this spectrum both magnetically nonequivalent sites have approximately the same g value, but the hfs of copper reaches a minimum for one site and almost a maximum for the other.

In Fig. 7 a spectrum of $Ag/Ni(but_2dsc)_2$ is shown. Apart from the silver ESR spectrum, lines are discernable which are due to $Cu(but_2dsc)_2$, present in the crystal as a small impurity. This impurity enabled us to compare very accurately the directions of the principal axes of the $\bar{\bar{g}}$ and $\bar{\bar{A}}$ tensors of the two complexes, because in this way they could be determined in the same coordinate system. Another spectrum which can be observed, is probably due to an unknown Ag(II) impurity: The g value variation of the impurity followed closely the variation in g value of the Ag(II) compound and never more than two lines originating from one site were observed. The most striking fact in Fig. 7 is the linewidth difference between the two sets of silver hyperfine lines. This is also observed in the Cu/Ni system but to a much smaller extent, so it can not be attributed to the above mentioned lattice distortions. An explanation could be the occurrence of unresolved hyperfine couplings. As van Rens pointed out [5], delocalization

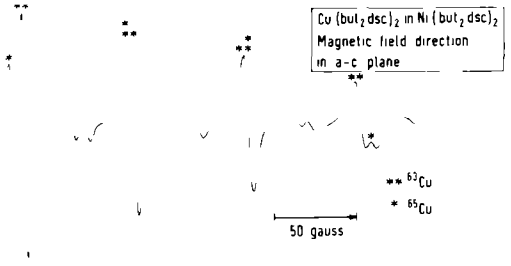

Fig.5 First derivative Q-band ESR spectrum of $Cu(but_2dsc)_2$ in a $Ni(but_2dsc)_2$ single crystal at room temperature. Not indicated lines are ^{77}Se satellites.

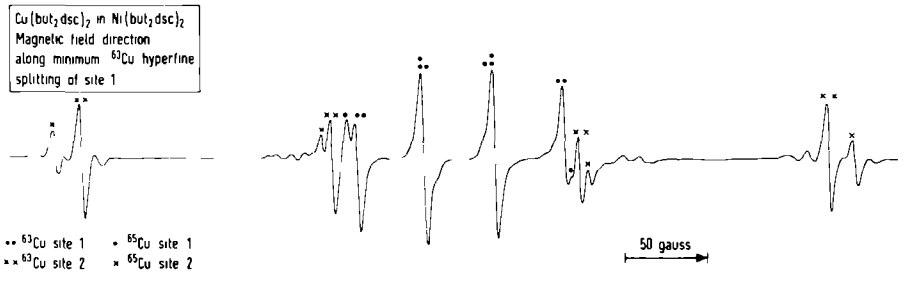

Fig.6 First derivative Q-band ESR spectrum of $Cu(but_2dsc)_2$ in a $Ni(but_2dsc)_2$ single crystal at room temperature. Not indicated lines are ^{77}Se satellites.

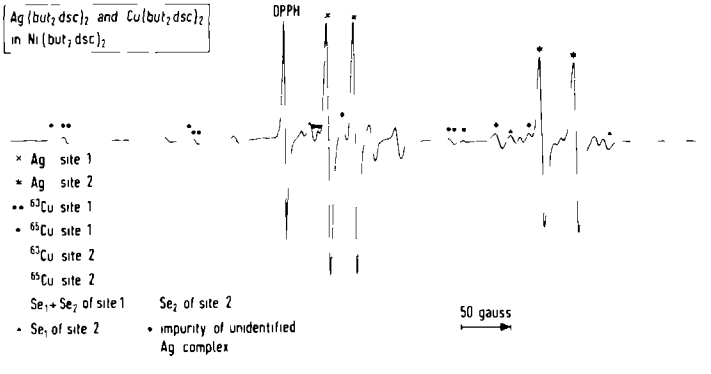

Fig.7 First derivative Q-band ESR spectrum of $Ag(but_2dsc)_2$ and $Cu(but_2dsc)_2$ in a $Ni(but_2dsc)_2$ single crystal at room temperature.

of the unpaired electron is more complete in the silver complex than in the Cu complex. This will cause a larger dipolar contribution to the ^{14}N hyperfine interaction in the case of the silver compound. Furthermore the second order hyperfine contribution will be larger due to the higher spin orbit coupling of silver. Therefore the ^{14}N couplings may be larger than in the Cu complex, but still not large enough to be resolved.

The principal axes and the principal values of the tensors were obtained by recording spectra in three different planes, according to the method described in chapter III. For $Cu/Ni(et_2dsc)_2$ and $Ag/Ni(but_2dsc)_2$ these planes were chosen arbitrarily, whereas in the case of $Cu/Ni(but_2dsc)_2$ the crystal was rotated approximately around the principal axes of the $\bar{\bar{g}}$ tensor of one site.

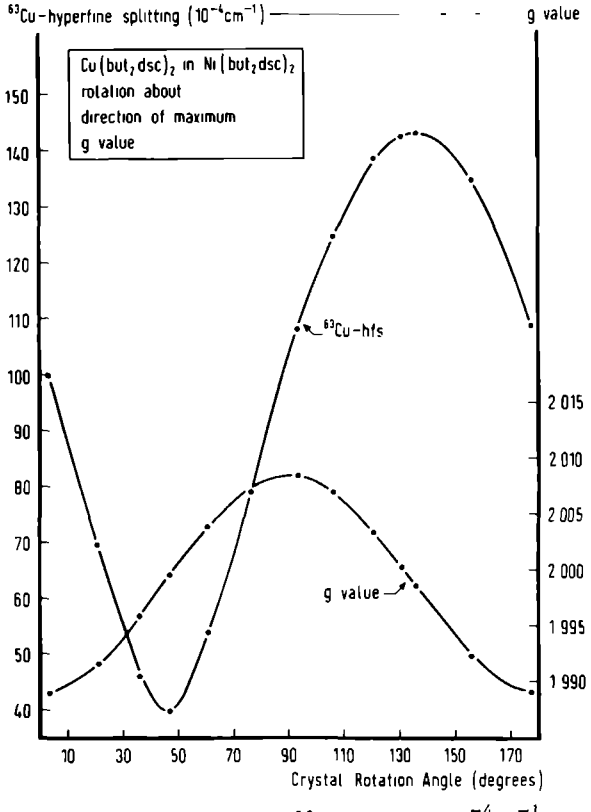

Fig.8 Angular variation of g value and ^{63}Cu hfs (in $10^{-4}cm^{-1}$) in $Cu/Ni(but_2dsc)_2$, upon rotation about the direction of maximum g value

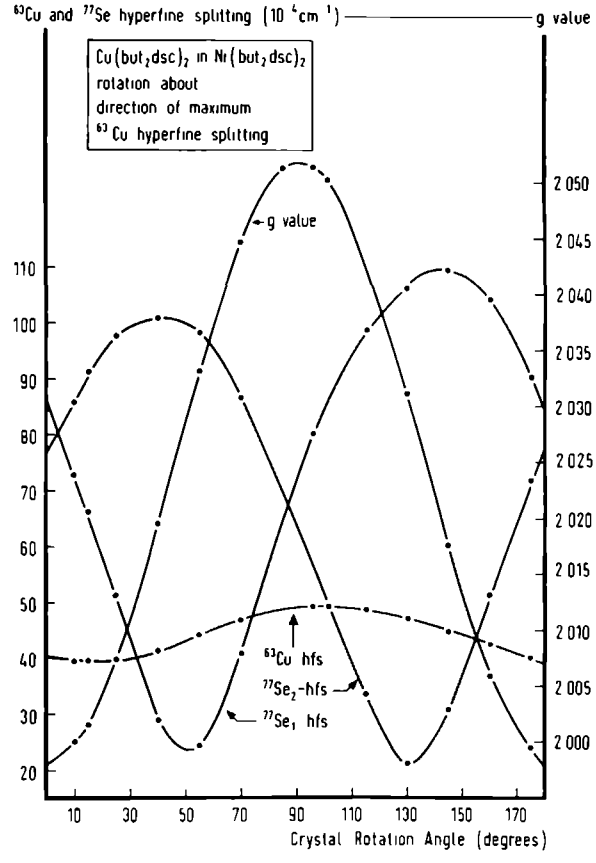

Fig. 9 Angular variation of g value, ^{63}Cu and ^{77}Se hfs's (in $10^{-4}cm^{-1}$) in $Cu/Ni(but_2dsc)_2$, upon rotation about the direction of maximum ^{63}Cu hfs.

IV A 2a The system $Cu/Ni(but_2dsc)_2$

Analysis of the spectra showed that none of the g value axes coincides with a principal axis of the Cu hfs tensor. This is clearly illustrated in Fig. 8 and 9. Fig. 8 gives the angular variation of the g value and Cu hfs upon rotation about the direction of maximum g value (g_1). Two principal axes of the Cu hfs tensor lie almost in the plane perpendicular to g_1 (A_1^{Cu} and A_3^{Cu}); their orientation is rotated by about 45^o with respect to the directions of extreme g values. Fig. 9 depicts the angular variation upon rotation about the direction of maximum Cu hfs (A_1^{Cu}). Apart from two principal axes of the $\bar{\bar{A}}^{Cu}$ tensor, this plane contains also a principal axis of the g tensor (g_1). The angle between g_1 and A_2^{Cu} is about 10^o. The hfs

components of both sets of magnetically equivalent Se atoms could also be determined quite accurately, although for certain ranges of orientations the positions of the Se satellites are obscured by other peaks.

The principal values and the angles between the principal axes and the the b axis are listed in Table IV.3. The orientation of the principal axes of the $\bar{g}$ and the Se hyperfine tensors with respect to the principal axes of the $\bar{A}^{Cu}$ tensor is listed in Table IV.4. The largest Cu hfs (A_1^{Cu}) is perpendicular to $A_1^{Se_1}$ and $A_1^{Se_2}$ and the angle between A_1^{Cu} and the b axis (48.7^o, Table IV.3) is in excellent agreement with the angle of 49.0^o between the b axis and the normal to the molecular plane [59]. Therefore it is assumed that A_1^{Cu} is perpendicular to the molecular plane and that the largest ^{77}Se hfs's point in the direction of the copper atom. In agreement with this assumption the angle between the directions of $A_1^{Se_1}$ and $A_1^{Se_2}$ is 80.6^o (see Fig. 9) close to the crystallographic angle Se_1-Ni-Se_2 which is 81.3^o. Similarly the angles of 60.4^o and 50.3^o between the b axis and $A_1^{Se_1}$ and $A_1^{Se_2}$ respectively, agree very well with the crystallographic angles of 61.5^o and 49.4^o between the Ni-Se_1 and Ni-Se_2 directions and the b axis. It is interesting to note that both the average and the purely anisotropic hfs (A_1-A_{av}) of Se_1 are larger than those of Se_2, whereas Se_1 has a larger distance to copper.

The orientations of the principal axes of the tensors in the molecular frame are sketched in Fig. 10. The maximum g value (g_1) bisects approximately the angle Se_1-Cu-Se_2, whereas the Cu hfs tensor is rotated around A_1^{Cu}: the angles of A_2^{Cu} with $A_1^{Se_1}$ and $A_1^{Se_2}$ are 36^o and 63^o respectively. The smallest selenium hyperfine splittings are found in directions making an angle of about 35^o with A_1^{Cu}.

Table IV.3 A. Experimentally obtained principal values of $\bar{\bar{g}}$ tensor, quadrupole coupling and hyperfine coupling tensors (in $10^{-4}cm^{-1}$) of Cu/Ni(met_2dsc)$_2$, Cu/Ni(et_2dsc)$_2$, Cu/Ni(but_2dsc)$_2$, Ag/Ni(but_2dsc)$_2$ and Ag/Pd(but_2dsc)$_2$[a].
B. Angles between principal axes and crystallographic b axis.

principal axes	A. principal values					B. angle with b axis		
	Cu/Ni $(met_2dsc)_2$	Cu/Ni $(et_2dsc)_2$	Cu/Ni $(but_2dsc)_2$	Ag/Ni $(but_2dsc)_2$	Ag/Pd $(but_2dsc)_2$	Cu/Ni $(et_2dsc)_2$	Cu/Ni $(but_2dsc)_2$	Ag/Ni $(but_2dsc)_2$
g_1	2.049	2.0511	2.0517	2.0820	2.086	59.2	82.6	83.2
g_2	2.005	2.0021	2.0084	1.9965	1.995	67.0	8.0	31.8
g_3	1.998	1.9941	1.9889	1.9280	1.928	40.2	87.2	59.0
b. g_{av}	2.017	2.0157	2.0163	2.0022	2.003			
c. g_{iso}	2.0210	2.0219	2.0231	2.0065	2.006			
Cu,Ag								
A_1	-140	-144.2	-142.5	+ 34.0	+ 34.8	63.2	48.7	49.4
A_2	- 48	- 50.6	- 48.8	+ 25.5	+ 27.3	61.2	93.3	88.9
A_3	- 43	- 44.0	- 39.6	+ 23.7	+ 24.0	41.3	41.5	40.6
b. A_{av}	- 77	- 79.6	- 77.0	+ 27.8	+ 28.7			
c. A_{iso}	- 75.6	- 76.3	- 76.5	+ 26.6	+ 27.6			
Se_1								
A_1	n.m.	+105.4	+109.3	+121.3	+119.7	26.6	60.4	59.1
A_2	n.m.	+ 22	+ 21	+ 17	+ 11	83	32	27
A_3	n.m.	+ 17	+ 17	+ 10	+ 9	64	79	50
b. A_{av}	n.m.	+ 48	+ 49	+ 49	+ 47			
c. A_{iso}	+ 43.3	+ 44.0	+ 44.9	+ 44.3	+ 45.9			
Se_2								
A_1	n.m.	+103.4	+101.0	+110.0	+113.0	76.4	50.3	49.7
A_2	n.m.	+ 20	+ 21	+ 16	+ 16	32	47	65
A_3	n.m.	+ 13	+ 15	+ 5	+ 9	62	70	47
b. A_{av}	n.m.	+ 45	+ 46	+ 44	+ 46			
c. A_{iso}	+ 43.3	+ 44.0	+ 44.9	+ 44.3	+ 45.9			
Cu								
P_1	n.m.	+ 0.3	+ 0.6			43	72	
P_2	n.m.	0.0	0.0			88	19	
P_3	n.m.	- 0.3	- 0.6			46	90	

a. values from Ref. [64].
n.m. = not measured.
b. average of principal values.
c. isotropic value, measured in liquid solution of chloroform.

Table IV.4 Angles between principal axes of $\bar{\bar{A}}^{Cu}$ and principal axes of $\bar{\bar{g}}$, $\bar{\bar{A}}^{Ag}$, $\bar{\bar{A}}^{Se}$ and $\bar{\bar{P}}^{Cu}$.

	Cu/Ni $(met_2dsc)_2$			Cu/Ni $(et_2dsc)_2$			Cu/Ni $(but_2dsc)_2$			Ag/Ni $(but_2dsc)_2$		
	A_1^{Cu}	A_2^{Cu}	A_3^{Cu}	A_1^{Cu}	A_2^{Cu}	A_3^{Cu}	A_1^{Cu}	A_2^{Cu}	A_3^{Cu}	A_1^{Cu}	A_2^{Cu}	A_3^{Cu}
g_1	90	0	90	90	3	87	89	10	109	90	14	104
g_2	58	90	148	57	92	33	46	97	135	80	76	17
g_3	32	90	58	33	88	123	44	84	47	10	93	100
Se_1												
A_1	n.m.	n.m.	n.m.	91	52	38	90	36	54	90	36	54
A_2	n.m.	n.m.	n.m.	87	39	128	53	62	130	79	55	143
A_3	n.m.	n.m.	n.m.	3	92	87	37	111	61	11	96	81
Se_2												
A_1	n.m.	n.m.	n.m.	91	49	41	90	63	27	89	62	28
A_2	n.m.	n.m.	n.m.	89	42	131	57	42	112	74	32	117
A_3	n.m.	n.m.	n.m.	5	91	88	33	119	76	16	104	82
Ag												
A_1										2	90	91
A_2										90	6	96
A_3										90	84	6
Cu												
P_1	n.m.	n.m.	n.m.	79	82	14	23	93	67			
P_2	n.m.	n.m.	n.m.	63	30	103	67	89	157			
P_3	n.m.	n.m.	n.m.	30	119	96	88	3	88			

n.m. = not measured.

IV A 2b The system $Ag/Ni(but_2dsc)_2$

The study of this system was started to verify the findings of Kirmse et al. [64], who studied the system $Ag/Pd(but_2dsc)_2$ and concluded that the principal axes of $\bar{\bar{g}}$ and $\bar{\bar{A}}^{Ag}$ coincide within the accuracy of their measurements. Compared with our results for the system $Cu/Ni(but_2dsc)_2$, this conclusion was very unexpected, even bearing in mind the different host lattices used. The structure of $Pd(but_2dsc)_2$ is not known but, from the ESR measurements, some conclusions may be drawn: 1. Kirmse et al. observed just two magnetically non equivalenc sites, which means that the structure certainly is not the one of $Pd(et_2dtc)_2$ [62] where four

(magnetically non equivalent) molecules in a unit cell are present.
2. The largest hfs's of the two non equivalent Se atoms differ by $6\ 10^{-4}\ cm^{-1}$, whereas the two Pd-S distances in $Pd(et_2dtc)_2$(of which the structure is known [65]) are equal. Hence the structure of the $Pd(but_2dsc)_2$ molecule must have some characteristics of the structure of $Ni(but_2dsc)_2$: two molecules in a unit cell and two significantly different metal-Se distances. Therefore it did not seem very likely that the principal axes of $\bar{\bar{g}}$ and $\bar{\bar{A}}^{Ag}$ would coincide. This conclusion is supported by the ESR powder spectrum of $Cu/Pd(but_2dsc)_2$ [66], also measured by Kirmse et al. He found the same rotation of principal axes as is observed in $Cu/Ni(but_2dsc)_2$, also indicating that the symmetry of the Ni and the Pd complexes is the same.

The principal values and the angles with the b axis measured by us are listed in Table IV.3, together with the principal values measured by Kirmse et al. The orientation of the principal axes in the molecular frame is sketched in Fig. 11, the angles with the principal axes of $\bar{\bar{A}}^{Cu}$ are listed in Table IV.5.

The results show that the axes of $\bar{\bar{A}}^{Ag}$ nearly coincide with those of $\bar{\bar{A}}^{Cu}$. Especially the angle of just 2^o between A_1^{Cu} and A_1^{Ag} shows that the molecule is built in in the same way as the Cu containing molecules. The Ag hyperfine axes certainly do not coincide with those of the $\bar{\bar{g}}$ tensor of the Ag-molecule: the largest angle between two axes is 10^o.

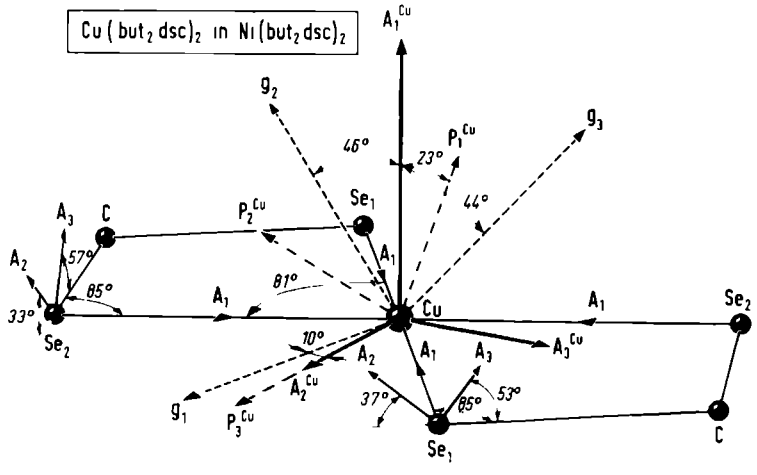

Fig. 10 Proposed orientations of the principal axes in $Cu/Ni(but_2dsc)_2$.

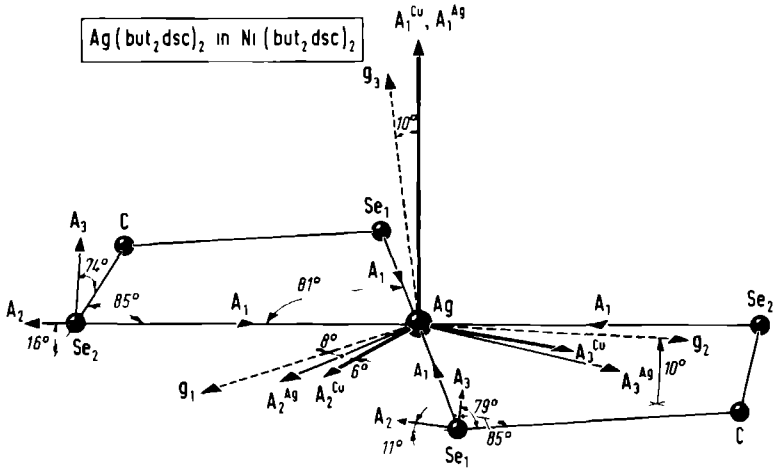

Fig. 11 Proposed orientations of the principal axes in $Ag/Ni(but_2dsc)_2$, together with the principal axes of the ^{63}Cu hfs in the same crystal.

IV A 2c The system $Cu/Ni(et_2dsc)_2$

The principal values and the directions of the principal axes are listed in Table IV.3 and IV.4 and sketched in Fig. 12. The most important differences with the results of $Cu/Ni(but_2dsc)_2$ are:

i. g_1 coincides with A_1^{Cu} (within 3°), bisecting the angle Se_1-Cu-Se_2.

ii. the angle between g_3 and A_1^{Cu} is decreased from 44° to 33°.

iii. The difference between $A_1^{Se_1}$ and $A_1^{Se_2}$ has been decreased from 8.3 to 2.0 $10^{-4}cm^{-1}$, which is in agreement with the decreased difference in the bonding distances Ni-Se_1 and Ni-Se_2. It is, of course, improbable that the built in Cu containing molecules have exactly the metal-selenium distances of the host molecules. However, the packing forces, which are responsible for the inequality of the Ni-Se distances, act also on the guest molecules. Although their effect on the Cu containing molecules is not known, it may be expected that the trend, on going from $Ni(et_2dsc)_2$ to $Ni(but_2dsc)_2$ will be followed.

iv. Similarly in agreement with the higher symmetry, the smallest Se hfs's are now parallel with A_1^{Cu}, perpendicular to the molecular plane.

v. the average Cu hfs has been increased by 2.3 $10^{-4}cm^{-1}$, whereas the anisotropic part did not change. This difference can also be explained on the basis of the higher symmetry as follows:
The magnitude of the average hfs is determined by

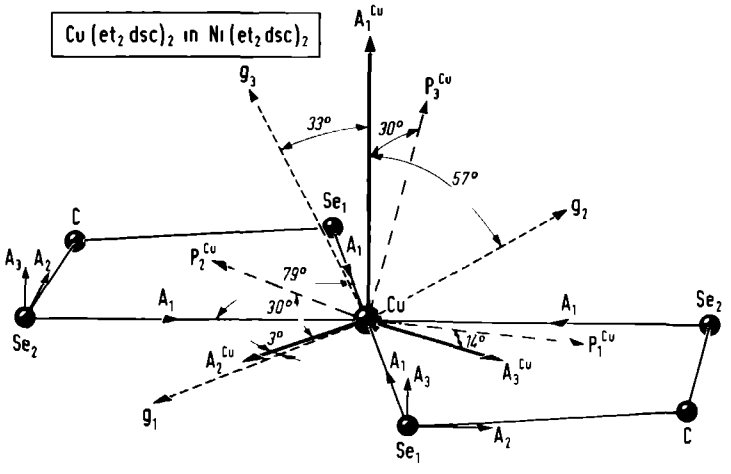

Fig.12 Proposed orientations of the principal axes in Cu/Ni$(et_2dsc)_2$.

a. the electron spin density on the nucleus (Eq.II.67), which may arise from
   a1. direct participation of s-orbitals in the wave function describing the unpaired electron, resulting in a positive contribution [53], and
   a2. spinpolarization of core s-orbitals by the unpaired electron, yielding a negative contribution [53].

b. the second order contributions to the anisotropic hfs tensor (Eq. II.64 and II.65). These yield a pseudo contact interaction which in our systems was calculated to be about +5 $10^{-4}cm^{-1}$.

Since the resulting average Cu hfs is negative, the contribution a2. dominates over a1. plus b.

Anticipating the results of the next chapter, the metal part of the MO of the unpaired electron consists mainly of one 3d AO pointing towards the ligand Se atoms, with some admixture of the other 3d AO's and the 4s orbital. The amount of admixture depends on the symmetry of the system: in case of exact D_{2h} symmetry it is zero and consequently the contribution a1. to the spin density at the nucleus vanishes, in cases of lower symmetry the coefficient of the 4s orbital will increase, resulting in a larger positive contribution to the average hfs, and thus in a smaller absolute value of the average hfs. Since the deviation from D_{2h} symmetry in Ni$(but_2dsc)_2$ is clearly much larger than in Ni$(et_2dsc)_2$, this effect explains the difference in the average Cu hfs

As will be pointed out in section B of this chapter, in a liquid solution the symmetry of $Cu(but_2dsc)_2$ is raised. From the near equality of the isotropic hfs's it may be concluded that the same holds for $Cu(et_2dsc)_2$.

IV A 3 Comparison with dithiocarbamates and conclusions

The measurements, described in this section, show that $Cu(R_2dsc)_2$ (R = et,but) and $Ag(but_2dsc)_2$ are built in in the corresponding Ni complexes as monomers, accepting the symmetry of the host crystal. In these monomers the highest g value is situated in the molecular plane, along the bisector Se_1-Metal-Se_2. The (in absolute value) largest central metal hyperfine splitting is perpendicular to the molecular plane and the largest selenium hyperfine splittings point from selenium to the central metal atom.

In all systems the $\bar{\bar{g}}$ tensor is rotated in the plane in which g is almost isotropic, the axis of rotation being g_1. The rotation angle depends on the central metal atom and on the extent to which the symmetry deviates from D_{2h}. Analogously the $\bar{\bar{A}}$ tensor of the metal atom is rotated in the plane of smallest anisotropy, which for this tensor is the molecular plane. Also this rotation depends on the central metal atom and the molecular symmetry.

When these results are compared with single crystal measurements of $Cu/Ni(et_2dtc)_2$ [12] and $Ag/Ni(et_2dtc)_2$ [5], the following differences are striking:

1. In the dithiocarbamates the highest g value is perpendicular to the molecular plane. In the molecular plane the anisotropy is much smaller than in the diselenocarbamate complexes. (Table IV.5)
2. Although the symmetry of $Ni(et_2dtc)_2$ deviates more from D_{2h} than the symmetry of $Ni(et_2dsc)_2$, the principal axes of the $\bar{\bar{g}}$ and $\bar{\bar{A}}$ tensor coincide. Therefore, the rotations of the principal axes of $\bar{\bar{g}}$ and $\bar{\bar{A}}$ in in the dsc complexes have to be ascribed to the presence of the heavy selenium atoms. The main reason might be a change of electron delocalization on going from a dtc to a dsc compound, or the large spin orbit coupling of Se. The calculations in the next chapter prove that the latter is the case.

Table IV.5 Experimentally obtained principal values of $\bar{\bar{g}}$ tensor and hyperfine coupling tensor (in 10^{-4} cm^{-1}) of $Cu/Ni(et_2dtc)_2$ [12] and $Ag/Ni(et_2dtc)_2$ [5].

	$Cu/Ni(et_2dtc)_2$	$Ag/Ni(et_2dtc)_2$
g_1	2.084	2.0355
g_2	2.025	2 0129
g_3	2.020	2.0052
A_1	-159.0	+38.0
A_2	- 42.0	+26.9
A_3	- 36.0	+23.0

IV B Single crystal measurements of $Cu(dsc)_2$ diluted in $Zn(dsc)_2$ and $Cu(dtc)_2$ in $Zn(dtc)_2$

The second diamagnetic host in which $Cu(dsc)_2$ was studied is the Zn(II) complex. Because of the results of the MO calculations (which are discussed in the next chapter) also the system $Cu/Zn(et_2dtc)_2$ was measured, although other authors had done this before [12].

IV B 1 Crystal structures

The structures of $Cu(et_2dsc)_2$ and $Cu(et_2dtc)_2$ are isomorphic, just as those of $Zn(et_2dsc)_2$ and $Zn(et_2dtc)_2$. The structures of the seleno compounds are given in the Figures 4 and 13.

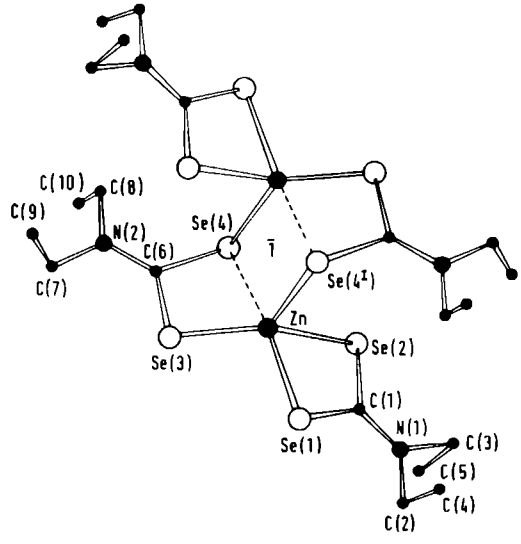

Fig. 13. Dimeric unit of $Zn(et_2dsc)_2$ [58].

Relevant bonding distances and angles of all complexes are tabulated in Table IV.6. All crystals belong to the space group $P2_{1/c}$, with two dimeric units in a unit cell. Because every dimer has inversion symmetry, it does not make a difference which Zn atom within one dimer is replaced by Cu.

The nearest neighbour environment of the Cu atom is about tetragonal pyramidal. The axial Cu - $S(e)_4$, distance is about 0.5 Å longer than the four equatorial Cu - S(e) distances. In the Zn compounds the distance Zn - $S(e)_4$, is smaller than the distance Zn - $S(e)_4$, in contrast to the situation in the Cu compounds. (see Table IV.6) Due to this difference, the

Table IV.6 Bonding distances (in Å) and angles of $Cu(et_2dsc)_2$ [58], $Cu(et_2dtc)_2$ [61], Zn(et dsc) [58] and $Zn(et_2dtc)_2$ [62].

	$Cu(et_2dsc)_2$	$Cu(et_2dtc)_2$	$Zn(et_2dsc)_2$	$Zn(et_2dtc)_2$
distances				
$M-S(e)_1$	2.438	2.317	2.568	2.443
$M-S(e)_2$	2.423	2.297	2.446	2.355
$M-S(e)_3$	2.421	2.301	2.435	2.331
$M-S(e)_4$	2.439	2.339	3.033	2.815
$M-S(e)_{4'}$	2.905	2.851	2.492	2.383
angles				
$S(e)_1-M-S(e)_2$	79.4°	77.3°	79.1°	75.8°
$S(e)_1-M-S(e)_3$	99.1°	101.5°	106.4°	106.9°
$S(e)_1-M-S(e)_4$	172.3°	172.3°	160.3°	160.0°
$S(e)_1-M-S(e)_{4'}$	94.0°	94.6°	104.7°	105.2°
$S(e)_2-M-S(e)_3$	159.3°	161.8°	134.3°	137.7°
$S(e)_2-M-S(e)_4$	99.6°	102.3°	89.3°	93.6°
$S(e)_2-M-S(e)_{4'}$	99.9°	97.8°	114.5°	112.1°
$S(e)_3-M-S(e)_4$	79.1°	76.5°	70.7°	69.6°
$S(e)_3-M-S(e)_{4'}$	100.8°	100.4°	107.9°	107.8°
$S(e)_4-M-S(e)_{4'}$	93.8°	93.1°	94.5°	94.4°

nearest neighbour environment of the Zn atom is no longer tetragonal pyramidal but can be described as nearly tetrahedal ($S(e)_1$, $S(e)_2$, $S(e)_3$ and $S(e)_{4'}$) or distorted trigonal pyramidal (through five S(e) atoms with $S(e)_1$ and $S(e)_4$ lying on the axial axes). In all four complexes the five S(e) atoms surrounding the metal atom are clearly all inequivalent.

IV B 2 Single crystal spectra

Except when the magnetic field is located either in the ac plane or along the b axis, the spectra consist of two different signals, belonging to the two magnetically non-equivalent dimers in the unit cell. No electron spin-electron spin interactions were observed, because not more than about 1% of the Zn atoms was replaced by Cu.

In $Cu/Zn(et_2dsc)_2$ there are five selenium atoms which have a distance from the Cu atom short enough to have a fairly high spin density. Experimentally it turned out that the hfs of only four of them could be measured accurately enough. The splittings caused by the fifth one are mostly hidden under the main peaks. Because the natural abundance of ^{77}Se

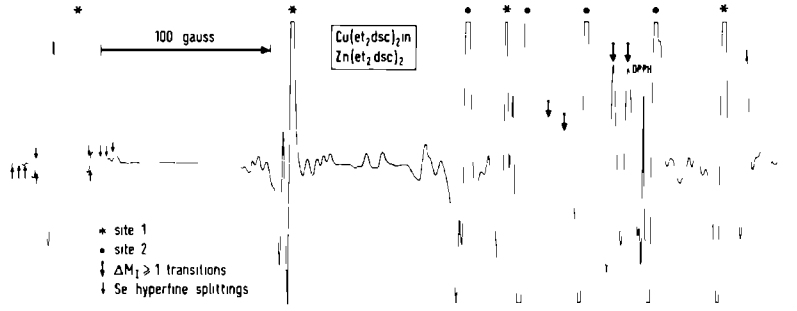

Fig.14 First derivative Q-band ESR spectrum of $Cu(et_2dsc)_2$ in a $Zn(et_2dsc)_2$ single crystal at room temperature. ↓ are ^{77}Se satellites of ^{63}Cu; ↑ are ^{77}Se satellites of ^{65}Cu.

is 7.5% and I = ½, each satellite has a relative intensity of 4% of a peak which is due to a molecule with no ^{77}Se hyperfine splittings. One spectrum, showing the satellites, is given in Fig.14. Due to the very low natural abundancy of ^{33}S (0.74%, I=3/2) no ^{33}S hfs's could be measured in $Cu/Zn(et_2dtc)_2$.

In both systems so called "forbidden" transitions (i.e. $\Delta M_I = \pm 1$ and +2 transitions, mentioned in section II A) are observed. Their relative intensity runs from zero up to more than 100% of some of the $\Delta M_I = 0$ transitions in the spectrum. This high intensity is caused by a co-operative effect of the nuclear Zeeman and the quadrupole interaction, as may be seen from Eq.II.19. This equation shows that the admixture of, for instance, the $|M_S, M_I + 1\rangle$ state in $|M_S, M_I\rangle$ is at a maximum when $g_n\mu_n Z_3 - M_S T_{33} - 3(M_I \pm \frac{1}{2})Q_{33}$ is small. This explains also why these transitions were not observed in the systems $Cu/Ni(R_2dsc)_2$. In the latter systems the minimum Cu hfs is much larger than in the systems we are discussing now, and furthermore the quadrupole interactions are smaller. In Fig.15 a spectrum of $Cu/Zn(et_2dtc)_2$ is given, showing these "forbidden" lines; they can also be discerned in the spectrum of $Cu/Zn(et_2dsc)_2$ in Fig.14.

IV B 2a The system $Cu/Zn(et_2dsc)_2$

The measured ESR data are listed in Table IV.7 and IV.8. Because of the selenium satellites the "forbidden" transitions could not be measured accurately enough. Therefore they were not used for the determination of the tensors. Since a dimer with one Cu and one Zn atom has no symmetry at

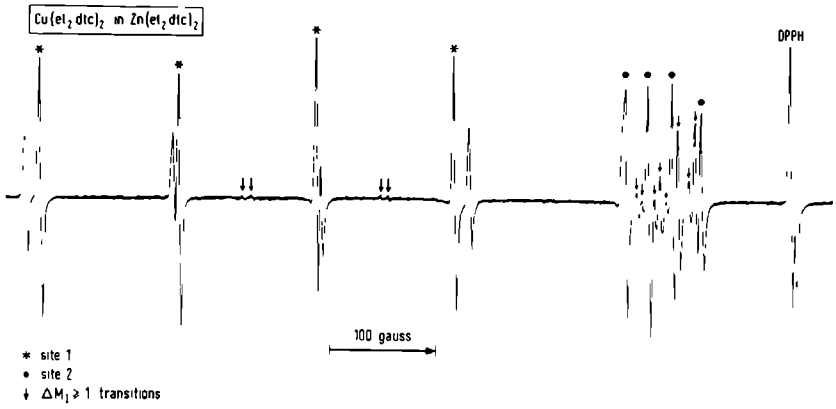

Fig.15 First derivative Q-band ESR spectrum of $Cu(et_2dtc)_2$ in a $Zn(et_2dtc)_2$ single crystal at room temperature.

Table IV.7 Experimentally obtained principal values of the $\bar{\bar{g}}$ tensor, the hyperfine coupling tensors and the copper quadrupole tensor (in $10^{-4}cm^{-1}$) of $Cu/Zn(et_2dsc)_2$.

		Cu		Cu	
g_1	2.0559	A_1	-127.6	P_1	+1.8
g_2	2.0213	A_2	- 40.4	P_2	-0.3
g_3	2.0068	A_3	- 26.6	P_3	-1.5
g_{av}	2.0280	A_{av}	- 64.9		

Se_1		Se_2		Se_3		Se_4	
A_1	118.3	A_1	97.3	A_1	91.6	A_1	101.5
A_2	22	A_2	19	A_2	19	A_2	23
A_3	12	A_3	15	A_3	17	A_3	19
A_{av}	51	A_{av}	44	A_{av}	43	A_{av}	48

all, it is not surprising that the principal axes of $\bar{\bar{g}}$ and of the $\bar{\bar{A}}$ tensor of Cu do not coincide.

An interesting question in this study is whether or not the copper containing dimer accepts the structure of the host crystal. Table IV.9 lists the experimentally obtained angles between the crystallographic b axis and the principal axes $A_1^{Se_i}$ together with the angles between the b axis and the metal-selenium bonds in $Cu(et_2dsc)_2$ and $Zn(et_2dsc)_2$. In the table the experimental results are arranged in such a way that the best agreement is obtained between both types of measurements. It is clear that (except for Se_2) the experimental values agree best with the angles in $Cu(et_2dsc)_2$. In Table IV.10 the mutual angles between the $A_1^{Se_i}$ axes are compared with the bonding angles in the pure compounds. Also these

Table IV.8 Experimentally obtained angles between the principal axes of $\bar{\bar{A}}^{Cu}$ and the principal axes of $\bar{\bar{g}}$, $\bar{\bar{P}}^{Cu}$ and $\bar{\bar{A}}^{Se_1}$ in $Cu/Zn(et_2dsc)_2$.

	g_1	g_2	g_3	Cu	P_1	P_2	P_3	Se_1	A_1	A_2	A_3
Cu											
A_1	85	7	86		2	89	89		93	100	10
A_2	24	96	67		91	7	96		104	17	81
A_3	112	92	23		91	84	7		15	76	85

	Se_2	A_1	A_2	A_3	Se_3	A_1	A_2	A_3	Se_4	A_1	A_2	A_3
Cu												
A_1		106	90	16		103	95	14		93	95	6
A_2		27	112	75		153	65	99		76	165	94
A_3		69	22	84		113	154	100		165	104	95

Table IV.9 a. Experimentally obtained angles between $A_1^{Se_1}$ principal axes and the crystallographic b axis in $Cu/Zn(et_2dsc)_2$.
b. Angles between M-Se bonding directions and b axis (M = Cu,Zn) in $Cu(et_2dsc)_2$ and $Zn(et_2dsc)_2$ [58].

	a	b	
		$Cu(et_2dsc)_2$	$Zn(et_2dsc)_2$
Se_1	35.8	34.8	40.8
Se_2	91.0	83.0	91.8
Se_3	108.2	107.7	122.4
Se_4	150.4	152.9	157.0
$Se_{4'}$		59.4	64.2

Table IV.10 a. Angles between principal axes $A_1^{Se_1}$ in $Cu/Zn(et_2dsc)_2$.
b. Bonding angles in $Cu(et_2dsc)_2$ and $Zn(et_2dsc)_2$ [58].

	a	b	
	exp.	$Cu(et_2dsc)_2$	$Zn(et_2dsc)_2$
Se_1-M-Se_2	81.6	79.4	79.1
Se_1-M-Se_3	98.7	99.1	106.4
Se_1-M-Se_4	173.8	172.3	160.3
Se_1-M-$Se_{4'}$		94.0	104.7
Se_2-M-Se_3	151.1	159.3	134.3
Se_2-M-Se_4	96.8	99.6	89.3
Se_2-M-$Se_{4'}$		99.9	114.5
Se_3-M-Se_4	79.8	79.1	70.7
Se_3-M-$Se_{4'}$		100.8	107.9
Se_4-M-$Se_{4'}$		93.8	95.5

experimental values agree best with the bonding angles in $Cu(et_2dsc)_2$; the strongest deviations occur for angles involving Se_2.

From the foregoing we conclude: 1. the copper containing dimer does

not have the structure of the host crystal, but has a structure which resembles very much that of the pure $Cu(et_2dsc)_2$ compound, 2. the $A_1^{Se_i}$ vectors point in the direction Se→Cu, 3. the four measured $\bar{\bar{A}}^{Se_i}$ tensors belong to the four selenium atoms which lie nearly in a plane, so that the Se atom of which the hfs was not measured is Se_4, (see Fig.4). This result is not surprising since the $Cu-Se_4$, distance is the largest distance in the Cu complex considered.

With the aid of these results, the principal axes of the tensors can be situated in the molecule, as is done in Fig.16. As opposed to the monomeric systems, discussed in section A of this chapter, A_1^{Cu} and g_2 nearly coincide. However, the largest rotation has taken place in the plane of one molecule: g_1 and g_3 approximately bisect the angles Se-Cu-Se, but A_2 and A_3 are rotated from these directions.

The principal values of $\bar{\bar{P}}^{Cu}$ and the directions of its principal axes have been obtained in two sites independently. Therefore it can be concluded that these data are meaningfull in spite of their small values. The tensor turns out to be far from axially symmetric. The principal axes almost coincide with those of $\bar{\bar{A}}^{Cu}$, the axis along which the highest P value has been measured is perpendicular to the molecular plane, similar to the orientation of the $\bar{\bar{A}}^{Cu}$ tensor.

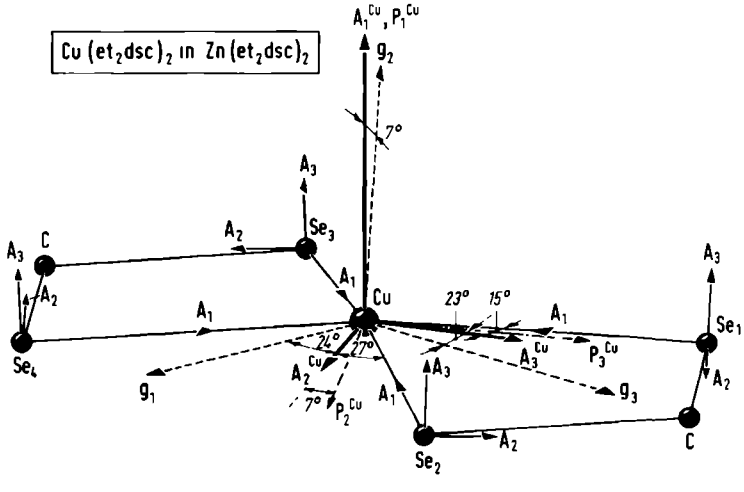

Fig.16 Proposed orientations of the principal axes in $Cu/Zn(et_2dsc)_2$. Note that the Cu atom and the Se atoms do not lie in a plane.

IV B 2b The system Cu/Zn(et_2dtc)$_2$

ESR spectra of single crystals of this system have been measured by Reddy and Srinivasan [11] and by Weeks and Fackler [12]; their results are listed in Table IV.11. Reddy and Srinivasan concluded to axial symmetry around the Cu atom and calculated the parameters of the spin hamiltonian on this basis. Apart from the principal values of the $\bar{\bar{g}}$ tensor and the copper hfs tensor, the nuclear quadrupole coupling tensor of copper was also determined. Because no detailed crystal structures were available at that time, they could not relate the principal magnetic axes to the geometry of the molecule in the crystal. When Weeks and Fackler carried out their study, the crystal structures of both guest and host molecule had been published [61,62]. Thus the angles between the principal axes of $\bar{\bar{g}}$ and $\bar{\bar{A}}^{Cu}$ and the crystallographic a, b and c axis could be determined. The angles with the b axis are given in Table IV.11. Weeks and Fackler found (within experimental error) the $\bar{\bar{g}}$ and $\bar{\bar{A}}$ tensor non axial, with coinciding principal axes. The maximum g value and Cu hfs is approximately normal to the least-squares plane through the four sulphur atoms of the formula unit. Of the two principal axes that lie in the plane of the sulphur atoms, g_1 lies along the S(4)-M-S(1) direction. Weeks and Fackler measured a very small A_3^{Cu} component. Compared with our result in the diselenocarbamato system (preceding section) this value seemed to be rather unlikely. Because an MO calculation (chapter V) also yielded a much higher value for A_3^{Cu}, we decided to remeasure this system. After the last refinements with the program "SPINHAM" (section III E) the function $\{\frac{1}{N}\sum_{i=1}^{N}(B^1_{observed} - B^1_{calculated})^2\}^{\frac{1}{2}}$ was reduced to 0.85 gauss. The summation ran over 168 $\Delta M_I=0$, 110 $\Delta M_I=\pm1$ and 20 $\Delta M_I=\pm2$ transitions. Neither Reddy and Srinivasan nor Weeks and Fackler reported $\Delta M_I>0$ transitions, probably because they measured at X-band frequency. Our results (Tables IV.11 and 12) confirm the non axiallity of the tensors, but differ from those of Weeks and Fackler in the smallest Cu hfs. Furthermore a small angle is found between the directions of g_3 and A_3^{Cu}. The values found for $\bar{\bar{P}}^{Cu}$ agree very well with those of Reddy and Srinivasan, except for the axial symmetry supposed by them.

Inspection of Table IV.11 shows that good agreement exists between the angles of the principal axes and the b axis, measured by Weeks and Fackler and us. The direction of the principal axes in the molecule is drawn in Fig.17. From the observation that g_3 lies along the S(4)-M-S(1) direction, which direction contains the pair of bonds that are

Table IV.11 Experimentally obtained principal values of $\bar{\bar{g}}$, $\bar{\bar{A}}^{Cu}$ and $\bar{\bar{P}}^{Cu}$ (in $10^{-4}cm^{-1}$) of $Cu/Zn(et_2dtc)_2$, and angles between the principal axes and the crystallographic b axis.

	principal axes			angles with b axis	
	a	b	c	a	b
g_1	2.1076	2.107	2.1085	56.9	56.4
g_2	2.0308	2.033	2.023	88.1	88.6
g_3	2.0230	2.025	2.023	33.1	33.3
g_{av}	2.0538	2.055	2.0515		
Cu					
A_1	-142.4	-143	-142.4	57.3	57.3
A_2	- 29.9	- 27	- 22.4	88.2	88.1
A_3	- 20.4	- 7	- 22.4	32.8	32.7
A_{av}	- 64.2	- 59	- 62.4		
Cu					
P_1	+ 2.1		+ 2	55.1	
P_2	- 0.5		- 1	22.1	
P_3	- 1.6		- 1	43.3	

a. this thesis.
b. results from Ref.12
c. results from Ref.11

Table IV.12 Experimentally obtained angles between the principal axes of $\bar{\bar{A}}^{Cu}$ and the principal axes of $\bar{\bar{g}}$ and $\bar{\bar{P}}^{Cu}$ in $Cu/Zn(et_2dtc)_2$.

	g_1	g_2	g_3	P_1^{Cu}	P_2^{Cu}	P_3^{Cu}
Cu						
A_1	0	90	90	6	94	86
A_2	90	4	94	85	22	111
A_3	90	86	4	93	68	22

considerably elongated in the zinc complex, Weeks and Fackler concluded that the copper ion environment in the doped $Zn(et_2dtc)_2$ is similar to that in pure $Cu(et_2dtc)_2$.

IV B 3 Conclusions

The measurements on $Cu/Zn(et_2dsc)_2$ prove that $Cu(et_2dsc)_2$ does not accept the structure of the host crystal, but retains the structure of the pure $Cu(et_2dsc)_2$. This was also found by Weeks and Fackler for the corresponding dithio system. A relevant correspondence between the dimeric system $Cu/Zn(et_2dsc)_2$ and the monomeric systems $Cu/Ni(R_2dsc)_2$ is that the maximum g value has been measured in the molecular plane. In the dithio systems,

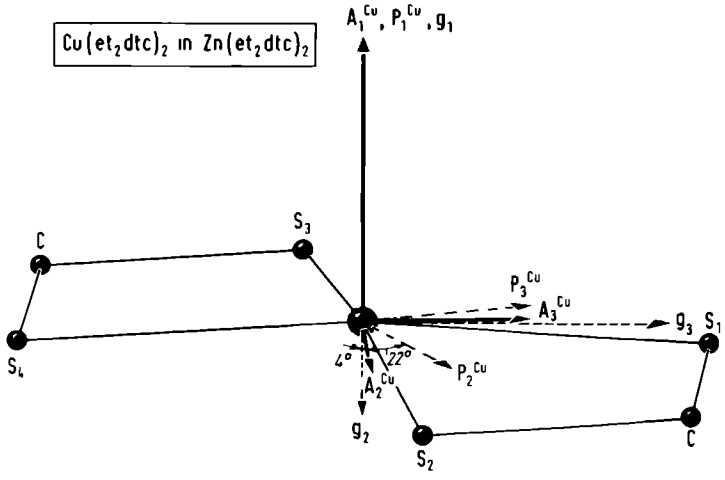

Fig.17 Proposed orientations of the principal axes in $Cu/Zn(et_2dtc)_2$.

however, the maximum g value is perpendicular to this plane, for both dimer and monomers. A difference between the monomeric and dimeric diseleno systems is that, in the dimeric system, the principal axes of the $\bar{\bar{g}}$ tensor and the $\bar{\bar{A}}^{Cu}$ tensor in the xz plane almost coincide. On the other hand, a rotation of the $\bar{\bar{A}}^{Cu}$ principal axes relative to those of $\bar{\bar{g}}$ in the molecular plane seems to be typical for the dimers, for the diseleno compounds as well as for the dithio compounds. Another difference between the monomers and dimers is the magnitude of the copper nuclear quadrupole coupling tensor. In the dimers P_1^{Cu} is $\sim 2\ 10^{-4} cm^{-1}$, whereas its value in the monomeric systems is $\sim 0.5\ 10^{-4} cm^{-1}$.

IV C Powder and glass measurements

IV C 1 Powder spectrum of $Cu/Ni(met_2dsc)_2$

When no single crystals are available, the anisotropic interaction parameters can be determined from a diluted powder spectrum. In powder and glass samples the molecules are distributed over all possible orientations. Consequently the absorption ESR spectrum is a summation of spectra corresponding with the various orientations. In the "strong field" approximation and neglecting the nuclear Zeeman and quadrupole interactions, the resonance condition for a molecule in an arbitrary orientation, where the magnetic field has spherical angles θ and ϕ relative to a chosen

molecular coordinate system, is:

$$B(\theta,\phi,m_I) = \frac{1}{g(\theta,\phi)\mu_b}(h\nu - m_I a(\theta,\phi)) \quad , \qquad \text{(IV.1)}$$

where $g(\theta,\phi)$ and $a(\theta,\phi)$ are defined by the expressions (III.2) and (III.3). In the first derivative ESR spectrum peaks occur for those values of the magnetic field for which applies

$$\frac{\delta B(\theta,\phi,m_I)}{\delta\theta} = \frac{\delta B(\theta,\phi,m_I)}{\delta\phi} = 0 \quad . \qquad \text{(IV.2)}$$

Schaafsma [67] has discussed a system with such a high symmetry that all principal axes of the $\bar{\bar{g}}$ tensor and hyperfine splitting tensor coincide. Then $B(\theta,\phi,m_I)$ is a function of $\cos^2\theta$ and $\cos^2\phi$, so that the peakpositions, derived from the conditions (IV.2), are

a. $\theta = 0$, ϕ indefinite.

b. $\theta = \frac{1}{2}\pi$, $\phi = 0$.

c. $\theta = \frac{1}{2}\pi$, $\phi = \frac{1}{2}\pi$.

For each of these orientations $2I + 1$ equidistant peaks are obtained, from which the principal values of $\bar{\bar{g}}$ and $\bar{\bar{A}}$ can be determined in a straightforward way.

In the case that none of the principal axes of $\bar{\bar{g}}$ and $\bar{\bar{A}}$ coincides, (which situation occurs in most of the systems discussed in this thesis) $B(\theta,\phi,m_I)$ is neither a function of $\cos^2\theta$ nor a function of $\cos^2\phi$. The conditions (IV.2) are not fulfilled by $\theta = 0,\frac{1}{2}\pi$; $\phi = 0,\frac{1}{2}\pi$. One obtains three sets of $2I + 1$ not equidistant peaks, from which the principal values can not be obtained.

If one pair of principal axes coincides, $B(\theta,\phi,m_I)$ is still a function of $\cos^2\theta$ (θ being measured relative to the unique axis) but not of $\cos^2\phi$. This case has been discussed by van Rens [5]. From the conditions (IV.2) it follows:

a. $\theta = 0$, ϕ indefinite. A set of $2I + 1$ equidistant lines, corresponding with the principal values of the coinciding axes.

b,c. $\theta = \frac{1}{2}\pi$, $\left.\frac{\delta B(\theta,\phi,m_I)}{\delta\phi}\right/_{\theta=\frac{1}{2}\pi} = 0$. Two sets of $2I + 1$ not equidistant lines, from which the remaining principal values cannot be determined. If, however, the principal values and the relative position of the principal axes are known (from a single crystal study), the peakpositions in the first derivative powder spectrum can be calculated under the assumptions for which equation IV.1 has been derived. Of course the same can be done by taking trial values for the principal values and the angle between the principal axes. By varying the trial values, optimum agreement between the

measured and calculated peakpositions can be obtained.

In this way the principal values of $Cu/Ni(met_2dsc)_2$ have been determined from the powder spectrum (Fig.18), with the assumption that the axes of g_1 and A_2^{Cu} coincide. In Table IV.13 the measured and calculated fieldpositions are listed. The calculated principal values have been reported in Table IV.3. The angle between the axes of g_2 and A_1^{Cu} appeared to be 58^o, almost as large as the angle in the ethyl compound.

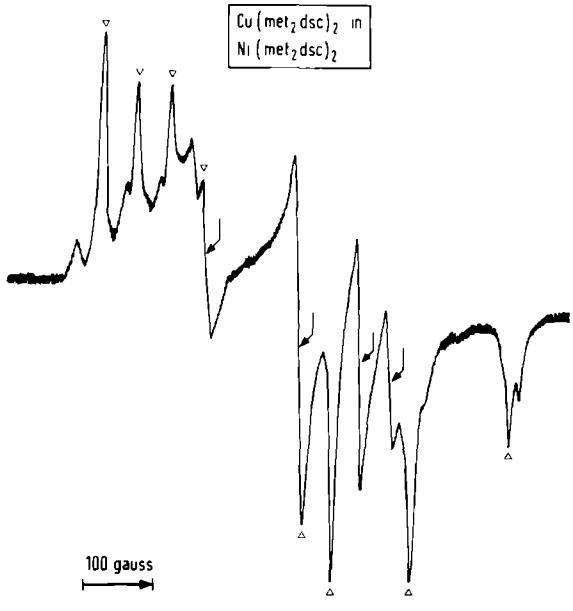

Fig.18 First derivative Q-band ESR spectrum of a powder of $Cu(met_2dsc)_2$ in $Ni(met_2dsc)_2$ at room temperature.

Table IV.13 Measured and calculated peakpositions in the Q-band powder spectrum of $Cu/Ni(met_2dsc)_2$.
Microwave frequency is 34.61 gHz, the angle between g_2 and A_1^{Cu} is 58^o. Principal values of $\bar{\bar{g}}$ and $\bar{\bar{A}}^{Cu}$ are listed in Table IV.3.

m_I	$B_{measured}$	$B_{calculated}$
-3/2	12139.9	12136.0
	12280.8	12279.8
-1/2	12280.8	12278.9
	12333.0	12328.7
+1/2	12370.2	12368.3
	12450.1	12445.8
+3/2	12415.7	12416.1
	12596.6	12593.1

IV C 2 Glass spectrum of $Cu(but_2dsc)_2$

The fact that the axes of the $\bar{\bar{g}}$ and $\bar{\bar{A}}^{Cu}$ tensor do not coincide in the systems $Cu/Ni(R_2dsc)_2$ was initially attributed to influences of neighbouring diselenocarbamate molecules. Therefore it was decided to check this in a liquid solution, because there the complexes are monomeric. Since it is not possible to obtain this information from the liquid solution spectrum itself, the spectrum of $Cu(but_2dsc)_2$ in a frozen solution of chloroform-toluene (40-60%) was recorded. Here the phenomenon occured that a reasonable intensity was measured only between -100 and $-140^{o}C$. Crystallization of the solvent below $-140^{o}C$ can be an explanation of this effect, but then it is not clear why this does not happen in the corresponding dithiocarbamate system where, down to $-190^{o}C$, a good intensity is measured.

The linewidth in the glass spectrum (Fig.19A) is much larger than in the powder spectrum (Fig.18). Therefore the glass spectrum could be interpreted only by using a simulation computerprogram. Only simulations based on coinciding principal axes and Lorentzian lineshapes of the resonance lines of each molecule were carried out. In Fig.19B the optimum spectrum is shown. The linewidth used is 12 gauss, the principal values are tabulated in Table IV.14.

Table IV.14 Experimentally obtained principal values of $Cu(but_2dsc)_2$ in a frozen solution of chloroform-toluene (40-60%) at $-125^{o}C$. (Hyperfine splittings in $10^{-4}cm^{-1}$.)

g_x	2.0020	A_x	- 40.2
g_y	2.0513	A_y	- 56.2
g_z	2.0021	A_z	-145.8
g_{av}	2.0185	A_{av}	- 80.7

The good agreement between the experimental spectrum and the simulated one makes it likely that the principal axes of $\bar{\bar{g}}$ and $\bar{\bar{A}}^{Cu}$ do coincide, although no simulations have been made with non coinciding axes. This should imply that the symmetry of the $Cu(but_2dsc)_2$ molecule in liquid solution is higher than in the doped single crystal of the nickel complex. The data in Table IV.14 show that the g value is almost isotropic in the xz plane, which means that, in fact, it is meaningless to speak about a rotation of the $\bar{\bar{g}}$ tensor relative to the $\bar{\bar{A}}^{Cu}$ tensor in the xz plane.

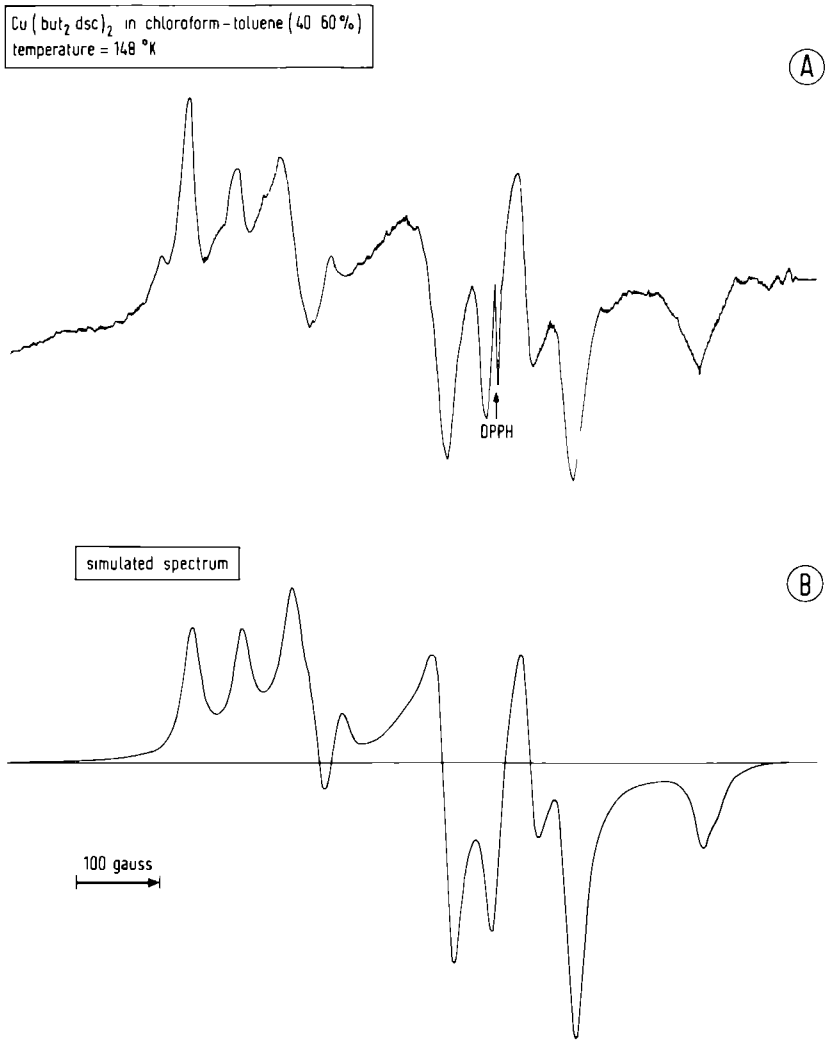

Fig.19A First derivative Q-band ESR spectrum of $Cu(but_2dsc)_2$ in a frozen solution of chloroform-toluene (40-60%) at a temperature of 148°K.
B Simulated spectrum assuming coinciding principal axes of $\bar{\bar{g}}$ and $\bar{\bar{A}}^{Cu}$, using Lorentzian lineshapes. ^{77}Se satellites have not been taken into account.

IV D. Liquid solution spectra

The room temperature liquid solution spectra of the diselenocarbamate complexes of copper (the spectrum of the ethyl complex is shown in Fig.20A) show the four major peaks of which the first and the last are partly split due to the presence of the ^{65}Cu isotope. The spectrum of $Ag(but_2dsc)_2$ (Fig.22) shows two major peaks which are not split by the presence of the two silver isotopes. Each peak is symmetrically flanked by a satellite pair with an intensity of about 16% of the major peaks. These satellites are due to the isotope ^{77}Se.

The isotropic g values (g_{iso}) and hyperfine splittings (A_{iso}) of $Cu(met_2dsc)_2$, $Cu(et_2dsc)_2$, $Cu(but_2dsc)_2$ and $Ag(but_2dsc)_2$ are listed in Table IV.15, together with g_{iso} and A_{iso} of the diethyldithiocarbamate complexes of copper [10] and silver [5]. In Table IV.3 they were listed already to facilitate comparison with the average values of the single crystal measurements. Recently Belford and Pilbrow pointed out that the average of the measured principal hyperfine splittings does not have to be equal to the isotropic hfs, if the hfs tensor is not symmetrical [68]. However, according to our MO calculations (chapter V) the asymmetry in the hfs tensor is never so large that these effects have to be taken into account.

Table IV.15 Experimentally obtained isotropic g values and hyperfine splittings (in $10^{-4}cm^{-1}$) of some diselenocarbamate and dithiocarbamate complexes of copper and silver.

complex	solvent	g_{iso}	$A^{Cu(Ag)}_{iso}$	A^{Se}_{iso}
$Cu(met_2dsc)_2$	chloroform	2.0210	-75.6	+43.3
$Cu(et_2dsc)_2$	chloroform	2.0219	-76.3	+44.0
$Cu(but_2dsc)_2$	chloroform	2.0231	-76.5	+44.9
$Ag(but_2dsc)_2$	chloroform	2.0065	+26.6	+44.3
$Cu(et_2dtc)_2$ a.	benzene	2.0453	-74	
$Ag(et_2dtc)_2$ b.	benzene	2.021	+28.6	

a. Ref.10
b. Ref.5

A liquid solution spectrum does not provide information about the location of the principal axes. On the other hand, a spectrum measured in a glassy solution can yield this information. In section IV C the

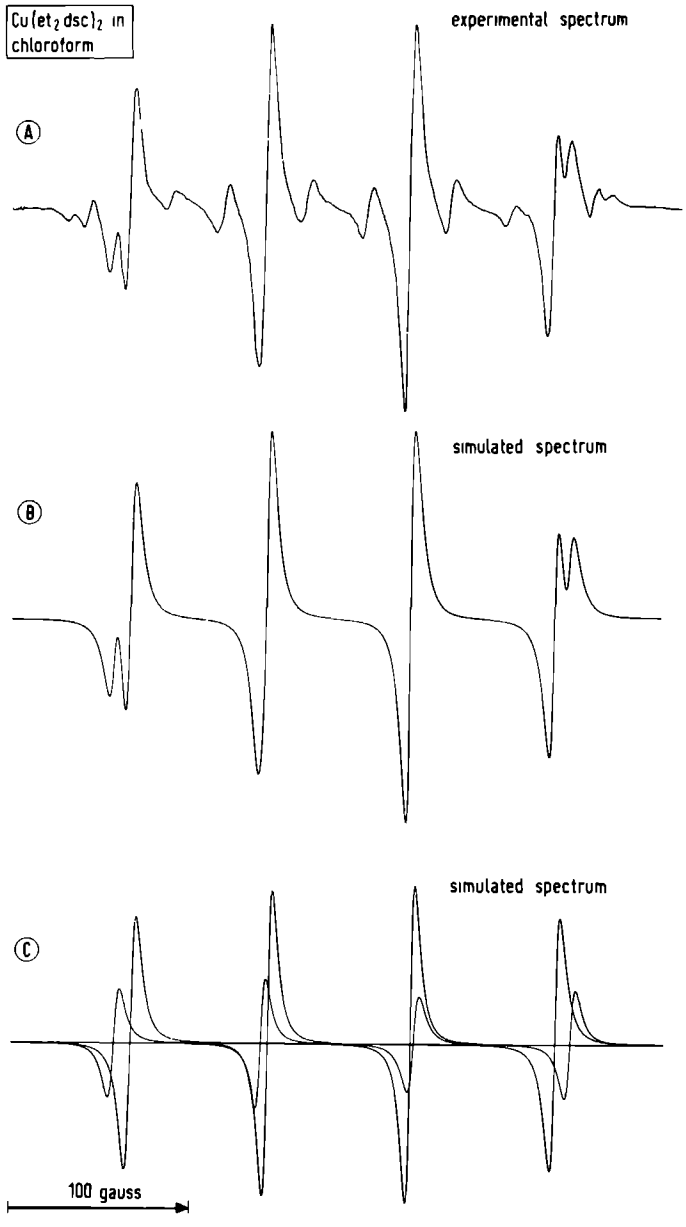

Fig.20A First derivative X-band ESR spectrum of a solution of $Cu(et_2dsc)_2$ in chloroform at room temperature.
B Simulated spectrum using Lorentzian line shapes and calculated line positions. ^{77}Se satellites have not been taken into account.
C Composing lines of the simulated spectrum.

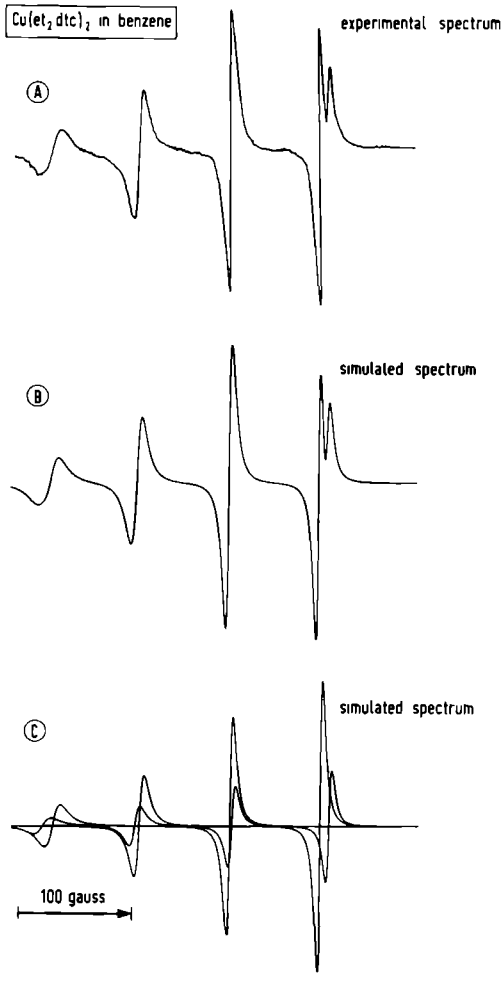

Fig.21A First derivative X-band ESR spectrum of a solution of $Cu(et_2dtc)_2$ in benzene at room temperature.
B Simulated spectrum using Lorentzian line shapes and calculated line positions.
C Composing lines of the simulated spectrum.

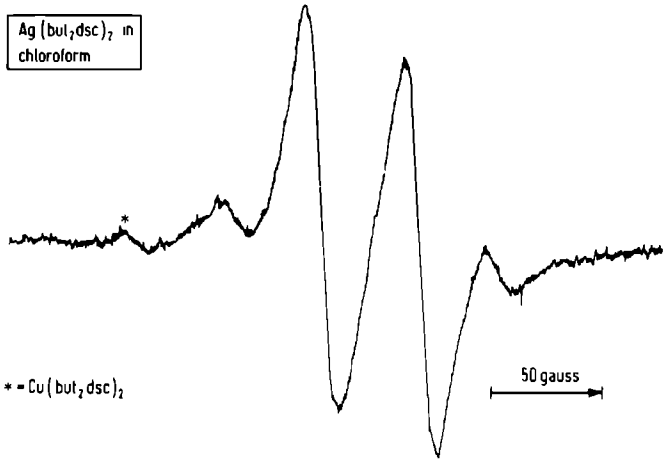

Fig.22 First derivative X-band ESR spectrum of a solution of $Ag(but_2dsc)_2$ in chloroform at room temperature.

spectrum of $Cu(but_2dsc)_2$ in a glassy solution of chloroform-toluene has been discussed. It turned out that the principal axes of $\bar{\bar{g}}$ and $\bar{\bar{A}}^{Cu}$ coincide. It is likely that the same is true for the other diseleno-carbamate complexes in solution, which means that in solution these complexes are planar with equal metal-selenium distances. This is in agreement with the observation of only one selenium hyperfine splitting.

IV D 1 Linewidth variation in spectra of copper complexes

The observed linewidth variation in the liquid solution spectra of the diselenocarbamates is very unusual for spectra of planar copper complexes. A typical example of a "normal" liquid solution ESR spectrum is the spectrum of the copper diethyldithiocarbamate complex, given in Fig.21A, which shows a gradual decrease in linewidth from low to high field. The "abnormal" linewidth variation in the spectra of the diselenocarbamate complexes is probably caused by the change in g values, which occurs in going from dtc to dsc: In all the planar copper complexes, studied up till now, the maximum g value and copper hfs coincide and are normal to the molecular plane. In the diselenocarbamates, however, the maximum Cu hfs is still perpendicular to the molecular plane, but the maximum g value lies in this plane. (See section A of this chapter). Using the relaxation theory of Kivelson [69] we will show

that this change in the relative orientation of the maximum g value and the maximum Cu hfs does result in a different linewidth variation.

Kivelson derived for the relaxation time T_2 of a room temperature spectrum in a diluted liquid solution:

$$T_2^{-1} = \frac{\tau_c}{60\hbar^2}\Big[\{[\,3I(I+1) + 5M_I^2\,]\,\mathrm{Tr}(\bar{\bar{A}}.\bar{\bar{A}}^T) + 8\,[\,\mathrm{Tr}(\bar{\bar{g}}.\bar{\bar{g}}^T) - \tfrac{1}{3}\,(\mathrm{Tr}\,\bar{\bar{g}})^2\,]\,\mu_b^2B^2 + 16\,[\,\mathrm{Tr}(\bar{\bar{g}}.\bar{\bar{A}})\,]M_I\mu_bB\,\} + \frac{1}{1+4\pi^2\nu^2\tau_c^2}\{[\,7I(I+1) - M_I^2\,]\,\mathrm{Tr}(\bar{\bar{A}}.\bar{\bar{A}}^T) + 6\,[\,\mathrm{Tr}(\bar{\bar{g}}.\bar{\bar{g}}^T) - \tfrac{1}{3}\,(\mathrm{Tr}\,\bar{\bar{g}})^2\,]\,\mu_b^2B^2 + 12\,[\,\mathrm{Tr}(\bar{\bar{g}}.\bar{\bar{A}})\,]M_I\mu_bB\,\}\Big]\,, \qquad \text{(IV.3)}$$

here $\bar{\bar{A}}$ is the traceless hyperfine coupling tensor and the $\bar{\bar{g}}$ tensor is diagonal. As has been mentioned earlier, no information is available about the principal values of the tensors in solution, but from the frozen glass spectrum it was deduced that the principal axes of $\bar{\bar{g}}$ and $\bar{\bar{A}}^{Cu}$ coincide. Instead of using the principal values derived from the frozen glass spectrum, which were measured at low temperature (148°K), we decided to use values measured in $Cu/Ni(et_2dsc)_2$, which are measured at room temperature. The principal values used are given in Table IV.16.

Table IV.16 Principal values of the $\bar{\bar{g}}$ tensor and central metal hyperfine splitting tensor (in $10^{-4}cm^{-1}$), used for the calculation of linewidths in liquid solution.

	$Cu(et_2dsc)_2$	$Cu(et_2dtc)_2$	$Ag(but_2dsc)_2$
g_x	1.9981	2.020	1.9280
g_y	2.0511	2.025	2.0820
g_z	1.9981	2.084	1.9965
g_{av}	2.0157	2.043	2.0022
$A_x - A_{av}$	+35.6	+43.0	- 4.0
$A^x - A^{av}$	+29.0	+37.0	- 2.2
$A^y - A^{av}$	-64.6	-80.0	+ 6.2
$A^z - A^{av}$	-79.6	-79.0	+27.8
A_{av}			

The values tabulated for $Cu(et_2dtc)_2$ are those published by Weeks and Fackler [12] for $Cu/Ni(et_2dtc)_2$. For $Cu(et_2dsc)_2$ the values for A_x, A_y,

A_z and g_y are taken from the system $Cu/Ni(et_2dsc)_2$ (section IV A). The values for g_x and g_z are the mean of g_2 and g_3 from the same system, because in the glassy spectrum it was found that the g value is isotropic in the xz plane.

The klystron frequency ν was taken to be 9.2 gHz. The correlation time τ_c was initially estimated using the relation

$$\tau_c = V\eta/kT \quad , \qquad (IV.4)$$

where η is the viscosity of the liquid (η = 0.585 10^{-3} kg/m.sec = 0.585 10^{-2} poises for chloroform at 20°C) and V is the molecular volume. Assuming the volume of the Cu complex in solution to be the same as the volume of the Ni complex in a single crystal (both being monomeric and planar), the volume is estimated to be 441 10^{-30} m^3, being half the volume of a unit cell in $Ni(et_2dsc)_2$ [58]. Substitution of these values of V and η yields for τ_c : 6.4 10^{-11} sec. Since it is well known that Eq.IV.4 overestimates the correlation time [70], the values of τ_c were subsequently changed until the observed and calculated linewidth of the first ^{63}Cu line were the same. The values of τ_c, obtained in this way, for $Cu(et_2dsc)_2$ and $Cu(et_2dtc)_2$ are 1.2 10^{-11} and 0.75 10^{-11} sec., respectively.

The experimental relaxation times were determined by simulation of the experimental spectra, using Lorentzian line shapes and calculated line positions (Fig.20B,C and 21B,C). They are listed in Table IV.17, together with the calculated ones.

Table IV.17 Measured and calculated relaxation times (in 10^{-10} sec.) in X-band liquid solution spectra.

	$Cu(et_2dsc)_2$				$Cu(et_2dtc)_2$				$Ag(but_2dsc)_2$			
	obs.		calc.		obs.		calc.		obs.		calc.	
isotope	63	65	63	65	63	65	63	65	107	109	107	109
M_I												
-3/2	666	653	666	582	296	269	296	268				
-1/2	732	712	660	588	459	429	450	405	274	274	263	263
+1/2	746	612	516	464	674	612	726	639	253	253	253	251
+3/2	666	653	361	325	779	720	1181	981				

The increase in T_2 observed on $Cu(et_2dtc)_2$, is reproduced in the calculated values, but the variation is too large, probably because of

overestimation of the M_I-dependent terms. The linewidth variation calculated for $Cu(et_2dsc)_2$ is indeed different. However, the experimentally observed M_I^2 dependence is not reproduced theoretically, probably because here too the M_I-dependent terms dominate. A calculation using the relative position of the principal axes of the system $Cu/Ni(et_2dsc)_2$ (section IV A) did not improve these results.

The linewidth calculations on $Cu(et_2dtc)_2$ have been performed earlier by Gibson [71]. He found a much better correspondence between the experimental and theoretical linewidths. This is due, however, to an error he made in the dimension of the hyperfine splitting. Moreover, his experimental linewidths refer to the total linewidths of the measured peaks. For a comparison with theoretical values these total linewidths should be decomposed into the widths of the two lines of the copper isotopes, as has been done in Fig.20C and Fig.21C.

IV D 2 Linewidths in the spectrum of $Ag(but_2dsc)_2$

For the calculation of the liquid solution linewidths, the single crystal principal values of $Ag/Ni(but_2dsc)_2$ were used (section IV A). It was assumed that the principal axes or $\bar{\bar{g}}$ and $\bar{\bar{A}}^{Ag}$ coincide. A calculation with the relative position of the axes of the system $Ag/Ni(but_2dsc)_2$ yielded almost the same values. The correlation time τ_c, which gives the experimental linewidth of the low field ^{107}Ag line, was $2.3\ 10^{-11}$ sec. The obtained relaxation times are listed in Table IV.17. Because of the very small anisotropy (see Table IV.16) there is practically no M_I dependence, experimentally as well as theoretically.

CHAPTER V

MOLECULAR ORBITAL CALCULATIONS

The purpose of the ESR experiments is to obtain information about the bonding properties of the transition metal complexes. To this end one often attempts to estimate the contribution of the metal and the ligand orbitals to the MO's from the measured $\bar{\bar{g}}$ tensor and hyperfine splitting tensors. This procedure can be employed in systems of a high symmetry where, in addition, only d-type antibonding MO's (i.e. the "d-orbitals") are important for the spin hamiltonian parameters, because otherwise too many unknowns are to be determined. In this way Maki and McGarvey [40] and Kivelson and Neiman [41] derived expressions for the spin hamiltonian parameters of a tetragonal copper(II) system and deduced numerical values for the LCAO coefficients in the antibonding d-type MO's. Since the symmetry in our systems is C_1 at the most, and since ligand orbitals can be important for the ESR parameters as well, we compare directly the measured ESR quantities with those, calculated by means of the iterative extended Huckel MO method [72]. The advantage of this procedure is that all metal and ligand orbitals can be included, and that the system may have any symmetry.

V A The lcao mo extended huckel method

The computerprogram used [73] was based on the self-consistent charge method. In this method a set of secular equations

$$\sum_j (H_{ij} - E\, S_{ij})\, C_j = 0 \qquad (V.1)$$

is constructed in a semi-empirical way. In these equations H_{ij} and S_{ij} are elements of the hamiltonian and overlap matrix, respectively

$$H_{ij} = \langle \phi_i | h_{eff} | \phi_j \rangle \qquad (V.2)$$

$$S_{ij} = \langle \phi_i | \phi_j \rangle \quad , \qquad (V.3)$$

where ϕ_i are atomic orbitals and h_{eff} is an effective one-electron hamiltonian. By solving these secular equations, the orbital energies ϵ_k and LCAO coefficients C_{jk} are obtained. After occupying the lowest MO's in agreement with the spin multiplicity of the ground state, the Mulliken charges for all atoms are calculated [49]. The hamiltonian matrix, which is chosen to be charge dependent, is recalculated with these charges. This

procedure is repeated until self-consistency is reached, i.e. until the differences between the atomic charges in two successive cycles are less than 0.001 charge unit.

V A 1 Input data

The required input data for the MO calculations are the structure, the atomic wave functions and the hamiltonian matrix.

V A 1a Structure

Because the ESR results have been obtained from single crystal studies in a diamagnetic host complex, the crystal structure of the host complex is used, unless stated otherwise. For copper in the nickel complexes (which are monomeric with C_1 symmetry) the cartesian coordinates of the atoms were computed in a coordinate system with the x and y axes along the bisectors of the angles S(e) - Cu - S(e) {S(e) means S or Se} and the z axis perpendicular to the plane of the copper and the four sulphur (or selenium) atoms.

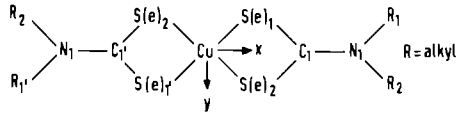

(V.4)

In the cases where the structure of the copper or the zinc complex has been used (both are dimeric and have no symmetry at all when they contain one Cu and one Zn atom) the coordinate system has been chosen such that it resembles as good as possible the above described one.

V A 1b Atomic wave functions

To limit the number of atomic wave functions, we have replaced the ethyl groups by hydrogen atoms and taken the N-H distance to be 1.01 Å. This substitution was justified by one sample calculation, carried out with the full ethyl groups, which showed that the effect of these groups on the calculated spin hamiltonian parameters is small. Moreover a 40% decrease of the N-H distance did not appreciably affect the calculated charge distributions except those on nitrogen and hydrogen. We have taken into account all valence orbitals, i.e. 45 for a monomer and 90 for a dimer calculation.

For the radial part of the atomic wave functions, we used Slater-type orbitals.

$$R_{nl} = \sum_i c_i r^{k_i-1} e^{-\zeta_i r}, \qquad l+1 \leq k_i \leq n. \tag{V.5}$$

Because these functions are used only to calculate the overlap matrix elements, it is sufficient to retain only the term with the highest power of r (k_i=n) and restrict the sum of exponentials for s and p functions to one term,

$$R_{nl} = cr^{n-1} e^{-\zeta r} \tag{V.6}$$

and for d functions to two terms,

$$R_{nl} = r^{n-1}(c_1 e^{-\zeta_1 r} + c_2 e^{-\zeta_2 r}). \tag{V.7}$$

The values of c_i and ζ_i were obtained from the literature [74-76] and are listed in Table V.1.

To calculate the expectation values of r^{-3}, required for the ESR parameters, the complete multiple-exponent Slater-type orbitals were used as published by Clementi [77].

V A 1c Hamiltonian matrix

Diagonal elements, H_{ii}. H_{ii}, which is the energy of an electron in the atomic orbital ϕ_i, is approximated by:

$$H_{ii} = -\alpha_i - \beta_i q_A - \gamma_i q_A^2, \tag{V.8}$$

where α_i is the valence state ionization energy (VSIE) of orbital ϕ_i, q_A is the Mulliken charge of the atom A on which the orbital ϕ_i is centred, and $\beta_i q_A + \gamma_i q_A^2$ describes the charge dependence of the VSIE. The values of α, β and γ were taken from Ref.78 or calculated from the data in Ref.79, and are listed in Table V.1.

The influence of surrounding atoms on H_{ii} is generally to lower the charge dependency. This effect can be taken into account by introducing a parameter k

$$H_{ii} = -\alpha_i - k\beta_i q_A - k^2 \gamma_i q_A^2 \quad (0 \leq k \leq 1). \tag{V.9}$$

Alternatively a point charge approximation can be used

$$H_{ii} = -\alpha_i - \beta_i q_A - \gamma_i q_A^2 - \sum_{B \neq A} \frac{q_B}{R_{AB}} \tag{V.10}$$

in which q_B is the Mulliken charge of the atom B and R_{AB} is the distance between the atoms A and B.

Off-diagonal elements, H_{ij}. The off-diagonal elements are approximated by the Wolfsberg-Helmholz relation [80]

$$H_{ij} = \tfrac{1}{2}KS_{ij}(H_{ii} + H_{jj}) \qquad (V.11)$$

where K is an empirical constant, which is usually taken between 1.5 and 3.0. Cusachs [81] and Jug [82] proposed overlap-dependent formulas for K: $K = 2-|S_{ij}|$ and $K = 2/(1 + S_{ij}^2)$, respectively. These formulas proved to be not very satisfactory for the calculation of the ESR parameters. Therefore, we have used the original relation and searched for the best value of K.

V B. Calculation of esr parameters

The elements of the $\bar{\bar{g}}$, $\bar{\bar{A}}$ and $\bar{\bar{P}}$ tensors were calculated according to the formulas II.57, II.66 and II.80. In the calculation of the $\bar{\bar{A}}$ tensors multiple-centre contributions were neglected, because all operators depend on r^{-3}. Lupei and McMillan [83] have studied the effect of this neglect on the central metal hfs in some Cu(II) square-planar complexes. As expected, they found from their numerical evaluations that the first order two-centre contributions depend strongly on the copper-ligand distance. Above 2.38 Å these contributions are negligible but, in a configuration with four nitrogen atoms at 1.86 Å, this correction represents about 7% of the one-centre contribution. Since in our systems the metal-ligand distances are 2.2 Å at least, the neglect of the multiple-centre contributions to the central metal hfs seems to be justified. The effect of the multiple-centre contributions on the hfs of the ligand atoms has been discussed by van Kemenade [84] for the octahedral ions $M(V)OX_5^{2-}$, with M being Cr, Mo, W and X = F, Cl, Br. For the oxyfluorides (the M-F distance varies from 1.70 to 1.85 Å) these contributions are almost as large as the one-centre first order contribution. For the oxychlorides and bromides (in which the M-X distances are more in agreement with the metal-ligand distances in our systems, namely 2.12 and 2.30 Å respectively) they are of less importance: in the order of 10% of the one-centre contribution. Since the surroundings of the central metal atoms in these ions are octahedral, it is questionable whether these results apply to our systems.

The radial parts of the integrals containing the spin-orbit

operator were not calculated, but approximated by the atomic spin-orbit coupling constants. They were obtained from the references 85, 86 and 87 or were calculated from the data in Ref.79. The values are listed in Table V.1.

Table V.1 Constants of atomic orbitals

		VSIE (eV)			radial function		spin orbit coupling
atom	orbital	α	β	γ	coefficient	exponent	constant (cm^{-1})
Cu	4s	7.72	8.16	1.49	1.0	1.55	-
	3d	10.64	14.74	1.22	0.593322 0.574421	5.95 2.30	828
	4p	3.91	5.30	1.38	1.0	1.73	925
Zn	4s	9.40	8.60		1.0	1.60	-
	3d	17.35	10.65		0.602937 0.561873	6.15 2.40	1088
	4p	5.00	6.90		1.0	1.43	583
S	3s	20.67	15.37	1.52	1.0	2.1223	-
	3p	11.58	12.21	1.63	1.0	1.8273	382
Se	4s	21.77	12.10	0.18	1.0	2.4394	-
	4p	9.75	12.38	-0.63	1.0	2.0718	1690
C	2s	21.20	17.51	3.47	1.0	1.6083	-
	2p	10.77	13.88	3.48	1.0	1.5679	28
N	2s	28.02	20.25	3.48	1.0	1.9237	-
	2p	16.04	14.13	3.72	1.0	1.9170	76
H	1s	13.60	27.18	13.62	1.0	1.0	-

After the calculation of the tensors, they were multiplied with their transposed and the resulting symmetric squared tensor was diagonalized. The principal values were obtained by taking the square root of the eigenvalues. The eigenvectors are the principal axes of the tensor itself.

V C Choice of empirical parameters

To obtain the best choice of the empirical parameters in the elements of the H matrix, the g values and hfs's of $Cu/Ni(et_2dtc)_2$ were calculated for varying parameter values. This system has been measured by Weeks and Fackler [12] and is a rather simple one, compared with the diseleno-carbamate systems: the principal axes of the $\bar{\bar{g}}$ tensor and $\bar{\bar{A}}^{Cu}$ tensor coincide and point along the coordinate axes as defined in V.4. The experimentally determined principal values are listed in Table V.2. The largest g value and (in absolute value) largest hfs point perpendicular to the molecular plane along the z axis. The smallest g value and hfs point along the x axis towards the ligands.

Table V.2 Experimentally determined principal values of $\bar{\bar{g}}$, $\bar{\bar{A}}^{Cu}$ and $\bar{\bar{P}}^{Cu}$ (in $10^{-4}cm^{-1}$) of $Cu/Ni(et_2dtc)_2$ [12,17].

$A_{xx} - A_{av}$	43.0 ± 1.9	g_{xx}	2.0200 ± 0.0010	P_{xx}	-0.25
$A_{yy} - A_{av}$	37.0 ± 1.9	g_{yy}	2.0250 ± 0.0010	P_{yy}	-0.25
$A_{zz} - A_{av}$	-80.0 ± 1.4	g_{zz}	2.0840 ± 0.0005	P_{zz}	+0.5
A_{av}	-79.0 ± 1.4				

Although it is likely that the Cu-S distances in the guest $Cu(et_2dtc)_2$ molecules are larger than the Ni-S distances (listed in Table IV.2), the structure of the Ni complex [60] has been used in the computations, because the calculated ESR parameters appeared to be rather insensitive to small changes in these distances.

V C 1 Molecular orbitals

Table V.3 lists the MO energies, the occupation numbers, and the atomic orbitals of copper, sulphur, and carbon which have a coefficient larger than 0.3, as computed with K = 2.5 (Eq.V.11) and k = 0.0 (Eq.V.9). It is striking that the MO's which are mainly composed of the metal d orbitals (and which correspond with the antibonding 3d orbitals in a crystal field model) are not in sequence: one of the MO's which are built up from ligand p orbitals is situated between them. This result is not due to the approximations of the extended Huckel method because Demuynck and Veillard [88] and also van der Lugt [89] found the same sort of ordening of the energy levels in $CuCl_4^{2-}$, by using much more sophisticated computation methods.

For all calculations it turned out that the MO of the unpaired electron has at most 60% $3d_{xy}$ character. For lower values of the Wolfsberg-Helmholz constant K, the difference between the results of various charge-dependent H_{ii} (Fq.V.9 and V.10) is considerable, but for increasing K this difference is reduced. This is clearly demonstrated in Fig.23 where the LCAO coefficient $C_o^{3d_{xy}}$ is shown as a function of K.

The computed Mulliken charges on the copper atom are shown in Fig.24. It appears that the ionicity decreases with increasing values for K and k. For the values of K above 2.1, calculations with the point charge correction yield a still higher ionicity. A calculation of the overlap population between the copper and sulphur atoms (O_{Cu-S}) indicates that the covalent bonding (for which the overlap population is a measure) between

Table V.3 $Cu(H_2dtc)_2$ with the structure of $Ni(et_2dtc)_2$.
Energies, occupation numbers, and symmetries of MO's, computed with K = 2.5 and k = 0.0, and the most important coefficients of copper, sulphur, and carbon atomic orbitals.

MO no.	No. of electrons	Energy	Symmetry	Orbitals of Cu	Orbitals of S(1)	Orbitals of S(2)	Orbitals of C(1)
1	0	91.2	u				+0.77s + 0.52x
2	0	90.5	g				+0.73s + 0.55x
3	0	61.7	u	0.89x	-0.54s - 0.52y	-0.49s + 0.48y	+0.55s - 0.45x
4	0	57.3	g	0.82s	-0.54s - 0.45y	-0.51s + 0.43y	+0.62s - 0.39x
5	0	39.0	g	0.80s			-0.37s - 0.31x
6	0	37.5	u	0.65x			-0.36s - 0.39x
7	0	35.9	u	0.49y	+0.37s	-0.41s	+0.57y
8	0	35.0	g				+0.56y
9	0	28.5	u	0.97y	+0.33s	-0.36s	
10	0	23.6	g	0.90s	+0.45x		+0.59x
11	0	22.1	g	0.30s		+0.35x - 0.34y	-0.61y
12	0	20.3	u	1.05x	+0.47x	+0.31x	+0.57x
13	0	17.2	u	0.81y	-0.42x	+0.54x	-0.61y
14	0	0.4	u	0.85z	-0.36x	-0.35x	+0.36z
15	0	- 2.4	g		+0.33z	+0.32z	-0.66z
16	0	- 4.2	u	0.60z			-0.57z
17	1	- 5.0	g	0.73xy	-0.37x	+0.38x	
18	2	- 9.7	g	0.81yz	+0.32z	-0.32z	
19	2	-10.2	g	0.94xz			
20	2	-10.3	g	$0.97x^2-y^2$			
21	2	-10.4	u		+0.45y	+0.44y	
22	2	-10.5	g	$0.96z^2$			
23	2	-10.9	u		+0.50z	-0.51z	
24	2	-11.6	g	0.44xy	-0.41y	-0.40y	
25	2	-11.8	u		+0.39x	+0.41x	
26	2	-11.9	g	0.59yz	-0.38z	+0.39z	
27	2	-13.3	g	0.31xz	+0.36z	+0.34z	
28	2	-13.4	g	0.42xy		-0.43x	
29	2	-13.4	u		+0.37z	+0.36z	
30	2	-13.5	g	0.33xy	+0.41x		
31	2	-14.6	u		+0.32x	-0.32x	
32	2	-15.0	u		+0.36y	-0.34y	
34	2	-18.2	g				+0.30z
35	2	-18.2	u				+0.30z
40	2	-23.9	g		+0.30s	-0.30s	
41	2	-24.2	u		+0.31s	-0.32s	

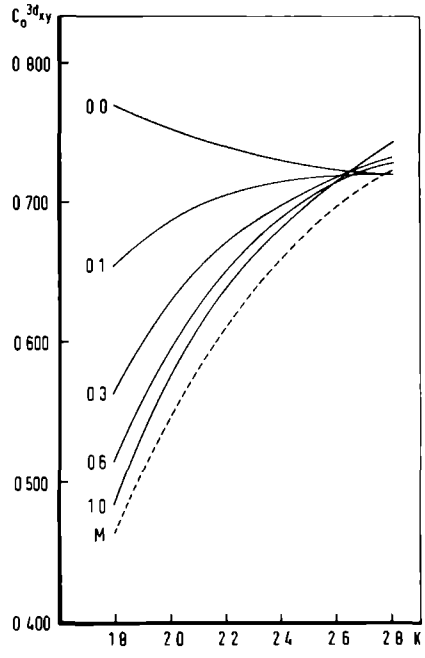

Fig.23 The LCAO coefficient $C_o^{3d_{xy}}$ of the $3d_{xy}$ atomic orbital in the MO of the unpaired electron in $Cu(et_2dtc)_2$ vs. the Wolfsberg-Helmholz parameter K. Solid lines refer to calculations with different values of the charge dependency parameter k. The dashed line represents calculations with a point charge approximation for the charge dependency of the hamiltonian matrix.

the copper and sulphur atoms increases when the ionicity decreases. An example of a rather ionic bonding is the calculation with K = 1.8 and k = 0.0 (q_{Cu} = 0.96; $q_{S(1)}$ = -0.51; $q_{S(2)}$ = -0.54; $O_{Cu-S(1)}$ = 0.11; $O_{Cu-S(2)}$ = 0.11 electron unit); an example of a nearly complete covalent bonding is the calculation with K = 2.8 and k = 0.0 (q_{Cu} = -0.24; $q_{S(1)}$ = -0.22; $q_{S(2)}$ = -0.24; $O_{Cu-S(1)}$ = 0.25; $O_{Cu-S(2)}$ = 0.24 electron unit). The calculation with k = 0.0 and K = 2.5 (for which the MO scheme has been given in Table V.3) yields a relatively strong covalent bonding with q_{Cu} = 0.01, $q_{S(1)}$ = -0.27, $q_{S(2)}$ = -0.30, $O_{Cu-S(1)}$ = 0.23, and $O_{Cu-S(2)}$ = 0.22 electron unit.

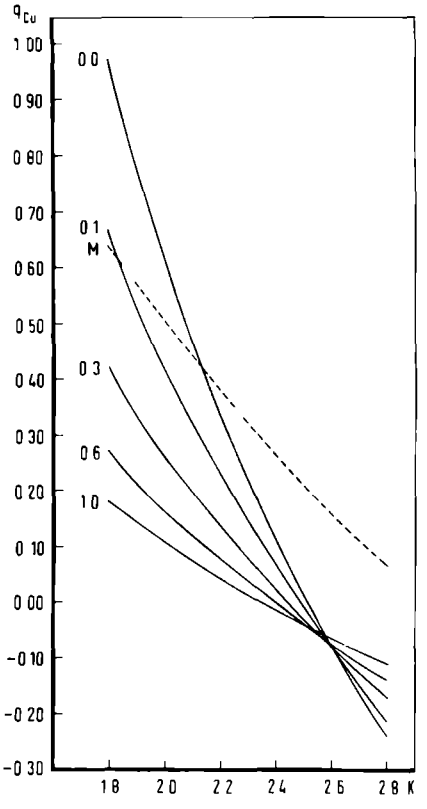

Fig.24 Mulliken charges (in electron units) on the copper atom in $Cu(et_2dtc)_2$ vs. the Wolfsberg-Helmholz parameter K. Details are given in the caption of Figure 23.

V C 2 $\bar{\bar{g}}$ Tensor

The computed g_{11} values are plotted in Figure 25A,B,C as a function of K. The plots show that g_{11} increases as k is lowered from 1.0 to 0.0. Further it is clear that this dependency on k decreases when K increases and almost vanishes for K ≈ 2.5.

A comparison with the observed values indicates that the best results for g_{11} are obtained for K = 2.5 and k = 0.0. The MO scheme, that was given in Table V.3, was also calculated with these values. The value k = 0.0 means that the charge dependency of H_{11} (Eq.V.9) is cancelled by the surrounding atoms. It means also that it suffices to use the non-iterative extended Huckel method, which saves much computer time.

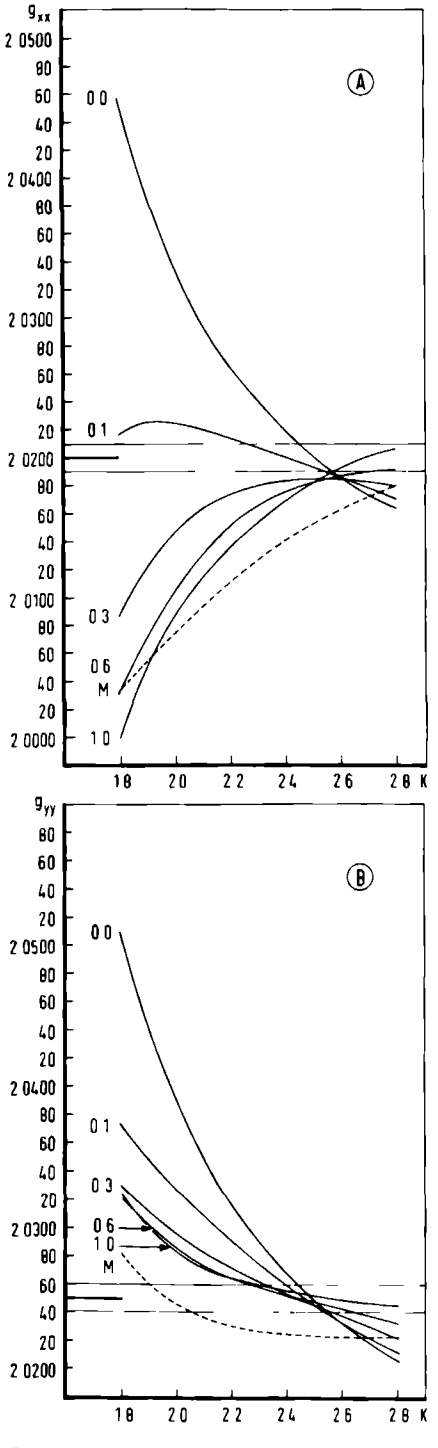

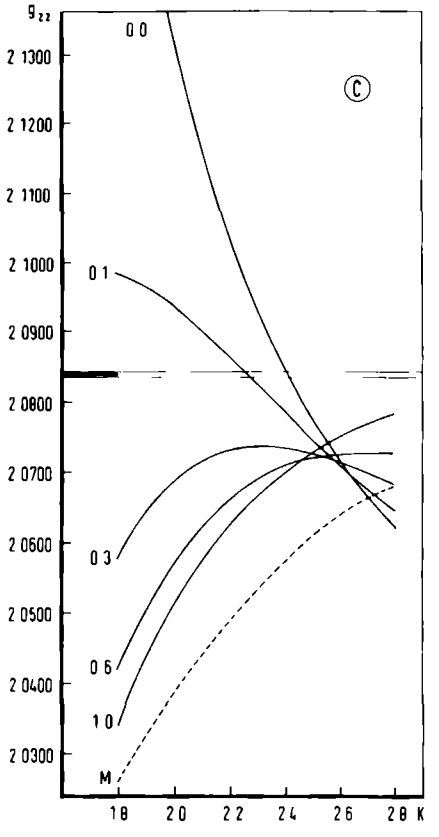

Fig.25
Calculated g values of $Cu(et_2dtc)_2$ vs. the Wolfsberg-Helmholz parameter K. The solid bars refer to the experimentally measured values of g_{ii}. The horizontal lines denote the experimental error. Further details are given in the caption of Fig.23.

Since the part of the MO of the unpaired electron that is centred on the copper atom consists mainly of the $3d_{xy}$ orbital, it follows from Eq.II.57 and Table V.4 that the main contributions to Δg_{xx} and Δg_{zz} (Δg_{ii} being $g_{ii} - 2.00229$) arise from excitations to the MO of the unpaired electron from MO's 19 and 20, respectively. This is due to the fact that these MO's have mainly $3d_{xz}$ or $3d_{x^2-y^2}$ character. The main contributions to Δg_{yy} arise from excitations from MO's 18 and 26 which have mainly $3d_{yz}$ character. The largest contribution is due to MO 26 (0.0204 relative to 0.0016), although the $3d_{yz}$ coefficient in this MO is smaller and the excitation energy is higher than the corresponding values in MO 18. This is caused by the fact that the metal and sulphur contributions to Δg_{yy} partly cancel for the excitation arising from MO 18, whereas they reinforce each other for the excitation from MO 26. This effect may lead to large errors if only excitations from "antibonding d levels" are taken into account.

As may be expected for a nearly D_{2h} symmetry, the directions of the principal axes are calculated to be along (within 1.25°) the x, y, and z axes (see V.4), which is in agreement with the experimentally observed directions [12].

Table V.4 Functions obtained from s, p, and d orbitals using the operators L_x, L_y, and L_z.

orbital	L_x	L_y	L_z
s	0	0	0
p_z	$-ip_y$	ip_x	0
p_x	0	$-ip_z$	ip_y
p_y	ip_z	0	$-ip_x$
d_{z^2}	$-i\sqrt{3}d_{yz}$	$i\sqrt{3}d_{xz}$	0
d_{xz}	$-id_{xy}$	$id_{x^2-y^2} - i\sqrt{3}d_{z^2}$	id_{yz}
$d_{x^2-y^2}$	$-id_{yz}$	$-id_{xz}$	$2id_{xy}$
d_{yz}	$id_{x^2-y^2} + i\sqrt{3}d_{z^2}$	id_{xy}	$-id_{xz}$
d_{xy}	id_{xz}	$-id_{yz}$	$-2id_{x^2-y^2}$

V C 3 Isotropic hyperfine coupling of copper

According to Eq.II.67, $a_{iso} = \frac{3\pi}{3} g_e \mu_b g_{Cu} \mu_n (C_o^{4s})^2 |\phi_{4s}(0)|^2 = 1131 (C_o^{4s})^2$, where C_o^{4s} is the coefficient of the 4s atomic orbital in the MO of the

unpaired electron. Because C_o^{4s} varies between 0.0038 and 0.0050 for different values of K and k, a_{iso} varies between 0.016 10^{-4} and 0.025 $10^{-4}cm^{-1}$. A comparison with the observed value of (-79.0 ± 1.4) $10^{-4}cm^{-1}$ shows that this contribution is negligibly small and has the wrong sign. A second contribution to a_{iso} originates from the second order terms in Eq.II.66, which yield a non-traceless tensor. This contribution has been calculated to vary between 2.4 10^{-4} and 19.3 $10^{-4}cm^{-1}$ and has also the wrong sign. Therefore the main contribution to a_{iso} must be the spin polarization of the inner-core s orbitals, which is indeed negative [53] but cannot be calculated with the extended Huckel method.

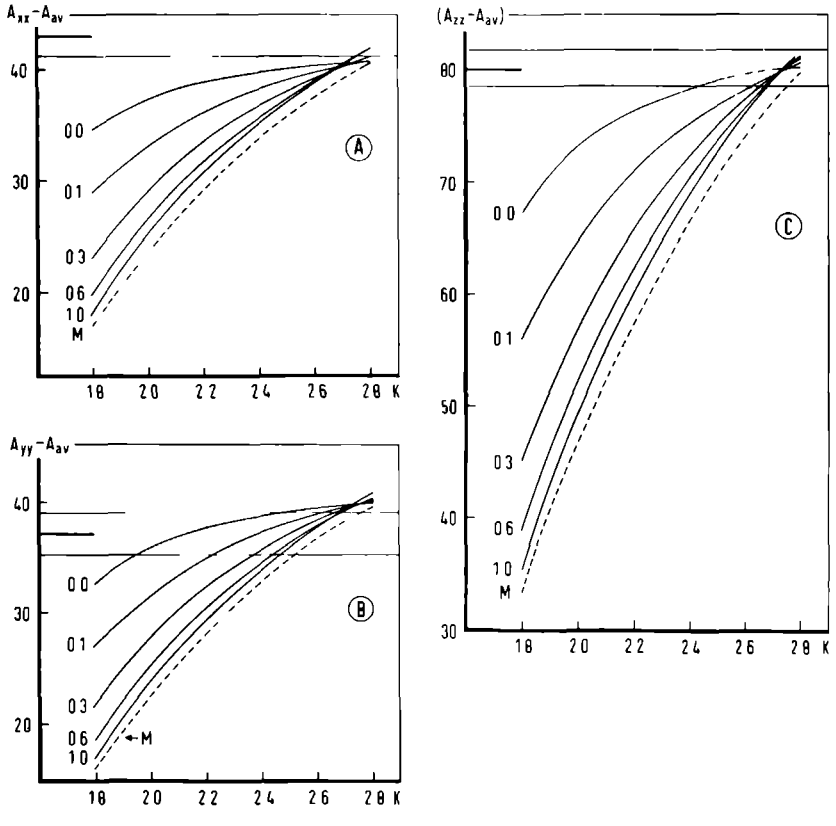

Fig.26 Absolute values of the anisotropic parts of the ^{63}Cu hyperfine couplings (in $10^{-4}cm^{-1}$) of $Cu(et_2dtc)_2$ vs. the Wolfsberg-Helmholz parameter K. The solid bars refer to the experimentally measured values of $(A_{11}-A_{av})$. The horizontal lines denote the experimental error. Further details are given in the caption of Fig.23.

V C 4 Anistropic hyperfine coupling of copper

The figures 26A,B,C show the principal values of the traceless hyperfine coupling tensor of copper as a function of K. The measured anisotropy in the xy plane is not reflected in the calculated results: the maximum calculated difference between $(A_{xx} - A_{av})^{Cu}$ and $(A_{yy} - A_{av})^{Cu}$ is 2.1 $10^{-4}cm^{-1}$, whereas the measured difference is 6 $10^{-4}cm^{-1}$. The calculated anisotropy can be influenced slightly by changing the copper-ligand distances.

From the figures it can be seen that good agreement between experimental and theoretical values is again obtained for K = 2.5 and k = 0.0. The calculated couplings for these parameter values are: $A_{xx} - A_{av} = +40.0\ 10^{-4}$, $A_{yy} - A_{av} = +39.0\ 10^{-4}$, and $A_{zz} - A_{av} = -79.0\ 10^{-4}cm^{-1}$. The main contribution to these values is due to the dipole-dipole interaction, which yields in first order $A_{xx} = A_{yy} = +47.9\ 10^{-4}cm^{-1}$ and $A_{zz} = -95.8\ 10^{-4}cm^{-1}$. The contributions due to the second order terms in Eq.II.66 are: $A_{xx} = -7.9\ 10^{-4}$, $A_{yy} = -8.9\ 10^{-4}$, and $A_{zz} = +16.8\ 10^{-4}cm^{-1}$, where we have subtracted the isotropic part. The second order contribution originates mainly from an excitation from MO 20, which consists almost entirely of the copper $3d_{x^2-y^2}$ orbital.

V C 5 Hyperfine coupling of sulphur

Although no results have been published about the hfs of sulphur in this system (probably because the only isotope with a magnetic moment, viz. ^{33}S, has a natural abundance of 0.74%) it is interesting to examine what these calculations predict for the ^{33}S hfs. The calculation with K = 2.5 and k = 0.0 yields, for both S(1) and S(2), a dipole-dipole interaction of $A_1^S = +10.1\ 10^{-4}$, $A_2^S = -5.0\ 10^{-4}$, and $A_3^S = -5.1\ 10^{-4}cm^{-1}$, and a second order contribution which is practically zero.

The calculated isotropic ^{33}S hfs's for S(1) and S(2) are 11.2 10^{-4} and 11.6 $10^{-4}cm^{-1}$ respectively. These isotropic hfs's are brought about by the density of the unpaired electron in the sulphur 3s orbitals and are not influenced by the second order contributions to the hfs. Since it is not expected that core polarization is important, these values may be compared directly with the value of 10.7 $10^{-4}cm^{-1}$ for the ^{33}S hfs of $Cu((iso\text{-}propyl)_2dtc)_2$ in benzene, measured by Pettersson and Vanngård [10]. The agreement is satisfactory.

V C. 6 Quadrupole coupling of copper

The quadrupole coupling of copper in this system has been measured by So and Belford [17]. Assuming an axial symmetry for all tensors, they have found $P_{zz} = 0.5\ 10^{-4} cm^{-1}$. It turns out that the extended Hückel method cannot reproduce these small numbers, probably because spin-orbit coupling effects and thermal mixing of states are neglected. The calculation yields a nearly axially symmetric tensor with principal value $P_{zz} = 2.7\ 10^{-4} cm^{-1}$.

V C 7 Conclusions

The calculations, discussed in this section, show that it is possible to calculate spin hamiltonian parameters for $Cu(et_2dtc)_2$ with the aid of the extended Hückel MO method, in agreement with the experimental values, employing reasonable values for the empirical parameters. These parameter values (viz. K = 2.5 and k = 0.0) were used in all other calculations in the rest of this chapter.

On the other hand, one may conclude that the MO's, calculated with these parameter values, give a fair description for the ground state of this complex. The bonding is largely covalent, with overlap populations between the copper and sulphur atoms of 0.22 electron unit. The Mulliken charges on the atoms are rather low: for instance, 0.008 on the copper atom and -0.27 and -0.30 on the sulphur atoms.

The unpaired electron is strongly delocalized; the density on the copper atom (obtained by summing squares of LCAO coefficients) is only 0.53, while the density on each sulphur atom is 0.15 electron units. The relatively high position of the MO of this single electron corresponds well with the experimentally observed redox behaviour of $Cu(R_2dtc)_2$: oxidation to $Cu(R_2dtc)_2^+$ is easy (half-wave potential 0.47 Volt with respect to a saturated calomel electrode in CH_2Cl_2), whereas reduction to $Cu(R_2dtc)_2^-$ appeared to be impossible [90].

V D. The monomeric systems $Cu(R_2dsc)_2$ and $Ag(R_2dsc)_2$ diluted in $Ni(R_2dsc)_2$

The study of the diselenocarbamate systems has been started because the hyperfine splitting of the ligand selenium atoms can be measured more easily than the hyperfine splitting of sulphur in the corresponding dithiocarbamate systems. These ligand hyperfine splittings should yield extra information about the electronic and the molecular structure of these complexes. A disadvantage of these systems is the large spin-orbit

coupling of selenium which results in large ligand contributions to the g values. Furthermore, an extra complication is found in the relative orientation of the principal axes of the $\bar{\bar{g}}$ tensor and the central metal hfs tensor, as has been discussed in chapter IV. In this section an explanation is given for the non-coincidence of the principal axes of these tensors. The results of the MO calculations give some insight in the bonding in these complexes.

V D 1 The systems Cu/Ni$(R_2dsc)_2$

As has been discussed in section IV A, the study of these monomeric systems was started, supposing that the structure of the guest copper complex resembles very much the structure of the host compound, the nickel complex. This supposition was justified by the observation of just two different selenium hfs's, which implies that the inversion centre is retained and hence that the central part of the molecule (consisting of copper and the four selenium atoms) has to be planar as in the host molecule. Also the angles between $A_1^{Se_1}$ and $A_1^{Se_2}$ agree very well with the crystallographic angle Se_1-Ni-Se_2. Other structural data, as the lengths of the distances Cu-Se, are hard to obtain from ESR results.

To study the effect of a deviation from the structure of the host, we have calculated the MO's and their energies with the extended Hückel method for a number of different structures.

V D 1a Molecular orbitals

In Table V.5 the most important coefficients and energies are listed assuming the structure of Ni$(et_2dsc)_2$. Compared with the dithio system (Table V.3), more ligand orbitals are found between the "antibonding d" levels. This is because the Se 4p orbital is much higher in energy than the S 3p orbital. Moreover, the delocalization of the copper d-electrons is more complete in the diselenocarbamate system. This is not true, however, for the MO's which contain $3d_{x^2-y^2}$ and $3d_{z^2}$; these MO's are almost non-bonding in both systems.

The energy difference between the two highest occupied MO's in the dsc compound is smaller than in the dtc complex. This is in accordance with the observations of Furlani c.s. [91] who found that the first d-d absorption in diselenocarbamates is always at a lower frequency. Van der Linden and Geurts [92] concluded from voltametric measurements

Table V.5 $Cu(H_2dsc)_2$ with the structure of $Ni(et_2dsc)_2$.
Energies, occupation numbers, and symmtries of MO's, computed with K = 2.5 and k = 0.0, and the most important coefficients of copper, selenium, and carbon atomic orbitals.

Mo no.	No. of electrons	Energy (eV)	Symmetry	Orbitals of Cu	Orbitals of Se(1)	Orbitals of Se(2)	Orbitals of C(1)
1	0	98.5	u				+0.74s + 0.62x
2	0	98.1	g				+0.71s + 0.64x
3	0	55.5	u	1.04x	-0.50s - 0.52y	-0.48s + 0.50y	+0.55s - 0.34x
4	0	53.4	g	1.12s	-0.53s - 0.44y	-0.51s + 0.43y	+0.52s - 0.28x
5	0	39.4	g	0.61s			-0.39s - 0.31x
6	0	37.8	u	0.58x			-0.31s - 0.42x
7	0	33.8	u	0.50y	+0.30s	-0.31s	+0.42y
8	0	33.2	g				+0.38y
9	0	28.6	u	1.14y	+0.36s - 0.29x	-0.38s + 0.30x	
10	0	19.0	g	0.79s	+0.48x	+0.36x	-0.33s + 0.59x
11	0	16.8	g			+0.36x - 0.38y	-0.69y
12	0	15.2	u	0.92x	+0.49x	+0.36x	-0.32s + 0.51x
13	0	12.7	u	0.61y	-0.40x	+0.51x	-0.67y
14	0	- 0.2	u	0.87z	-0.35z	-0.35z	+0.33z
15	0	- 2.9	g		+0.33z	+0.32z	-0.63z
16	0	- 4.4	u	0.57z			-0.56z
17	1	- 4.4	g	0.64xy	-0.40x	+0.40x	
18	2	- 8.9	g	0.51yz	+0.44z	-0.45z	
19	2	- 9.0	u		+0.41y	+0.40y	
20	2	- 9.2	u		+0.46z	-0.46z	
21	2	-10.0	g	0.82xz			
22	2	-10.3	u		+0.37x	+0.38x	
23	2	-10.3	g	$0.47z^2$			
				$-0.83x^2-y^2$			
24	2	-10.5	g	$0.80z^2$			
				$+0.53x^2-y^2$			
25	2	-10.5	g	0.42xy	-0.38y	-0.38y	
26	2	-11.1	g	0.86yz			
27	2	-11.7	u		+0.38z	+0.37z	
28	2	-11.8	g	0.55xz	+0.31z	+0.30z	
29	2	-11.9	g	$0.31z^2$			
30	2	-12.4	g	0.66xy			
31	2	-13.2	u		+0.31x	-0.30x	
32	2	-14.2	u		+0.32y	-0.31y	
34	2	-18.1	g				+0.30z
35	2	-18.1	u				+0.30z
40	2	-24.3	g		+0.33s	-0.34s	
41	2	-24.6	u		+0.34s	-0.35s	

that copper diselenocarbamate complexes are more easily oxidized than the sulphur analogs. This observation too is in accordance with the results of the extended Huckel method: the calculated energy of the MO of the unpaired electron in dsc is higher than in dtc.

V D 1b Hyperfine coupling of copper

The larger delocalization of the unpaired electron in the dsc compounds is reflected in the calculated dipole-dipole contribution of the copper hfs: $A_1 = -73.0\ 10^{-4}$ and $A_2 = A_3 = +36.5\ 10^{-4} cm^{-1}$, while in the dithiocarbamate system the values are $-95.8\ 10^{-4}$ and $+47.9\ 10^{-4} cm^{-1}$, respectively. By adding the second order contributions, the values are obtained which are listed in Table V.6. The data in this table show that the agreement between the calculated and the experimentally obtained (purely anisotropic) hfs's of copper is very good. Furthermore it appears that the calculated anisotropy in the xy plane is much better than in the dithiocarbamate system.

The calculated rotation of the Cu hfs in the xy plane is too small: about 1^o whereas the experimental rotation angle in the ethyl system is 3^o and in the butyl system 10^o (see Table IV.4 and Figures 10 and 12). The larger angle in the butyl complex can be attributed to the large difference between the Cu-Se_1 and Cu-Se_2 distances: the calculated angle between g_1 and A_2^{Cu} increases when the difference between the Cu-Se_1 and Cu-Se_2 distances is enlarged. In that case mixing occurs of the $3d_{xy}$ orbital with $3d_{z^2}$ and $3d_{x^2-y^2}$. This brings about a first order contribution to A_{xy}. A second order contribution arises from mixing of the $3d_{xz}$ and $3d_{yz}$ orbitals.

V D 1c Hyperfine coupling of selenium

Like the Cu hfs, the calculated selenium hfs's agree very well with the experimental ones (Table V.6). The agreement of the isotropic splittings suggests that contributions of inner-shell s electrons can be neglected, as has been done in these calculations. Since the isotropic part due to the second order terms in Fq.II.66 is small, (it does not exceed 2% of the total calculated value) the coefficient C_o^{4s} of the Se 4s orbital in the MO of the unpaired electron can be obtained rather accurately from the experiment:

$$A_{av}^{Se} = \frac{8\pi}{3} g_e \mu_b g_{Se} \mu_n |\phi_{4s}(0)|^2 (C_o^{4s})^2 , \qquad (V.12)$$

where $|\phi_{4s}(0)|^2$ is the 4s electron density at the nucleus. The coefficients, obtained in this way, are 0.103 and 0.100 for Se_1 and Se_2, respectively. The theoretically obtained coefficients are 0.101 and 0.100.

The second order contribution to the anisotropic traceless Se hfs tensor is larger than in the dithiocarbamate system. For the axial component A_1^{Se}, however, this contribution is only 3% of the calculated value. This means that it is possible to determine the coefficients of the Se 4p orbitals in the MO of the unpaired electron from the observed anisotropic hyperfine values. The experiment shows that A_1^{Se} points from Se towards Cu and hence the Se 4p orbital points in this direction. In the coordinate system of Eq.V.4 the normalized Se 4p orbital which

Table V.6 Experimentally obtained and calculated principal values of $\bar{\bar{g}}$, $\bar{\bar{A}}^{Cu}$, $\bar{\bar{P}}^{Cu}$, and $\bar{\bar{A}}^{Se}$ in the system $Cu/Ni(et_2dsc)_2$.

	obs.	calc.		obs.	calc.		obs.	calc.
Cu			Se_1			Se_2		
$A_1 - A_{av}$	-64.6	-62.3	$A_1 - A_{av}$	+57.2	+55.7	$A_1 - A_{av}$	+58.0	+55.4
$A_2 - A_{av}$	+29.0	+28.8	$A_2 - A_{av}$	-26.1	-27.0	$A_2 - A_{av}$	-25.5	-26.7
$A_3 - A_{av}$	+35.6	+33.5	$A_3 - A_{av}$	-31.1	-28.7	$A_3 - A_{av}$	-32.5	-28.7
A_{av}	-79.6		A_{av}	+48	+45.5	A_{av}	+45	+46.5
			Cu					
g_1	2.0511	2.0591	P_1	+0.3	+1.7			
g_2	2.0021	2.0533	P_2	0.0	-0.8			
g_3	1.9941	1.9912	P_3	-0.3	-0.9			

points in the direction from Se to Cu can be written:

$$4p^{Se} = \cos\alpha\ 4p_x^{Se} + \sin\alpha\ 4p_y^{Se} , \qquad (V.13)$$

where α is the angle between the x axis and the Cu-Se bond. This expression holds if the molecule is perfectly planar, otherwise the $4p_z$ function must be taken into account. For the nearly planar monomeric systems under investigation, V.13 is therefore a good approximation. For p orbitals the first order contribution in Eq.II.66 can be rewritten:

$$A_1^{Se} = \frac{4}{5} g_e \mu_b g_{Se} \mu_n \langle r^{-3} \rangle (C_o^{4p})^2 . \qquad (V.14)$$

Here C_o^{4p} is the coefficient of the 4p orbital (defined in Eq.V.13) in

the MO of the unpaired electron and $\langle r^{-3} \rangle$ is the expectation value of r^{-3} of a Se 4p atomic orbital. No information can be obtained on the Cu-Se distance from C_o^{4p} because of its complicated dependence on this distance and because Eq.V.13 is only dependent on the angle between the Cu-Se direction and the x-axis. The experimentally obtained coefficients of the $4p_x$ and $4p_y$ orbitals are 0.351 and 0.312 for Se_1 and 0.363 and 0.314 for Se_2. The theoretically calculated coefficients are 0.397 and 0.262 for Se_1 and 0.398 and 0.262 for Se_2.

As discussed in section IV A, in $Cu/Ni(but_2dsc)_2$ the largest Se hfs (both the averaged value and the axial component A_1^{Se}) belongs to the Se atom with the largest distance to Cu. Since the angles between $A_1^{Se_1}$ and $A_1^{Se_2}$ in $Cu/Ni(but_2dsc)_2$ and $Cu/Ni(et_2dsc)_2$ are the same, it can be expected that in the latter system the largest Se hfs similarly belongs to the atom with the largest distance to Cu. From the measurements on this system it appeared that Se_2 (the atom with the largest distance if the Cu containing molecule has the structure of the host crystal) has indeed the largest axial component of the traceless tensor but, on the other hand, the smallest isotropic hfs (Table V.6). Therefore, it is not possible to decide from these experimental values which Se atom in the system $Cu/Ni(et_2dsc)_2$ has the largest distance to Cu. From the extended Hückel calculation on the ethyl system it appears that the atom with the smallest distance (Se_1) has the largest axial component and the smallest averaged hfs. In view of these results we conclude that the order of the actual Cu-Se distances in $Cu/Ni(et_2dsc)_2$ is reversed compared with the Ni-Se distances in the host crystal. To check the reliability of this conclusion, a calculation with an enlarged difference between the distances Cu-Se_1 and Cu-Se_2 (as is the case in the butyl system, see Table V.2) has been carried out. This calculation confirmed the experimental result of the $Cu/Ni(but_2dsc)_2$ system: the Se atom with the largest distance to Cu has the largest value of both, A_1^{Se} and A_{av}^{Se}.

V D 1d $\bar{g}$ Tensor

As has been discussed in chapter IV, in all the monomeric diselenocarbamate complexes studied, the largest g value is found in the y direction (see Eq.V.4 for the coordinate system) whereas in the xz plane the g value is much smaller and almost isotropic. In the dithiocarbamates, however, the largest g value points along the z-axis and the anisotropy in the molecular plane is much smaller than in the diselenocarbamates.

The extended Hückel calculations reproduce the g values in the molecular plane very well. As was shown in section C of this chapter, the empirical parameters could be chosen such that the calculated g values of $Cu/Ni(et_2dtc)_2$ agree very well with the measured values. The difference in g anisotropy in the xy plane between dsc and dtc can be understood on the basis of our MO calculations. If the spin-orbit coupling of the ligand is small, as in dtc (Table V.1), the contributions to Δg_{xx} arise mainly from the MO's which contain the central metal $3d_{xz}$ orbital (see Table V.4), since the MO of the unpaired electron (MO 17) contains mainly $3d_{xy}$ (see Table V.5). If the ligand spin-orbit coupling is large, as is the case in the diselenocarbamates, contributions to Δg_{xx} arise also from the ligand p_z orbitals since the ligand part in the MO 17 consists mainly of the p_x and p_y orbitals. In this way a large negative contribution to Δg_{xx} (viz. -0.0314) arises from the MO 15 (which mainly consists of ligand p_z orbitals), whereas in $Cu/Ni(et_2dtc)_2$ the contribution due to MO 15 (also consisting of ligand p_z orbitals) is -0.0018 and can be neglected. The same effect applies to the g_{yy} values. In both systems the main contributions to Δg_{yy} are due to excitations from the MO's 18 and 26, which contain the metal $3d_{yz}$ and the ligand p_z orbitals. Because of the large spin-orbit coupling of selenium, in dsc these contributions are 0.0204 and 0.0363 for the MO's 18 and 26, respectively, whereas in dtc they are 0.0016 and 0.0204 (see section V C.2). Hence the difference in the g values in the xy plane can be ascribed to the spin-orbit interactions of the ligands and, to a less extent, to the enlarged delocalization of the unpaired electron in the dsc compounds compared to the dtc compounds. This conclusion is sustained by a calculation for dtc, in which the spin-orbit coupling constant of S 3p was taken equal to that of Se 4p. The values g_{xx} and g_{yy} calculated for dsc were reproduced.

Another difference between the dtc and dsc systems is the rotation of the principal axes of the $\bar{\bar{g}}$ tensor relative to those of $\bar{\bar{A}}^{Cu}$ in the xz plane, which occurs only in the dsc systems. This property is not reflected in the results of the MO calculations: the calculated g_2 and g_3 principal axes point along the z and x-axis, respectively. A condition for obtaining a rotation in the xz plane is that the two principal values in this plane are nearly equal. In that case a small off-diagonal element g_{xz} or g_{zx} will result in a rotation. Comparing the experimental with the calculated values of g_2 and g_3 in Table V.6, it is evident that the calculated value of g_2 (which points in the z direction) is far too large,

which prevents a rotation of the calculated tensor. From Table V.4 follows that the contributions to Δg_{zz} come from MO's which contain the metal $3d_{x^2-y^2}$ orbital and/or the Se $4p_x$ and $4p_y$ orbitals. This is the case for MO 23, 24 and 33. The latter MO contributes 0.0175 and the first two MO's contribute 0.0370. In order to find an explanation for the rotation in the xz plane it is necessary to find a mechanism that lowers these contributions to g_{zz}, or that yields an extra, negative, contribution. Since the structure of the ligand in the Cu containing guest molecules is not known, MO calculations have been carried out using various structures. Since the metal and the ligand hfs's show that the central part of the molecule is planar with C_1 symmetry, and since enlarging of the difference between the Cu-Se distances results only in a rotation of the $\bar{\bar{A}}^{Cu}$ tensor in the xy plane (section V D.1b), only those structures were considered in which the ligands are rotated in the same direction about the axes Se_1-Se_2 and $Se_{1'}$-$Se_{2'}$. These structures retain the C_1 symmetry. It turned out that unrealistically large rotation angles of 30^o or more are needed to obtain a rotation of 1^o of the $\bar{\bar{g}}$ tensor in the xz plane. The rotation of the ligands has practically no effect on the g_{zz} value itself, so that this structure deformation alone is not capable of explaining the effect. Thereupon the effect of Se 4d functions was investigated. Taking into account these atomic orbitals results in a number of MO's which contain mainly the Se 4p and 4d orbitals and which lie in energy above the MO of the unpaired electron. It appears that excitations to these MO's affect the g_{zz} value more than the two other g values. The amount in which the g values are changed depends strongly on the exponent in the radial function of the 4d orbital and, to a smaller extent, on the spin-orbit coupling of this orbital. As both parameters are unknown, several values were used. The VSIE of this orbital has been calculated from the data in Ref.79 (1.89) The best g values are obtained for an exponent of about 1.5 in the radial function and a Se 4d spin-orbit coupling constant of 800 cm^{-1} The value for the radial exponent is not unrealistic, as other authors have used an exponent of 1.878 [93]. Table V.7 lists the g values calculated with these parameters and with the structure of the host crystal. It is clear that inclusion of the Se 4d orbitals yields the desired effect, the difference between g_2 and g_3 is lowered from 0.06 to 0.02 and the $\bar{\bar{g}}$ tensor is rotated around g_1 by an angle of 7^o. If the ligands are rotated by an angle of 30^o in the way described above, the calculated angle between A_1^{Cu} and g_2 is 29^o.

Table V.7 Experimentally obtained and calculated g values and angles χ between A_1^{Cu} and g_2 in $Cu/Ni(et_2dsc)_2$. "calc a" are the calculated values without inclusion of the Se 4d orbitals, "calc b" and "calc c" the values obtained with these orbitals. In "calc c" the ligands have been rotated by 30°.

	obs.	calc a	calc b	calc c
g_1	2.0511	2.0591	2.0582	2.0432
g_2	2.0021	2.0533	1.9855	1.9910
g_3	1.9941	1.9912	1.9646	1.9296
χ	57°	0°	7°	29°

Finally it was checked whether the sulphur 3d orbitals could effect the same result in the dithiocarbamate systems. It appeared that this was not the case due to the relatively small spin-orbit coupling of the sulphur orbitals.

In a recent article Buluggiu and Vera [94] investigated also the intriguing problem of the g tensor orientation in the system $Cu/Ni(et_2dsc)_2$. These authors considered only metal d orbitals. As shown above, ligand orbitals play a very important role and should be included in the calculation of the g tensor components. As happens often, a more complete calculation does not lead always to better agreement with experiment. Such a situation occurred here, inclusion of charge-transfer states does increase the g tensor anisotropy in the xz plane, rendering more difficult a rotation of the g tensor. Only by including Se 4d functions the g anisotropy decreased again. As shown above, good agreement is then obtained with the experimental data.

V D 2 The system $Ag/Ni(but_2dsc)_2$

We have not carried out extended Huckel calculations for this system, because of the disappointing results obtained with this method for the system $Ag/Ni(et_2dtc)_2$ [5]. From the ligand hfs's conclusions can be drawn about the LCAO coefficients in the MO of the unpaired electron, as has been pointed out in section V D.1c. The average Se couplings are about equal to the average couplings in the corresponding copper systems (Table V.8). Therefore we conclude that the coefficient of the Se 4s orbital in the MO of the unpaired electron in the Ag system is the same as in the Cu system. From the difference between the purely anisotropic hfs's of the two inequivalent Se atoms in the two systems (Table V.8) we conclude that the

Table V.8 Experimentally obtained principal values of the $\bar{\bar{A}}^{Se}$ tensors in the systems $Cu/Ni(but_2dsc)_2$ and $Ag/Ni(but_2dsc)_2$ (in $10^{-4}cm^{-1}$).

	$Cu/Ni(but_2dsc)_2$	$Ag/Ni(but_2dsc)_2$
Se_1		
A_1-A_{av}	+60	+72
A_2-A_{av}	-28	-32
A_3-A_{av}	-32	-39
A_{av}	+49	+49
Se_2		
A_1-A_{av}	+55	+66
A_2-A_{av}	-25	-28
A_3-A_{av}	-31	-39
A_{av}	+46	+44

difference between the metal-selenium distances in the silver and copper systems is equal. The fact that the axial splittings in the silver system are ~ 20% larger than in the corresponding copper system means that the coefficients of the Se $4p_x$ and $4p_y$ orbitals in the MO of the unpaired electron are ~ 10% larger than in the copper system. From these coefficients of the selenium orbitals and with the help of the normalization condition, the density of the unpaired electron on the silver atom can be calculated if it is assumed that the other ligand atoms have a negligible spin density and if the required overlap integrals are taken to be equal to those of the copper system. In this way, a density is calculated of 0.20 which is approximately half the calculated density on the metal atom in the corresponding copper system (see Table V.4). This result is in very good agreement with the values obtained for the corresponding dithiocarbamates. van Rens [5] found for $Ag/Ni(et_2dtc)_2$ a spin density of 0.26 at the silver atom, which is also about half the calculated density on the copper atom in the corresponding $Cu/Ni(et_2dtc)_2$ system (section V C).

V D 3 Conclusions

The results of the extended Huckel calculations show that neither the principal g values nor the hyperfine couplings of the central metal atom can be used to calculate the LCAO coefficients in the MO's with a reasonable accuracy directly from experimental data. The reason is that, besides the metal orbitals, also ligand orbitals contribute, so that the number of unknown coefficients and MO energies is too large. This dilemma can be circumvented by calculating the LCAO coefficients and MO energies by means of a theoretical method, assuming a realistic structure for the

complex studied. The obtained LCAO coefficients and MO energies can then be used to calculate the parameters occurring in the spin hamiltonian. If reasonable agreement is found with the experimental values, some confidence can be given to the calculated MO's and the energy scheme.

Without the 4d functions of Se, all calculated hyperfine couplings (those of copper as well as those of selenium, hence 9 principal values) and two of the principal g values are found in very good agreement with the experimental ones. The third principal g value can be brought into agreement with the experimental value if the 4d functions of selenium are taken into account. In doing this, also the rotation of the principal axes of $\bar{\bar{g}}$ relative to those of $\bar{\bar{A}}^{Cu}$ in the xz plane can be understood. The measured differences between the magnitudes and the directions of the principal g values of copper dithiocarbamate and copper diselenocarbamate are caused by the spin-orbit coupling of selenium, which is much larger than that of sulphur. The change in delocalization plays only a minor role in this respect.

The results of the extended Hückel calculations show that the hyperfine couplings of the ligand atoms are determined almost completely by the MO of the unpaired electron. This enabled us to calculate the selenium part of this MO with a reasonable accuracy, directly from the experiment. If it is assumed that other ligand atoms have a negligible spin density and if the required overlap integrals are known, the density of the unpaired electron on the central metal atom can be calculated with the help of the normalization condition. When this procedure is applied to the system $Ag/Ni(but_2dsc)_2$, it appears that the delocalization of the unpaired electron to the selenium atoms is much larger than in the corresponding copper system. The spin density on the silver atom is only 0.2, compared to 0.4 on the copper atom.

V E The dimeric systems $Cu(et_2dsc)_2$ and $Cu(et_2dtc)_2$ diluted in the Zn complexes

In section IV B we concluded from the experimental data that the copper containing dimer does not accept the structure of the host crystal, but has a structure which resembles very much that of the pure copper complex. With the help of MO calculations we will try to verify this conclusion.

V E 1a The molecular structure

We have carried out MO calculations for a dithiocarbamate dimer with one copper and one zinc atom, using both the structure of the pure Zn dimer and that of the pure Cu dimer. In Table V.9 the calculated spin hamiltonian parameters are listed, together with the experimentally determined values. For practically all the listed parameters the calculation based on the structure of the pure copper complex yields the best values. This confirms the conclusion drawn by Weeks and Fackler [12]. However, the reasoning they used is open to discussion. These authors based their conclusion on the expectation that for the Zn structure the largest g value should fall along the direction S(1)-M-S(4) because this direction contains the two bonds which are considerably elongated . This expectation, however, is not supported by our results where, for the Zn as well for the Cu structure, the largest g value is directed approximately along the Cu-S(4') direction (deviation in the Cu structure 1^o, in the Zn structure 10^o).

Table V.9 Experimentally obtained and calculated principal values of $\bar{\bar{g}}$, $\bar{\bar{A}}^{Cu}$ and $\bar{\bar{P}}^{Cu}$ (in units of $10^{-4}cm^{-1}$) in Cu/Zn(et_2dtc)$_2$. Cu(et_2dtc)$_2$ or Zn(et_2dtc)$_2$ means· calculated using the structure of this complex.

	obs.	calc.	
		Cu(et_2dtc)$_2$	Zn(et_2dtc)$_2$
g_1	2.1076	2.1010	2.1664
g_2	2.0308	2.0321	2.0619
g_3	2.0230	2.0251	2.0359
g_{av}	2.0538	2.0527	2.0881
Cu			
A_1-A_{av}	-78.2	-70.8	-51.7
A_2-A_{av}	+43.7	+40.5	+38.2
A_3-A_{av}	+34.3	+30.3	+13.5
A_{av}	-64.2		
Cu			
P_1	+ 2.1	+ 3.4	+ 3.9
P_2	- 0.5	- 1.5	- 1.4
P_3	- 1.6	- 1.9	- 2.5

V E 1b Molecular orbitals

No complete table will be given of the calculated MO's and their energies, but some remarks will be made about differences and similarities with the MO scheme of the monomeric system (section V C).

For the Cu dimer structure the MO of the unpaired electron consists of the copper $3d_{xy}$ orbital and the sulphur $3p_x$ and $3p_y$ orbitals. The LCAO coefficients are almost equal to the coefficients in the monomer. The largest coefficient of an orbital that belongs to the Zn containing part of the dimer is only 0.07, which means that the unpaired electron is fully localized on the copper containing part of the dimer. The energy of this MO is 1.4 eV lower than the corresponding one in the monomer.

The following, doubly occupied, MO is centred on the zinc part of the dimer and contains the Zn $3d_{xy}$ orbital and the sulphur $3p_x$ and $3p_y$ orbitals. The density on the Zn atom is only about 0.2.

The following five MO's consist mainly of the Cu 3d orbitals. The order is the same as in the monomeric system and their energies are not changed, with the exception of the energy of the MO which contains $3d_{z^2}$. This energy has been raised by 0.6 eV so that it follows second after the MO of the unpaired electron. The delocalization in these MO's is, in general, somewhat larger than in the monomeric system.

The remaining "d-orbitals" of zinc are very low in energy and lie about 10 eV below the orbital of the unpaired electron.

V E 1c Spin hamiltonian parameters

Inspection of Table V.9 learns that the absolute values of all the calculated hyperfine couplings are not large enough. This is possibly due to a too large delocalization of the unpaired electron, resulting in a small dipolar contribution. It is more likely that the too small couplings are caused by the second order contributions. This contribution is nearly zero for A_2 and A_3, but $+30\ 10^{-4}cm^{-1}$ for A_1. This large value is due to the relatively small energy gap between the MO of the unpaired electron and the MO's which contain mainly the $3d_{x^2-y^2}$ orbitals.

The calculated principal values of the quadrupole coupling tensor agree very well with the experimental values, bearing in mind the approximations made in deriving the expressions for the tensor elements (see section II D). It is important that the calculated signs of the principal values agree with the experimentally determined ones. The signs of the experimental values depend on the choice of the signs of the copper hyperfine couplings and if the latter are chosen in the opposite sense, the signs of the quadrupole

Table V.10 Experimentally obtained and calculated angles between the principal axes of $\bar{\bar{A}}^{Cu}$ and the principal axes of $\bar{\bar{g}}$ and $\bar{\bar{P}}^{Cu}$ in $Cu/Zn(et_2dtc)_2$.

	g_1		g_2		g_3		P_1		P_2		P_3	
	obs.	calc.	obs.	calc.	obs.	calc.	obs.	calc.	obs.	calc.	obs.	calc.
A_1	0	1	90	90	90	91	6	1	94	90	86	90
A_2	90	90	4	15	94	105	85	90	22	17	111	107
A_3	90	89	86	75	4	15	93	91	68	73	22	17

principal values also reverse. The good agreement between the experimentally and theoretically obtained values confirms the choice made.

The principal axes numbered 2 and 3 of all three tensors have been rotated from the x and y axis (see Eq.V.4). The rotation of the $\bar{\bar{g}}$ tensor is caused by the mixing of the $3d_{xz}$ and $3d_{yz}$ orbital, which results in a non-zero value of the off-diagonal element g_{xy}. The rotation of the $\bar{\bar{A}}^{Cu}$ tensor is a first order effect of the mixing of the $3d_{xy}$ and the $3d_{z^2}$ and $3d_{x^2-y^2}$ orbitals, so that the matrix element $\langle\psi_n|F_{xy}/r^3|\psi_n\rangle$ (Eq.II.66) is non-zero.

In Table V.10 the calculated angles between the principal axes of $\bar{\bar{A}}^{Cu}$ and the principal axes of $\bar{\bar{g}}$ and $\bar{\bar{P}}^{Cu}$ are compared with the experimentally determined values. The agreement is rather good, although the calculated angles between A_2^{Cu} and A_3^{Cu} on one side and g_2, g_3, P_2^{Cu} and P_3^{Cu} on the other side are too large. This could mean that the distance between the copper atom and the plane of the four surrounding sulphur atoms is smaller than in the structure of the pure copper compound.

V E 2 The system $Cu/Zn(et_2dsc)_2$

For this system too MO calculations were carried out based on the structure of the pure guest or of the pure host crystal. No Se 4d orbitals were taken into account in these calculations. It may be expected that this affects mainly the g values and to a smaller extent the other spin hamiltonian parameters. The calculated spin hamiltonian parameters are listed in Table V.11, together with the experimentally observed ones.

V E 2a The molecular structure

Although the results, obtained with the structure of $Cu(et_2dsc)_2$, are not very good, they are much better than those obtained with the structure of the host crystal. Hence, here too the conclusion can be drawn that the

Table V.11 Experimentally obtained and calculated principal values of $\bar{\bar{g}}$, $\bar{\bar{A}}^{Cu}$, $\bar{\bar{A}}^{Se}$ and $\bar{\bar{P}}^{Cu}$ (in units of $10^{-4}cm^{-1}$) in $Cu/Zn(et_2dsc)_2$. $Cu(et_2dsc)_2$ or $Zn(et_2dsc)_2$ means: calculated using the structure of this complex.

	obs.	calc.	
		$Cu(et_2dsc)_2$	$Zn(et_2dsc)_2$
g_1	2.0559	2.0634	2.1036
g_2	2.0213	2.0591	2.0721
g_3	2.0068	2.0079	2.0195
g_{av}	2.0280	2.0435	2.0651
Cu			
A_1-A_{av}	-62.7	-50.3	-24.1
A_2-A_{av}	+38.3	+31.4	- 3.7
A_3-A_{av}	+24.5	+18.9	+27.8
A_{av}	-64.9		
Cu			
P_1	+1.8	+2.3	+1.6
P_2	-0.3	-0.9	-0.5
P_3	-1.5	-1.3	-1.1
Se_1			
A_1-A_{av}	+68	+49.3	+41.1
A_2-A_{av}	-29	-22.8	-18.1
A_3-A_{av}	-39	-26.5	-23.0
A_{av}	+51	+25.2	+ 5.4
Se_2			
A_1-A_{av}	+54	+43.8	+26.5
A_2-A_{av}	-25	-20.2	-11.5
A_3-A_{av}	-29	-23.6	-15.0
A_{av}	+44	+20.6	+ 2.7
Se_3			
A_1-A_{av}	+49	+48.5	+23.2
A_2-A_{av}	-23.5	-23.5	- 9.8
A_3-A_{av}	-25.5	-25.0	-13.4
A_{av}	+43	+21.8	+ 4.0
Se_4			
A_1-A_{av}	+54	+56.6	+63.1
A_2-A_{av}	-25	-26.9	-28.6
A_3-A_{av}	-29	-29.5	-34.5
A_{av}	+48	+15.0	+ 6.2
$Se_{4'}$			
A_1-A_{av}		+ 1.0	+16.5
A_2-A_{av}		- 0.5	+ 7.2
A_3-A_{av}		- 0.5	+ 9.3
A_{av}		+ 4.7	+ 1.3

structure of the copper containing dimer resembles the structure of the pure copper complex.

V E 2b Molecular orbitals

The MO scheme is roughly the same as in the corresponding dithiocarbamate system. the energy of the MO of the unpaired electron is lowered, compared to the monomer, and the next occupied MO is centred on the Zn part of the dimer. The MO's which contain the copper 3d orbitals are, however, more delocalized than in the dithiocarbamate system and also more than in the monomer. Another difference with the dithiocarbamate system is, that a number of ligand orbitals lies between the MO of the unpaired electron and the other "3d" MO's.

V E 2c Spin hamiltonian parameters

Since no Se 4d orbitals have been taken into account, the calculated value of g_2 (in the Cu structure) is too large. The other g values agree rather well.

As in the calculation on the corresponding thio system (section V E.1) the calculated hfs's of copper are not large enough. In the present system this can be due to a too large calculated delocalization of the unpaired electron. While in the dimeric thio system the calculated density of the unpaired electron at the copper nucleus was nearly equal to the calculated density in the monomer, in the seleno system it is much smaller than in $Cu/Ni(et_2dsc)_2$. 0.35 relative to 0.41. However, the alternative explanation, too large calculated second order contributions, cannot be excluded.

It is striking that all the calculated isotropic Se hfs's are too small. This could mean that the copper atom lies in the plane of the four nearest by lying Se atoms, and not above it as is the case in the copper compound.

The anisotropic parts of the Se hfs's agree better with the experimental values, especially for Se_3 and Se_4 the agreement is very good. The fact that the agreement is rather bad for Se_2 is not surprising since the experiments showed that this atom does not have the position which it occupies in the pure copper complex (section IV B.2a). The large hfs of Se_1, however, cannot be understood from this calculation.

The calculated hfs's of Se_4, (the atom which has a large distance from Cu) are so small that only in the direction of A_1 one might hope to resolve this splitting.

V E. 3 Conclusions

The extended Hückel calculations confirm the conclusions which were drawn from the experimental data: the dimeric units with one zinc and one copper atom do not accept the structure of the host crystals but have a structure which resembles very much the structure of the pure copper complexes.

The MO schemes are about the same as in the monomeric systems $Cu/Ni(dsc)_2$ and $Cu/Ni(dtc)_2$, with some exceptions:

a. The energy of the unpaired electron MO has been lowered.
b. The energy of the MO which contains mainly the copper $3d_{z^2}$ orbital has been raised.
c. Delocalization of the "copper d-electrons" is more complete (especially in the diselenocarbamate system).
d. Mixing of atomic orbitals is stronger, which results in rotations of the various principal axes relative to each other in the xy plane.

SUMMARY

In this thesis the results are discussed of an ESR study of the N,N-dialkyldiselenocarbamate complexes of copper and silver {$Cu(R_2dsc)_2$ and $Ag(R_2dsc)_2$} and the N,N-dialkyldithiocarbamate complexes of copper {$Cu(R_2dtc)_2$}. Since the interaction parameters, which have to be determined, are anisotropic, these paramagnetic molecules were built in diamagnetic host lattices. To this end the corresponding nickel and zinc compounds were used. Measurements were also carried out in liquid and in frozen solutions. The interaction parameters were determined from single crystal measurements with the help of a minimization program that uses the expressions derived in chapter II for the peakpositions of the ESR transitions and their transition probabilities. These expressions were obtained without making assumptions about the relative direction of the principal axes of the tensors.

In all diselenocarbamate systems studied, it was found that the principal axes of the hyperfine splitting tensor of the central metal atom do not coincide with those of the $\bar{\bar{g}}$ tensor. Other authors found that in the corresponding dithiocarbamate systems these principal axes do coincide. This difference can not be ascribed to differences between the molecular structures, because in the diselenocarbamates the deviations from D_{2h} ssymmetry are smaller than in the dithiocarbamates. This means that an explanation has to be found in the large spin-orbit coupling of selenium and/or in a different covalency in the diselenocarbamate compounds.

The complexes of copper and zinc have a dimeric structure. When copper is built in the zinc crystal in a low concentration, dimers are formed which contain one copper and one zinc atom. The similarity of the angles between the axes of highest principal values of the selenium hyperfine splitting tensors and the corresponding bonding angles Se-Cu-Se in the pure copper compound indicates that the structure of such a paramagnetic dimer resembles very much the structure of the dimers in the pure copper diselenocarbamate complex and not the structure of the dimers in the host crystal.

The complexes of nickel consist of monomers. When copper diselenocarbamate is built in the corresponding nickel lattice, it appears from the measured hyperfine splittings that indeed the structure of the host crystal is adopted.

With the aid of the iterative extended Huckel MO method it was tried to verify the conclusions about the molecular structure which were drawn from the experimental data. To this end the parameters of the spin

hamiltonian were expressed in the parameters of the molecular orbital method. Special attention was paid to the influence of multicentre integrals and the problem of gauge invariance. The experimentally determined interaction parameters of $Cu/Ni(et_2dtc)_2$ could be reproduced very well with reasonable values for the empirical constants occurring in the extended Huckel method. Using the same empirical constants, the hyperfine splittings of copper as well as the hyperfine splittings of the selenium atoms in the system $Cu/Ni(et_2dsc)_2$ could be calculated in agreement with the experimentally determined values. The principal values of $\bar{\bar{g}}$ and also the rotation of the principal axes of this tensor relative to those of $\bar{\bar{A}}^{Cu}$ could be reproduced only when the 4d orbitals of selenium were taken into account. The differences with the dithiocarbamate system are caused mainly by the large spin-orbit coupling of selenium.

The calculations on the dimeric systems $Cu/Zn(et_2dsc)_2$ and $Cu/Zn(et_2dtc)_2$ show that the results which are obtained if the structure of the pure copper complex is used, are better than those obtained assuming the structure of the pure host compound. This is in accordance with the conclusion drawn from the experimental data.

From the MO calculations it appears that neither the hyperfine splittings of the central metal atom nor the g values are suitable to obtain information about the LCAO coefficients in the MO's, directly from the experiment. This is due to the fact that the ligand orbitals contribute considerably to the interaction parameters. As a consequence the number of unknowns in the expressions for these parameters exceeds the number of quantities which can be measured. The hyperfine splittings of the ligands, on the contrary, are determined mainly by the MO of the unpaired electron. This means that these experimental data yield direct information about the extent of the delocalization of the unpaired electron. When this method is applied to the monomeric systems $Cu/Ni(dsc)_2$ and $Ag/Ni(dsc)_2$ it appears that delocalization of the unpaired electron is more complete in the silver molecule than in the copper molecule.

The MO calculations show that the bonding in the molecules studied is highly covalent with a large delocalization of the metal "d-electrons". This delocalization is larger in the dimeric than in the monomeric systems. In the dimeric systems the unpaired electron is fully localized on the molecule that contains the paramagnetic centre.

SAMENVATTING

In dit proefschrift worden de resultaten besproken van een ESR onderzoek aan de N,N-dialkyldiselenocarbamaat kompleksen van koper en zilver {$Cu(R_2dsc)_2$ en $Ag(R_2dsc)_2$} en aan het N,N-dialkyldithiocarbamaat kompleks van koper {$Cu(R_2dtc)_2$}. Aangezien de te bepalen interaktieparameters anisotroop zijn, werden deze paramagnetische molekulen ingebouwd in diamagnetische gastheerroosters. Hiervoor werden de overeenkomstige nikkel- en zinkverbindingen gebruikt. Daarnaast werden ook metingen uitgevoerd aan vloeibare en bevroren oplossingen. De interaktieparameters werden bepaald uit metingen aan éénkristallen m.b.v. een minimalisatie programma dat gebruik maakt van de in hoofdstuk II afgeleide uitdrukkingen voor de piekposities van de ESR overgangen en hun overgangswaarschijnlijkheden. Deze uitdrukkingen zijn afgeleid zonder aannamen te maken over de relatieve ligging van de hoofdassen der tensoren.

In alle bestudeerde diselenocarbamaat systemen is gevonden dat de hoofdassen van de hyperfijnsplitsings tensor van het centrale metaal atoom niet samenvallen met die van de $\overline{\overline{g}}$ tensor. Andere auteurs vonden dat in de overeenkomstige dithiocarbamaat systemen deze hoofdassen wel samenvallen. Dit verschil kan niet toegeschreven worden aan verschillen tussen de molekulaire strukturen omdat afwijkingen van D_{2h} symmetrie in de diselenocarbamaten kleiner zijn dan in de dithiocarbamaten. Dit houdt in dat een verklaring gezocht moet worden in de grote spin-baankoppeling van seleen en/of in een verschillende kovalentie in de diselenocarbamaat verbindingen.

De kompleksen van koper en zink hebben een dimere struktuur. Wanneer koper in lage concentratie wordt ingebouwd in het zink kristal, worden dimeren gevormd die een koper en een zink atoom bevatten. Uit de overeenkomst van de hoeken die de assen van de grootste seleen hyperfijnsplitsing met elkaar maken en de overeenkomstige bindingshoeken Se-Cu-Se in de zuivere koper verbinding blijkt dat de struktuur van zo'n paramagnetisch dimeer veel lijkt op die van de dimeren in het zuivere koper diselenocarbamaat kompleks en niet op de struktuur van de dimeren in het gastheerkristal.

De kompleksen van nikkel bestaan uit monomeren. Wanneer koper diselenocarbamaat wordt ingebouwd in het overeenkomstige nikkel rooster, dan blijkt uit de gemeten hyperfijnsplitsingen dat wel de struktuur van het gastheerkristal wordt overgenomen.

Met behulp van de iteratieve extended Huckel MO methode werd gepro-

beerd de konklusies over de molekulaire struktuur te verifieren die getrokken zijn uit de eksperimentele gegevens. Daartoe werden eerst de parameters van de spin hamiltoniaan uitgedrukt in de parameters van het "molecular orbital" model, waarbij speciaal aandacht werd besteed aan de invloed van meer-centrum integralen en aan het probleem van "gauge" invariantie. De rekenmethode werd geijkt aan het systeem $Cu/Ni(et_2dtc)_2$ waarbij bleek dat het goed mogelijk is om de eksperimenteel bepaalde interaktieparameters te reproduceren met redelijke waarden voor enige empirisch te bepalen konstanten uit de extended Huckel methode. Met gebruik making van dezelfde empirische konstanten konden de hyperfijnsplitsingen van koper zowel als van de seleen atomen in het systeem $Cu/Ni(et_2dsc)_2$ berekend worden in overeenstemming met de eksperimenteel gevonden waarden. De hoofdwaarden van de $\bar{\bar{g}}$ tensor en ook de draaiing van de hoofdassen van deze tensor t.o.v. die van $\bar{\bar{A}}^{Cu}$ bleken echter alleen dan goed berekend te kunnen worden wanneer de 4d orbitals van seleen in rekening gebracht werden. De verschillen met de dithiocarbamaat systemen worden voornamelijk veroorzaakt door de grote spin-baan koppeling van seleen.

De berekeningen aan de dimere systemen $Cu/Zn(et_2dsc)_2$ en $Cu/Zn(et_2dtc)_2$ laten zien dat uitgaande van de struktuur van het zuivere koper kompleks veel betere resultaten verkregen worden dan met de struktuur van de zuivere gastheer verbinding. Dit is in overeenstemming met de konklusie die getrokken was uit de eksperimentele gegevens.

Uit de MO berekeningen blijkt dat noch de hyperfijnsplitsingen van het centrale metaal atoom noch de g waarden geschikt zijn om, direkt uit het eksperiment, gegevens te verkrijgen over de LCAO koefficienten in de MO's. Dit vindt zijn oorzaak in het feit dat ligand orbitals belangrijke bijdragen leveren aan de interaktieparameters waardoor het aantal onbekenden in de uitdrukkingen voor deze parameters groter wordt dan het aantal grootheden dat gemeten kan worden. De liganden hyperfijnsplitsingen, daarentegen, worden voornamelijk bepaald door de MO van het ongepaarde elektron. Dit betekent dat deze eksperimentele grootheden direkte informatie verschaffen over de mate van delokalisatie van het ongepaarde elektron. Wanneer deze methode wordt toegepast op de monomere systemen $Cu/Ni(dsc)_2$ en $Ag/Ni(dsc)_2$ blijkt dat de delokalisatie van het ongepaarde elektron in het zilver molekuul veel groter is dan in het koper molekuul.

De MO berekeningen wijzen op een vrij sterk kovalente binding in de bestudeerde molekulen met grote delokalisatie van de metaal "d-elektronen". Deze delokalisatie is in de dimere systemen groter dan in de monomeren. In de dimere systemen is het ongepaarde elektron volledig gelokaliseerd op het molekuul dat het paramagnetische centrum bevat.

REFERENCES

1. H.C. Brinkhoff, Thesis, Nijmegen, 1970.
2. J.H. Noordik, Thesis, Nijmegen, 1971.
3. J.L.K.F. de Vries, Thesis, Nijmegen, 1972.
4. J.G.M. van der Linden, Thesis, Nijmegen, 1973.
5. J.G.M. van Rens, Thesis, Nijmegen, 1974.
6. P.T. Beurskens, J.A. Cras, and J.J. Steggerda, Inorg. Chem. 7, 810 (1968).
7. H.C. Brinkhoff, J.A. Cras, J.J. Steggerda, and J. Willemse, Rec. Trav. Chim. 88, 633 (1969).
8. J. Willemse, P.H.F.M. Rouwette, and J.A. Cras, Inorg. Nucl. Chem. Letters 8, 389 (1972).
9. J.A. Cras, J. Willemse, A.W. Gal, and B.G.M.C. Hummelink-Peters, Rec. Trav. Chim. 92, 641 (1973).
10. R. Petterson and T. Vänngård, Arkiv Kemi 17, 249 (1961).
11. T.R. Reddy and R. Srinivasan, J. Chem. Phys. 49, 3696 (1968).
12. M.J. Weeks and J.P. Fackler, Inorg. Chem. 7, 2548 (1968).
13. A.K. Gregson and S. Mitra, J. Chem. Phys. 49, 3696 (1968).
14. A. Davison, N. Edelstein, R.H. Holm, and A.H. Maki, Inorg. Chem. 2, 1227 (1963).
15. A.H. Maki, N. Edelstein, A. Davison, and R.H. Holm, J. Am. Chem. Soc. 86, 4580 (1964).
16. E. Billig, R. Williams, I. Bernal, J.H. Waters, and H.B. Gray, Inorg. Chem. 3, 663 (1964).
17. Hyunsoo So and R. Linn Belford, J. Am. Chem. Soc. 91, 2392 (1969).
18. R.M. Golding and W.C. Tennant, Mol. Phys. 24, 301 (1972).
19. B. Bleany, Phil. Mag. 42, 441 (1951).
20. W. Low, "Paramagnetic Resonance in Solids", Academic Press, New York (1960), 1st ed., p. 57.
21. R.M. Golding, "Applied Wave Mechanics", Van Nostrand, New York (1969), 1st ed., p. 452.
22. R.E.D. McClung, Can. J. Phys. 46, 2271 (1968).
23. W.C. Lin, Mol. Phys. 25, 247 (1973).
24. R.M. Golding and W.C. Tennant, Mol. Phys. 25, 1163 (1973).
25. L.D. Landau and E.M. Lifshitz, "Quantum Mechanics", Pergamon Press, London (1959), 2nd ed., p. 137.
26. A. Abragam and B. Bleany, "Electron Paramagnetic Resonance of

Transition Ions", Clarendon Press, Oxford (1970), 1st ed., p. 136.
27. A.J. Stone, Proc. Roy. Soc. A 271, 424 (1963).
28. A.J. Stone, Thesis, Cambridge, 1963.
29. Ch.P. Slichter, "Principles of Magnetic Resonance", Harper & Row, New York (1963), 1st ed., p. 195.
30. M.H.L. Pryce, Proc. Phys. Soc. A 63, 25 (1950).
31. Ph. de Montgolfier and J.E. Harriman, J. Chem. Phys. 55, 5262 (1971).
32. J.S. Griffith, "The Theory of Transition-Metal Ions", University Press, Cambridge (1964), 2nd ed., p. 122.
33. J.D. Jackson, "Classical Electrodynamics", Wiley and Sons, New York (1962), 1st ed., p. 179.
34. Reference 33, p. 181.
35. H.H. Tippins, Phys. Rev. 160, 343 (1967).
36. P.W. Atkins and A.M. Jamieson, Mol. Phys. 14, 425 (1968).
37. Reference 32, p. 126.
38. J.A. Pople and D.L. Beveridge, "Approximate Molecular Orbital Theory", McGraw-Hill, New York (1970), 1st ed., p. 59.
39. D.W. Smith, J. Chem. Soc. A 1970, 3108.
40. A.H. Maki and B.R. McGarvey, J. Chem. Phys. 29, 31 (1958).
41. D. Kivelson and R. Neiman, J. Chem. Phys. 35, 149 (1961).
42. W.H. Moores and R. McWeeny, Proc. Roy, Soc. A 332, 365 (1973).
43. A. Dalgarno, T.N.L. Patterson, and W.B. Somerville, Proc. Roy. Soc. A 259, 100 (1960).
44. J.C. Slater, "Quantum Theory of Atomic Structure", vol. II, McGraw-Hill, New York (1960), 1st ed., p. 256.
45. T.P. Das and E.L. Hahn, Solid State Phys. suppl. 1 (1968).
46. J.L.K.F. de Vries, C.P. Keijzers, and E. de Boer, Inorg. Chem. 11, 1343 (1972).
47. W.D. White and R.S. Drago, J. Chem. Phys. 52, 4717 (1970).
48. C.T. O'Konski and T.K. Ha, J. Chem. Phys. 49, 5354 (1968).
49. R.S. Mulliken, J. Chem. Phys. 23, 1833 (1955).
50. D. Barnard and D.T. Woodbridge, J. Chem. Soc. 1961, 2922.
51. G. Gattow and M. Dräger, Z. Anorg. Allg. Chemie 343, 11 (1966).
52. F. James and M. Roos, MINUITS, CERN, Geneve, program no. D-506 CERN.
53. B.R. McGarvey, J. Phys. Chem. 7, 51 (1967).
54. D.S. Schonland, Proc. Roy. Soc. 73, 788 (1959).
55. "Handbook of Chemistry and Physics", The Chemical Rubber Co., Cleveland (1972), 52nd ed., p. B-245.

56. R.M. Sternheimer, Phys. Rev. 164, 10 (1967).
57. J.G.M. van Rens, C.P. Keijzers, and H. van Willigen, J. Chem. Phys. 52, 2858 (1970).
58. M. Bonamico and G. Dessy, J. Chem. Soc. A 1971, 264.
59. J.H. Noordik and J.M.M. Smits, Cryst. Struct. Comm., in press.
60. M. Bonamico, G. Dessy, C. Mariani, A. Vaciago, and L. Zambonelli, Acta Cryst. 19, 619 (1965).
61. M. Bonamico, G. Dessy, A. Mugnoli, A. Vaciago, and L. Zambonelli, Acta Cryst. 19, 886 (1965).
62. M. Bonamico, G. Mazzone, A. Vaciago, and L. Zambonelli, Acta Cryst. 19, 898 (1965).
63. J.H. Noordik, Private Communication.
64. R. Kirmse, W. Windsch, and E. Hoyer, Z. Anorg. Allg. Chemie 386, 213 (1971).
65. P.T. Beurskens, J.A. Cras, Th.W. Hummelink, and J.H. Noordik, J. Cryst. Mol. Struct. 1, 253 (1971).
66. R. Kirmse, S. Wartewig, W. Windsch, and E. Hoyer, J. Chem. Phys. 56, 5273 (1972).
67. T.J. Schaafsma, Thesis, Groningen, 1966.
68. R.L. Belford and J.R. Pilbrow, J. Magn. Res. 11, 381 (1973).
69. D. Kivelson, J. Chem. Phys. 33, 1094 (1960).
70. A. Spernol and K. Wirtz, Z. Naturforsch. 8a, 522 (1953).
71. J.F. Gibson, Trans. Faraday Soc. 60, 2105 (1964).
72. R. Hoffmann, J. Chem. Phys. 39, 1397 (1963).
73. The author wishes to thank Professor P. Ros and Dr. W.Th.A.M. van der Lugt for making the extended Huckel program available to him.
74 J. Richardson, W. Nieuwpoort, R. Powell, and W. Edgell, J. Chem. Phys. 36, 1057 (1962).
75. J. Richardson, R. Powell, and W. Nieuwpoort, J. Chem. Phys. 38, 796 (1963).
76. E. Clementi and D. Raimondi, J. Chem. Phys. 38, 2686 (1963).
77. E. Clementi, IBM J. Res. Dev. Suppl. 9, 2 (1965).
78. H. Basch, A. Viste, and H.B. Gray, Theoret. Chim. Acta 3, 458 (1965).
79. C.E. Moore, Natl. Bur. Stds. (U.S.) Circ. 467, vol. I (1949); II II (1952); and III (1958).
80. M. Wolfsberg and L. Helmholz, J. Chem. Phys. 20, 837 (1952).
81. L.C. Cusachs, J. Chem. Phys. 43, S157 (1965).
82. K. Jug, Theoret. Chim. Acta 19, 301 (1970).

83. A. Lupei and J.A. McMillan, J. Chem. Phys. 57, 827 (1972).
84. J.T.C. van Kemenade, Thesis, Delft, 1970.
85. C.A. Bates, Proc. Phys. Soc. 79, 69 (1962).
86. A. Carrington and A.D. McLachlan, "Introduction to Magnetic Resonance", Harper & Row, New York (1967), 1st ed., p. 138.
87. Reference 32, p. 437.
88. J. Demuynck and A. Veillard, Chem. Phys. Letters 6, 204 (1970).
89. W.Th.A.M. van der Lugt, Intern. J. Quantum Chem. 6, 859 (1972).
90. J.G.M. van der Linden and H.G.J. van de Roer, Inorg. Chim. Acta 5, 254 (1971).
91. C. Furlani, E. Cerrone, and F. Diomedi Camassei, Inorg. Chem. 7, 265 (1968).
92. J.G.M. van der Linden and P.J.M. Geurts, Inorg. Nucl. Chem. Letters 8, 903 (1972).
93. H.L. Hase and A. Schweig, Theoret. Chim. Acta 31, 215 (1973).
94. E. Buluggiu and A. Vera, J. Chem. Phys. 59, 2886 (1973).

LEVENSLOOP

De auteur van dit proefschrift werd geboren op 13 oktober 1945 te Oss. Nadat in 1964 het eindexamen HBS-B was afgelegd aan het Titus Brandsma Lyceum te Oss, werd in datzelfde jaar begonnen met de studie in de scheikunde aan de Katholieke Universiteit te Nijmegen.
Het kandidaatsexamen (S3) werd afgelegd op 20 november 1967. De doctoraal-studie omvatte als hoofdrichting Fysische Chemie en als bijvakken Theoretische Chemie en Natuurkunde. Op 6 juli 1970 werd het doctoraal-examen cum laude behaald. Sindsdien heeft hij als SON medewerker, verbonden aan de afdeling Molecuulspectroscopie, een promotie-onderzoek verricht.

STELLINGEN

I

De door Schlupp en Maki voorgestelde baansymmetrie voor de grondtoestand van bis(maleonitriledithiolato) goud(II) is, gezien de resultaten van Mossbauer experimenten en "molecular orbital" berekeningen, hoogst twijfelachtig

II

Bij de experimentele bepaling van de nulveldsplitsings-tensor in bis(diethyldithiocarbamato) koper(II) gaan Kumari Cowsik en Srinivasan uit van niet geverifieerde aannamen omtrent de ligging van de hoofdassen van deze tensor

R Kumari Cowsik and R Srinivasan, Pramāna 1, 177(1973)

III

Het door Lesk gegeven bewijs dat de restricted Hartree Fock methode niet in staat is de lange afstands van der Waals attractie van twee edelgas atomen te verklaren, berust op de niet bewezen veronderstelling dat bij toenemende afstand de elektrostatische potentiele energie minder snel afneemt dan de exchange interaktie

A M Lesk, J Chem Phys 59, 44(1973)

IV

De door Christoffersen en Baker voorgestelde definitie van "gross lading" voldoet niet aan de door deze auteurs gestelde eis dat deze lading niet groter mag zijn dan twee, zoals blijkt uit de door hen zelf uitgevoerde berekeningen

R E Christoffersen and K A Baker, Chem Phys Letters 8, 4(1971)

V

De door Manoussakis en Tsipis uitgevoerde NMR studie aan de interaktie van benzeen met enige tris(dithiocarbamato) kompleksen toont slechts aan dat per dithiocarbamaat ligand een benzeen molekuul addeert maar kan geen uitspraak doen over de stoichiometrie van het kompleks als geheel

G E Manoussakis and C A Tsipis, Z anorg allg Chem 398, 88(1973)

VI

Het verdient aanbeveling om aan een verkiezingsprogramma een verslag toe te voegen van de aktiviteiten uit de voorbije bestuursperiode

VII

De uitspraak van Burgemeester en Wethouders van de Gemeente Nijmegen " de gerichte inzaai van onkruiden is geen succes geworden bepaalde soorten ontwikkelen zich welig en verstikken de andere soorten" doet vermoeden dat de betrokken gemeentelijke instanties niet of niet voldoende kennis hebben genomen van de ideeen over dynamisch natuurbeheer zoals die o a door Louis G Le Roy zijn ontwikkeld

Nota van Aanbieding bij de begroting 1974 van de Gemeente Nijmegen, afdeling 3, pagina 15

VIII

Het begrip "schertsstelling" dreigt een pleonasme te worden

NIJMEGEN, 3 mei 1974 C P KEIJZERS